Pathogenic impact of immune cells in mouse models of neuronal ceroid lipofuscinosis

Dissertation zur Erlangung des
naturwissenschaftlichen Doktorgrades
der Julius-Maximilians-Universität Würzburg

vorgelegt von
Janos Michael Groh
aus Schweinfurt

Würzburg, 2013

Eingereicht am: ……………………

Mitglieder der Promotionskommission:

Vorsitzender: Prof. Dr. Wolfgang Rössler

Gutachter: Prof. Dr. Rudolf Martini

Gutachter: Prof. Dr. Erich Buchner

Tag des Promotionskolloquium: …………………..

Doktorurkunde ausgehändigt am: …………………

Eidesstattliche Erklärung

Hiermit erkläre ich, die vorliegende Arbeit selbständig angefertigt und keine anderen als die angegebenen Quellen und Hilfsmittel verwendet zu haben.

Diese Arbeit hat weder in gleicher noch in ähnlicher Form in einem anderen Prüfungsverfahren vorgelegen.

Ich habe in keinem früheren Verfahren einen akademischen Grad erworben oder zu erwerben versucht.

Würzburg, den ………………… ………………………………...

Janos Groh

Table of contents

Parts of the results presented in this thesis have been published:

Groh J, Kuhl TG, Ip CW, Nelvagal HR, Sri S, Duckett S, Mirza M, Langmann T, Cooper JD, Martini R (2013) Immune cells perturb axons and impair neuronal survival in a mouse model of infantile neuronal ceroid lipofuscinosis. Brain 136:1083-1101.

The published manuscript and this thesis contain similar text passages in adapted form in some sections.

1. Abstract

The neuronal ceroid lipofuscinoses (NCLs) are fatal neurodegenerative disorders in which the visual system is affected in early stages of disease. A typical accompanying feature is neuroinflammation, the pathogenic impact of which is presently unknown. In this study, the role of inflammatory cells in the pathogenesis was investigated in *Palmitoyl-protein thioesterase 1*-deficient ($Ppt1^{-/-}$) and *Ceroid-lipofuscinosis, neuronal 3*-deficient ($Cln3^{-/-}$) mice, models of the infantile and juvenile forms of NCL, respectively.

Focusing predominantly on the visual system, an infiltration of CD8+ cytotoxic T-lymphocytes and an activation of microglia/macrophage-like cells was observed early in disease. To analyze the pathogenic impact of lymphocytes, $Ppt1^{-/-}$ mice were crossbred with mice lacking lymphocytes ($Rag1^{-/-}$) and axonal transport, perturbation and neuronal survival were scored. Lack of lymphocytes led to a significant amelioration of neuronal disease and reconstitution experiments revealed a crucial role of CD8+ cytotoxic T-lymphocytes. Lack of lymphocytes also caused an improved clinical phenotype and extended longevity.

To investigate the impact of microglia/macrophage-like cells, $Ppt1^{-/-}$ and $Cln3^{-/-}$ mice were crossbred with mice lacking sialoadhesin ($Sn^{-/-}$), a monocyte lineage-restricted cell adhesion molecule important for interactions between macrophage-like cells and lymphocytes. Similar to the lack of lymphocytes, absence of sialoadhesin significantly ameliorated the disease in $Ppt1^{-/-}$ and $Cln3^{-/-}$ mice.

Taken together, both T-lymphocytes and microglia/macrophage-like cells were identified as pathogenic mediators in two distinct forms of fatal inherited neurodegenerative storage disorders. These studies expand the concept of secondary inflammation as a common pathomechanistic feature in some neurological diseases and provide novel insights that may be crucial for developing treatment strategies for different forms of NCL.

2. Zusammenfassung

Die Neuronalen Ceroid Lipofuszinosen (NCL) sind tödlich verlaufende neurodegenerative Erkrankungen, bei denen das visuelle System frühzeitig im Krankheitsverlauf betroffen ist. Eine typische Begleiterscheinung sind Entzündungsreaktionen, deren pathogenetischer Einfluss bisher ungeklärt ist. In dieser Studie wurde die Rolle von Entzündungszellen bei der Pathogenese in *Palmitoyl-protein thioestease 1*-defizienten (*Ppt1$^{-/-}$*) und *Ceroid-lipofuscinosis, neuronal 3*-defizienten (*Cln3$^{-/-}$*) Mäusen untersucht, den jeweiligen Modellen der Infantilen und Juvenilen Formen der NCL.

Mit besonderem Augenmerk auf das visuelle System wurde früh in der Krankheit ein Aufkommen von CD8+ zytotoxischen T-Lymphozyten und eine Aktivierung von Mikroglia/Makrophagen-ähnlichen Zellen beobachtet. Um den pathogenetischen Einfluss der Lymphozyten zu klären, wurden *Ppt1$^{-/-}$* Mäuse mit Mäusen verkreuzt, welche keine Lymphozyten besitzen (*Rag1$^{-/-}$*). An den generierten Doppelmutanten wurden axonaler Transport, axonale Schädigung und neuronales Überleben bestimmt. Die Abwesenheit von Lymphozyten führte zu einer signifikanten Abmilderung der neuronalen Schädigung und Rekonstitutions-Experimente zeigten, dass CD8+ zytotoxische T-Lymphozyten eine entscheidende Rolle spielen. Die Abwesenheit dieser Lymphozyten führte außerdem zu einem abgemilderten klinischen Phänotyp und einem verlängerten Überleben.

Um den Einfluss von Mikroglia/Makrophagen zu untersuchen wurden *Ppt1$^{-/-}$* und *Cln3$^{-/-}$* Mäuse mit Sialoadhesin-defizienten Mäusen (*Sn$^{-/-}$*) verkreuzt. Sn ist ein Monozyten-spezifisches Zelladhäsionsmolekül, das wichtig für Interaktionen zwischen Makrophagen-ähnlichen Zellen und Lymphozyten ist. Ähnlich wie die Abwesenheit von Lymphozyten führte die Abwesenheit von Sialoadhesin zu einer signifikanten Abmilderung der Krankheit in *Ppt1$^{-/-}$* und *Cln3$^{-/-}$* Mäusen.

Zusammengefasst wurden sowohl T-Lymphozyten als auch Mikroglia/Makrophagen-ähnliche Zellen als pathogenetische Mediatoren in zwei verschiedenen Formen von tödlich verlaufenden erblichen neurodegenerativen Speicherkrankheiten identifiziert. Diese Untersuchungen erweitern das Konzept der sekundären Entzündungsreaktion als verbreitete pathomechanistische Erscheinung in einigen neurologischen

Erkrankungen und liefern neue Perspektiven für die Entwicklung von Behandlungsstrategien für verschiedene Formen der NCL.

3. Introduction

In order to enable higher biological functions as well as rapid and coordinated responses to changes in the environment, the vertebrate nervous system is structurally and functionally dependent on complex cellular interactions. Thus, in order to understand underlying processes both in the context of normal function and disease of the nervous system, cell intrinsic actions as well as interactions between different cells or cellular systems have to be investigated.

The immune system is organized as an effective set of components that incorporate specificity and adaptation. It is able to promptly react to perturbations with specific processes that, depending on the context, can be beneficial or detrimental to the function of cellular systems. Increasing evidence is gained that the mammalian central nervous system (CNS), which has classically been viewed as an immune-privileged structure, reciprocally interacts with the immune system in an intricate way, both in healthy and diseased condition.

3.1 Cellular composition and interaction of the nervous system

The mammalian nervous system is a complex network of specialized cells and coordinates the actions of an organism by perceiving, processing and storing information from the environment and enabling reactions to these stimuli. The peripheral nervous system (PNS) transmits afferent and efferent signals between the peripheral organs and the CNS.

Neurons are the main signaling units of the nervous system and form specific signaling networks using synaptic connections. Neurons are electrically excitable by alterations in voltage gradients across their plasma membranes and transmit action potentials along axons, specialized cellular extensions that terminate in synaptic connections (Kandel et al., 2000). At these synapses action potentials trigger synaptic transmission, allowing chemical or electrical communication with other cells. Usually, action potentials at presynaptic axon terminals initiate release of neurotransmitters that bind to postsynaptic receptors, leading to activation of short term or long term changes in the postsynaptic cell. The connections between different neurons determine the behavioral function of individual cells and enable integration of unique information in complex neural maps. The plasticity of these

connections contributes to adaptability of behavior and cognitive functions (Caroni et al., 2012).

The efficient and fast signal conduction along axons is supported by specialized glial cells. Schwann cells in the PNS and oligodendrocytes in the CNS ensheath large caliber axons and form an insulating myelin layer, enabling saltatory conduction of action potentials along nodes of Ranvier (Kettenmann and Ransom, 2005). These nodes are non-myelinated compartments where adjacent myelinating glial cells meet and are characterized by a complex molecular architecture (Salzer *et al.*, 2008; Rasband, 2011). Nodal, paranodal and juxtaparanodal domains differ from each other and the myelinated internodes by specific structure, densities of axonal ion channels, cell adhesion and anchoring molecules. In the PNS, each Schwann cell myelinates one axon, whereas oligodendrocytes in the CNS enwrap multiple axons. Myelin consists of lipids, glycolipids and a specific set of myelin proteins and its formation and thickness is tightly controlled by reciprocal signaling between axon and glial cell (Martini, 2001; Nave and Salzer, 2006; Brinkmann *et al.,* 2008).

Glial cells fulfill additional roles besides myelination and structural support for neurons. Schwann cells in the PNS are important for trophic support, nerve development and axonal regrowth after injury, phagocytosis of cell debris and modulation of synaptic activity at neuromuscular junctions (Kettenmann and Ransom, 2005; Rousse and Robitaille, 2006; Nave and Trapp, 2008; Armati and Mathey, 2010). In addition, Schwann cells are recognized to have immunoregulatory functions (see below) and, together with endoneurial fibroblasts, synthesize the extracellular matrix. Oligodendrocytes in the CNS are also suggested to provide trophic and metabolic support for axons (Nave, 2010; Funfschilling et al., 2012). In contrast to Schwann cells, their plasticity and ability to provide a regeneration-supporting environment for neurons in injury or disease appears limited (Armati and Mathey, 2010).

Another cell type with many supporting functions and extensive interactions in the CNS is the astrocyte. Astrocytes are supposed to modulate vascular blood flow, transmitter release at "tripartite" synapses and ion concentrations in the extracellular space (Attwell et al., 2010; Nedergaard and Verkhratsky, 2012). In addition, they supply biochemical support to neural and endothelial cells, which form the blood-brain barrier (BBB) and provide nutrients to the nervous tissue. The blood-brain

barrier shields the CNS from free diffusion of cells and molecular components in the blood in order to protect from toxic or pathogenic substances (Quaegebeur et al., 2011).

Despite this separation and only low expression of major histocompatibility complex class I (MHC-I), an important recognition molecule for presentation of cytosolic antigenic peptides, the CNS is not excluded from constant immune surveillance. Similar to hematogenously derived resident macrophages in the PNS, microglial cells sample the CNS parenchyma and act as first line of defense against infectious agents and injury-related products (Nimmerjahn et al., 2005; Raivich, 2005). Recent studies have demonstrated that microglia derive from erythromyeloid precursors from the yolk sac during embryogenesis, while infiltrating monocytes can enter the CNS under pathological conditions (Ginhoux et al., 2010; Ajami et al., 2011; Ransohoff, 2011; Kierdorf et al., 2013). In response to diverse pathological changes, microglia can rapidly augment expression of molecules for antigen presentation and activation of T-lymphocytes like MHC molecules, CD86, CD80, CD40, CD11a, CD54 and CD58 (Ousman and Kubes, 2012). In addition, microglia is able to promote inflammatory responses and eliminate pathogens by release of a variety of cytokines, reactive oxygen species, nitric oxide and phagocytosis. Microglia possess the molecular machinery to strongly activate the adaptive immune system if required and under normal conditions these reactions are tightly controlled by regulatory mechanisms (Neumann, 2001). This is necessary, since many factors and mechanisms which are used for defense against pathogens are also detrimental to neural cells and can be harmful when immune reactions become inappropriate (Block et al., 2007; Cunningham, 2013).

At a much lower frequency, also non-resident, peripherally derived cells inspect the healthy CNS for harmful agents. T-cells may gain entry into the CNS at specialized sites which allow extravasation (Ransohoff et al., 2003). T-cells can also be found in the healthy peripheral nerves at a low frequency (Schmid et al., 2000). Depending on the subset, effector T-lymphocytes can fulfill a variety of functions related to adaptive immune reactions: cytotoxic, helper and regulatory T-cells are equipped with distinct molecules to efficiently act in different ways. Antigens presented in the context of MHC class I and II molecules are recognized by CD8+ and CD4+ T-lymphocytes, respectively. Classically, CD4+ T-lymphocytes were mainly considered as helper or

regulatory T-cells, while CD8+ T-cells were supposed to be mainly cytotoxic (Murphy et al., 2007). Meanwhile, after early less appreciated observations, many studies have shown that both CD8+ and CD4+ T-cells can fulfill regulatory functions, showing that the classical distinction is an oversimplification (Cantor et al., 1976; Cosmi et al., 2003; Rifa'i et al., 2004; Shi et al., 2009).

Other peripherally derived immune cells, such as macrophages and dendritic cells, professional antigen presenting cells, are strategically located at the interface between blood and brain, at perivascular regions or in the meninges. These cells appear to be continuously replaced by bone marrow-derived monocytes and survey the environment for presentation of antigens (Hickey, 2001).

Cells belonging to the immune system do not only screen the nervous system for pathogens or remove debris (e.g. after injury), but are increasingly recognized to fulfill other functions important for neural structure and physiology (Aguzzi et al., 2013). Aspects that underline the interaction between neurons and cells of the immune system are obvious in neural development. In the central nervous system it has recently been shown that microglia play an important part in synaptic pruning (Schafer et al., 2012). Moreover, there are concepts emerging that postulate nursing of synapses by microglia (Wake et al., 2009) and an immune-mediated control of synaptic plasticity by diffusible factors, implicating a possible role in encoding and retaining of memory (Di Filippo et al., 2008).

The intricate connection between distinct cells in the nervous system is also obvious in disease. Mutations in genes that encode CNS proteins can often lead to pathological alterations that affect different cells, which do not express the protein. For example, mutations in oligodendrocytic myelin proteins can lead to axonal degeneration (Griffiths et al., 1998; Edgar et al., 2009). In addition, mutations or conditions which cause inappropriate inflammation or affect the physiological role of immune cells can lead to detrimental consequences for neurons or glial cells (Block et al., 2007; Chen et al., 2010; Lassmann, 2010; Rademakers et al., 2012). Considering that many neurological diseases with completely different causes show an increased activation or recruitment of immune cells and similar neuropathological alterations (e.g. axonal loss), detrimental immune reactions might represent a widespread pathomechanistic aspect. However, depending on the context, inflammatory reactions may be either beneficial or detrimental in distinct situations

(Mueller, 2013). Therefore, the contribution of inflammatory components has to be clarified in a disease specific manner. In some lysosomal storage diseases, an activation of immune cells is known (see below), but the pathogenic relevance (beneficial, detrimental or not relevant) of these reactions is obscure.

3.2 Lysosomal storage diseases

Lysosomal storage diseases are a group of metabolic disorders that are caused by mutations in proteins important for lysosomal functions. The majority of lysosomal storage diseases impairs the functional integrity of the central nervous system and leads to progressive decline in cognitive and motor performance. While the individual forms are rare, their combined prevalence is estimated to be one in 8000 (Bellettato and Scarpa, 2010; Schultz et al., 2011). Lysosomal storage diseases affect mostly children and the patients often die at a young age or after years of suffering from various symptoms of their particular disorder.

When lysosomal function is impaired, metabolic end products destined for breakdown and recycling are stored in the cell. Depending on the type of primary storage material, lysosomal storage diseases are classified as lipid storage disorders, including sphingolipidoses, gangliosidosis and leukodystrophies, mucopolysaccharidoses, glycoprotein storage disorders and mucolipidoses (International Classification of Diseases-10).

As primary degradative organelle, the lysosome is dependent on a network of membrane-bound proteins and soluble enzymes to efficiently degrade metabolic end products and substrates derived from various pathways including endocytosis, phagocytosis and autophagy. Recessive monogenic mutations that cause defects in these proteins or in proteins important for their proper synthesis or trafficking lead to the typical accumulation of substrate and lysosomal storage in the diseases. The accumulation of storage material can alter many cellular processes, including lysosomal pH regulation, synaptic release, endocytosis, vesicle maturation, autophagy, exocytosis and Ca^{2+} homeostasis (Ballabio and Gieselmann, 2009; Kiselyov et al., 2010; Vitner et al., 2010). However, lysosomal dysfunction does not seem to disturb normal brain development and the mechanisms by which deficiencies in these proteins disrupt cellular and especially neuronal viability remain ambiguous.

The composition and structure of the storage material is diverse and can at least in some cases not be easily deduced from the function of the deficient protein (Seehafer and Pearce, 2006). In addition, the functions of some proteins involved in lysosomal storage diseases are not clarified yet. Investigation of the disturbed cellular processes might also reveal information about the normal functions of the deficient proteins.

There are currently no cures available for the lysosomal storage diseases and treatment is mostly symptomatic. Enzyme replacement therapy and bone marrow transplantation have been tested in clinical trials with success in some of the lysosomal storage diseases (Schultz et al., 2011). In addition, substrate reduction therapy is being evaluated and gene therapy trials are in progress, which might offer cures in the future. However, such treatments are not yet available or feasible for most lysosomal storage diseases and delivery of recombinant enzymes into the CNS is a problem when dealing with strategies to correct the primary protein defects (Desnick and Schuchman, 2012). In addition, approaches like enzyme replacement are at present poorly feasible for deficiency in membrane-bound lysosomal proteins.

3.3 Neuronal ceroid lipofuscinosis

The neuronal ceroid lipofuscinoses (NCLs) are a group of fatal hereditary lysosomal storage disorders that severely affect the CNS (Kohlschutter et al., 1993). Although the genetic causes have been identified for several subtypes (Jalanko and Braulke, 2009) and some insights into disease mechanisms have been gained (Zhang et al., 2006; Ahtiainen et al., 2007), there are so far no effective therapies for these disorders (Cooper, 2008; Wong et al., 2010). Despite their genetic heterogeneity, the NCLs have certain histopathological and clinical characteristics in common (Cooper, 2010). All forms of NCL display selective degeneration of CNS neurons and an increased accumulation of autofluorescent storage material in several cell types that resembles lipofuscin or ceroid. Clinically, deterioration of vision is typically one of the earliest symptoms, followed by blindness, motor abnormalities, epilepsy, dementia and ultimately premature death (Haltia, 2006).

Historically, the NCLs were classified based upon age of onset into infantile, late infantile, juvenile, and adult forms. More recent classifications (Table 1) divide them

according to the associated mutated gene into at least 9 forms (Williams and Mole, 2012). The functions of many of the respective gene products are not clarified, but it is known that both soluble and membrane proteins can be affected. Discovery of the mutant genes also allowed the development of non-vertebrate and vertebrate animal models, in order to investigate the neurobiology of the NCLs, decipher disease staging and assess possible treatment approaches (Cooper et al., 2006). The present study is focused on two mouse models of the infantile and juvenile forms of NCL.

	Gene symbol	Protein	Diseases[a]
Soluble lysosomal enzyme deficiencies	CTSD	Cathepsin D	CLN10 disease, congenital
	CLN10		CLN10 disease, late infantile
			CLN10 disease, juvenile
			CLN10 disease, adult
	PPT1	Palmityl protein thioesterase 1, PPT1	CLN1 disease, infantile
	CLN1		CLN1 disease, late infantile variant
			CLN1 disease, juvenile
			CLN1 disease, adult
	TPP1	Tripeptidyl peptidase 1, TPP1	CLN2 disease, late infantile
	CLN2		CLN2 disease, juvenile
Nonenzyme deficiencies (functions of identified proteins poorly understood at the current time)	CLN3	Transmembrane protein	CLN3 disease, juvenile
	CLN5	Soluble	CLN5 disease, late infantile
		Lysosomal	CLN5 disease, juvenile
			CLN5 disease, adult
	CLN6	Transmembrane protein; ER	CLN6 disease, late infantile
			CLN6 disease, adult Kufs type A
	MFSD8	Transmembrane protein; endolysosomal transporter	CLN7 disease, late infantile
	CLN7		
	CLN8	span lang=NLTransmembrane protein; ER, ER-Golgi intermediate complex	CLN8 disease, late infantile
			CLN8 disease, EPMR
	DNAJC5	Soluble cysteine string protein α	CLN4 disease, adult autosomal dominant
	CLN4		
Others: those whose classification is uncertain because of incomplete diagnostic investigations or absence of confirmed gene/ mutation designation, or where NCL is a minor mutation-specific phenotype	?	Mutations not yet defined in any gene	Congenital/infantile variants
	?	Mutations not yet defined in any gene	Late infantile variants
	?(CLN9)	Mutations not yet defined in any gene	Juvenile variants
	?	Mutations not yet defined in any gene	Late onset/adult variants
	CLCN6	Mutations not yet found on both disease alleles in human disease	Chloride transport defect, adult onset
	SGSH	Mutations usually cause MPSIIIA	Adult onset

Abbreviation: NCL = neuronal ceroid lipofuscinosis.
[a] Diseases listed are those already described. It is possible that further cases of later onset, e.g., CLN2 disease, adult, or those with atypical progression, e.g., CLN3 disease, juvenile, will yet be recognized.

Table 1 Present classification nomenclature of different forms of NCL; adapted from (Williams and Mole, 2012)

Infantile NCL (INCL or CLN1 disease, infantile) is a severe and early-onset form of NCL caused by mutations in the *PPT1* (also known as *CLN1*) gene that encodes for palmitoyl protein thioesterase 1 (PPT1), a soluble lysosomal enzyme. PPT1 removes

thioester-linked fatty acyl groups from cysteine residues during lysosomal degradation (Camp et al., 1994). Patients suffering from INCL initially show normal development until they become symptomatic at around 12 months of age and usually die by 10 years of age (Santavuori et al., 1973; Santavuori et al., 1974). The primary mechanisms leading to the profound deficits caused by *PPT1* mutations remain poorly understood. Murine models of INCL that have been generated by disruption of the *Ppt1* gene mimic the deficits observed in patients, including early neuropathology in many brain regions, motor abnormalities, spontaneous seizures and a reduced life span (Gupta et al., 2001; Jalanko et al., 2005; Kielar et al., 2007).

Juvenile NCL (JNCL or CLN3 disease, juvenile) is caused by mutations in the *CLN3* gene, encoding for a lysosomal transmembrane protein of so far unknown function. JNCL is the most prevalent NCL subtype and is clinically characterized by an age of onset at around 4-7 years and death in the second or third decade of life (Haltia, 2003). The most common mutation is a 1kb deletion leading to a frameshift and premature termination, resulting in impaired transport of the mutant protein to lysosomes and cellular projections (Jarvela et al., 1999). Murine models have been generated by mimicking this common mutation via a "knock-in" approach or by "knockout" approaches disrupting different exons of the *Cln3* gene (Katz et al., 1999; Mitchison et al., 1999; Cotman et al., 2002).

Interestingly, previous studies in several NCL mouse models revealed an early occurrence of innate immune reactions within the brain, which have been proposed but not proven to play a role in the disease (Pontikis et al., 2004; Kielar et al., 2007; Partanen et al., 2008).

In addition, some observations have suggested that the adaptive immune system might also contribute to disease progression in some models of NCL. On the one hand, antibodies have been suggested to contribute to detrimental autoimmune reactions (Seehafer et al., 2011) and on the other hand, there are some reports about increased numbers of T-lymphocytes present within the CNS in a mouse model of JNCL (Lim et al., 2007). However, the nature and role of these immune reactions in the disease have not yet been clarified.

The possibility that immune reactions might contribute to disease severity in NCL could have substantial implications for putative therapeutic strategies. Several

specific immunomodulatory drugs are in development or already available for the treatment of other immune-mediated diseases and immunomodulation might represent an easier and more feasible approach compared with other strategies such as gene therapy.

3.4 The role of inflammation in neural perturbation of the peripheral and central nervous system in other neurological disorders

Are there hints from other neurological diseases that inflammation could play a role in NCL? Previous studies have demonstrated that immune reactions can be detrimental or protective in different animal models of diseases of the PNS and CNS. While some PNS disorders like the Guillain-Barré-syndrome (GBS) or chronic inflammatory demyelinating polyneuropathy (CIDP) have been recognized as classical immune-mediated disorders (Ueda and Kusunoki, 2011), several studies using mouse models of Charcot-Marie-Tooth neuropathy type 1 (CMT1) revealed that low-grade and chronic activation of immune cells can also significantly contribute to diseases which were classically not considered as being immune-mediated (Ip et al., 2006a).

$P0^{+/-}$, $Cx32^{def}$ and $PMP22^{tg}$ mice, as models for CMT1B, CMT1X and CMT1A respectively, show an age-dependent increase in the number of both F4/80+ macrophages and CD8+ T-lymphocytes compared with wild-type mice in the quadriceps nerve, a branch of the femoral nerve containing a relatively high number of fibers from motor neurons (Schmid et al., 2000; Kobsar et al., 2002; Kobsar et al., 2005). The phenotype of the $P0^{+/-}$ and $Cx32^{def}$ mouse models can be significantly ameliorated by crossbreeding with $Rag1$-deficient mice, lacking mature T- and B-lymphocytes, demonstrating that reactions of the adaptive immune system are pathogenetically relevant (Schmid et al., 2000; Kobsar et al., 2003). In contrast, $PMP22^{tg}$ mice do not display any significant amelioration of neuropathy in the absence of mature T- and B-lymphocytes (Kohl et al., 2010b) and homozygous $P0^{-/-}$ mice, a model for the severe Dejerine-Sottas syndrome (DSS), even show an aggravated phenotype when crossbred with $Rag1$-deficient mice (Berghoff et al., 2005).

A detrimental contribution of reactions of the innate immune system in these models has been confirmed by crossbreeding with distinct mutants deficient in macrophage-

related factors. Both the *P0*^{+/-} and *Cx32*[def] mouse models displayed a profound and persistent amelioration of neuropathy when activation and proliferation of macrophages in the peripheral nerves was blocked by absence of CSF-1 (Carenini et al., 2001; Groh et al., 2012). In addition, absence of sialoadhesin (Sn), a monocyte-lineage restricted cell adhesion molecule involved in the interaction between macrophages and T-lymphocytes, also led to an amelioration of demyelination in *P0*^{+/-} mice (Kobsar et al., 2006). Several studies could demonstrate that mutant Schwann cells in *P0*^{+/-}, *Cx32*[def] and *PMP22*[tg] mice show increased MEK-ERK signaling and a subsequently upregulated expression of chemokines like MCP-1 that recruit and activate macrophages in the peripheral nerves. Attenuation of this increased expression by crossbreeding experiments resulted in significant amelioration of the neuropathological phenotype, demonstrating that communication between the primarily diseased glial cells and cells of the innate immune system might be a conserved mechanism in different diseases that can detrimentally affect structure and function (Fischer et al., 2008b; Fischer et al., 2008a; Groh et al., 2010; Kohl et al., 2010a).

Immune reactions have also been identified to contribute to neurological diseases of the CNS. In addition to CNS disorders which are classically considered as immune-mediated like multiple sclerosis or some viral infections of the CNS, there is increasing evidence that genetically caused diseases are influenced by reactions of the immune system. Importantly, previous studies in a mouse model of leukodystrophy, also belonging to the lysosomal storage diseases, have highlighted the role of low-grade inflammation comprising CD8+ T-lymphocytes in neural perturbation. Proteolipid protein (PLP) overexpressing mice show demyelination and axonal perturbation in the CNS and crossbreeding experiments with *Rag1*-deficient mice led to a significant amelioration of these alterations (Ip et al., 2006b). In subsequent experiments, clonally expanded CD8+ cytotoxic T-lymphocytes were shown to cause axonal damage in an antigen-dependent manner in these myelin mutants (Leder et al., 2007; Kroner et al., 2010). Granzyme B and perforin were additionally identified as cytotoxic effector molecules that perturb axonal structure and functional integrity, as measured by retrograde axonal transport (Ip et al., 2012). In this model, the primary defect clearly affects oligodendrocytes, as PLP is a major component of the compact myelin and the overexpression leads to increased expression of MHC class I molecules on oligodendrocytes (Ip et al., 2006b). The

exact mechanisms how secondary inflammation caused by primary glial defects leads to perturbation of axonal integrity are not yet fully understood. Nevertheless, the observations demonstrate that in addition to supporting interactions between neurons and glial cells, a contribution of the immune system to neuronal perturbation has to be considered.

In line with the proposed role for sialoadhesin in interactions between microglia/macrophage-like cells and T-lymphocytes and a contribution of activated microglia to disease in the PLP-transgenic mice, crossbreeding experiments using $Sn^{-/-}$ mice also resulted in ameliorated demyelination and reduced axonal pathology (Ip et al., 2007). Interestingly, despite the increased frequency of CD8+ cytotoxic T-lymphocytes and CD11b+ microglia/macrophage-like cells in the CNS of these PLP mutants, no significant alterations in blood-brain barrier integrity compared with healthy mice were observed and the numerical increase in CD11b+ cells appeared to be mostly due to local CNS-intrinsic expansion (Ip et al., 2008). As an example of beneficial reactions of the innate immune system in CNS disease it has been shown that microglia/macrophages are required for removal of myelin debris and remyelination in a mouse model of globoid cell leukodystrophy (Kondo et al., 2011).

Taken together, immune reactions have been shown to significantly impact a variety of neurological diseases of the PNS and CNS.

3.5 Aim of the study

The aim of this study was to analyze the pathogenic impact of immune cells in mouse models of INCL ($Ppt1^{-/-}$) and JNCL ($Cln3^{-/-}$) by addressing the following specific goals.

1) Analysis of the visual system as a readout system for characterizing pathological alterations, since visual impairment is an early alteration and a hallmark of NCL.

2) Detailed characterization of immune cells in the CNS and after isolation from the CNS and investigation of the integrity of the blood-brain barrier.

3) Investigation of the functional impact of immune reactions by crossbreeding of the NCL models with *Rag1*-deficient mice and *Sn*-deficient mice and detailed morphological and functional analyses of the resulting double mutants.

4) Reconstitution of the *Rag1*-deficient double mutants with bone marrow from wild-type, CD8-deficient and CD4-deficient mice to determine which type of lymphocytes (CD4+, CD8+ T-lymphocytes, B-lymphocytes) is involved in the pathogenesis of INCL and JNCL.

4. Material and Methods

4.1 Equipment, buffers and solutions, antibodies and primer sequences

Technical equipment (Appendix 8.1), buffers and solutions (Appendix 8.2) as well as antibodies for immunohistochemistry and flow cytometry (Appendix 8.3) and primer sequences for genotyping (Appendix 8.4) are listed in detail in the appendices.

4.2 Animals and determination of genotypes

Mice were kept in the animal facility of the Department of Neurology under barrier conditions at a constant light-dark-cycle of 14 hours in the light and 10 hours in the dark. To avoid alterations in the light-dark-cycle, all animal experiments were performed in the light and at approximately the same hour (before noon). All animal experiments were approved by the Government of Lower Franconia.

Ppt1-deficient (*Ppt1$^{-/-}$*) mice with disruption of exon 9 (Gupta et al., 2001) were crossbred with *Rag1*-deficient (*Rag1$^{-/-}$*) mice (Mombaerts et al., 1992). *CD4$^{-/-}$* (Rahemtulla et al., 1991), *CD8$^{-/-}$* (Fung-Leung et al., 1991) and wild-type (wt) mice were used as donors for bone marrow transplantation experiments. *Ppt1$^{-/-}$* mice as well as *Cln3*-deficient (*Cln3$^{-/-}$*) mice (Mitchison et al., 1999) were crossbred with sialoadhesin-deficient (*Sn$^{-/-}$*) mice (Oetke et al., 2006). All mouse strains were on a uniform C57BL/6 genetic background except the *Cln3$^{-/-}$* mice which were on a 129/Sv genetic background. The genotypes were determined by conventional PCR reaction using isolated DNA from tail biopsies. Primer sequences for detection of the corresponding alleles are described in Appendix 8.4.

Analyses of heterozygous *Ppt1$^{+/-}$* or *Cln3$^{+/-}$* mice as well as *Rag1$^{-/-}$* and *Sn$^{-/-}$* single mutant mice did not display any differences compared with wt mice in the described experiments (except the typical lack of lymphocytes in all *Rag1$^{-/-}$* genotypes and the lack of Sn in all *Sn$^{-/-}$* genotypes) and are not shown. In addition, heterozygous *Rag1$^{+/-}$* mice (*Ppt1$^{+/+}$Rag1$^{+/-}$* or *Ppt1$^{-/-}$Rag1$^{+/-}$*) did not show any differences to *Rag1$^{+/+}$* mice (wt or *Ppt1$^{-/-}$Rag1$^{+/+}$*) and are also not shown. Similar observations were made with heterozygous *Sn$^{+/-}$* mice.

4.3 Dissection and processing of nervous tissue

Mice were killed by asphyxiation with CO_2 (according to guidelines by the State Office of Health and Social Affairs Berlin) and transcardially perfused with phosphate buffered saline (PBS) containing heparin. Retinal ganglion cells (RGCs) were quantified in flat mounted preparations. Eyes were dissected, cut, and corneas and lenses were removed before fixation in 4% paraformaldehyde (PFA) in PBS for 30 minutes. Retinae (4 retinal leaves) were flat mounted to charged slides (SuperFrost® plus; Langenbrinck) and air dried for cresyl violet staining or directly embedded in DABCO after retrograde labeling (see below). For immunohistochemistry, freshly dissected tissue was embedded and frozen in OCT medium (Tissue-Tek; Sakura) and 10 µm-thick non-adjacent sections were cut and stored at -20°C until use. For isolation of total RNA and protein, tissue was snap frozen in liquid nitrogen and stored at -80°C. For flow cytometry, tissue was freshly dissected and stored in PBS on ice before further processing. For electron microscopy, animals were transcardially perfusion-fixed with 4% PFA and 2% glutaraldehyde (GA) in 0.1M cacodylate buffer for 15 minutes and the dissected tissue was post-fixed over night in the same solution. In order to quantify Nissl stained neurons in thalamic brain regions, mice were perfusion-fixed with 4% PFA in PBS, the tissue was post-fixed for 2 hours and then cryoprotected using 30% sucrose in PBS. After embedding and freezing in OCT medium, 30 µm-thick coronal sections were cut and air-dried on charged slides.

4.4 Histochemistry and immunofluorescence

Retinal flat mount preparations were stained with 0.1% cresyl violet for 10 minutes, rinsed, dehydrated and mounted in Vitro-Clud® (Langenbrinck) for microscopy. For quantification of Nissl stained RGCs, digital images were acquired (inner, middle, outer region of the flattened retina) and the density of RGCs was determined. Only cells that were clearly Nissl stained and displayed the typical shape of RGCs were counted (Drager and Olsen, 1981). Middle regions of the flattened retinae are shown in the figures. Similarly, Nissl stained neurons in the laterodorsal thalamic nucleus (LGNd) from 3-month-old mice were quantified in 30 µm thick coronal brain sections. For this purpose, three non-adjacent sections per animal were photographed and the Nissl stained cells were related to the analyzed area.

Sections of fresh frozen tissue were thawed and post-fixed in either ice-cold acetone or 4% PFA in PBS depending on the used primary antibody (Appendix 8.3). After fixation, sections were rinsed in PBS and a serum blocking step using 5% bovine serum albumin (BSA) in PBS was performed for 30 minutes. Primary antibodies were incubated over night at 4°C in 1% BSA in PBS (see Appendix 8.3 for dilutions). Depending on the antigen, 0.3% or 0.1% Triton X-100 was added to the blocking solution and the diluted primary antibodies. Sections were washed three times with PBS and incubated with secondary antibodies (Appendix 8.3) for 60 minutes at room temperature. For fluorescence microscopy, cell nuclei were stained with DAPI (Sigma-Aldrich) for 10 minutes. Sections were washed, embedded in DABCO and sealed with Vitro-Clud® (Langenbrinck) or embedded in Aqua-Poly/Mount® (Polysciences).

For chromogenic detection, biotinylated secondary antibodies were visualized by incubation with streptavidin–biotin–peroxidase complex (Vector Laboratories) for 30 minutes, followed by washing and incubation with diaminobenzidine–HCl and H_2O_2. Cell nuclei were stained with haematoxylin. For immunohistochemistry against non-phosphorylated neurofilaments, sections were incubated in methanol containing 0.3% H_2O_2 after post-fixation with 4% PFA in PBS and treated with avidin-biotin blocking reagents (Vector Laboratories) after incubation with primary antibodies. After chromogenic detection, sections were washed with distilled water and embedded in Aquatex medium (Merck).

4.5 Retrograde labeling of retinal ganglion cells

To study integrity of retinal ganglion cells via retrograde axonal transport, 1.5 µl of 4% fluorogold (Fluorochrome, LCC) in 0.9% saline were injected into each superior colliculus of both brain hemispheres. Mice were anesthetized and placed into a stereotactic frame. Using a micro drill (Fine Science Tools) and a syringe pump (Stoelting) injections were made into the superior colliculus at stereotactic coordinates -3.6 mm caudal, -0.6 mm lateral and -1.8 mm ventral to the bregma. After 6 or 12 days, retinal flat mount preparations were photographed as described above and fluorogold-positive profile density was determined by manual counting of fluorescently labeled cells.

4.6 Electron microscopy

Nervous tissue from perfusion-fixed mice was prepared for electron microscopy as previously described (Ip et al., 2006b). Post-fixation over night was followed by osmification, dehydration and embedding in Spurr's medium. Semithin sections (0.5 μm) were stained with alkaline methylene blue for light microscopy and ultrathin sections (70 nm) were mounted to copper grids and counterstained with lead citrate. Ultrathin longitudinal and cross-sections were investigated using a ProScan Slow Scan CCD (ProScan) camera mounted to a Leo 906 E electron microscope (Zeiss) and corresponding software iTEM (Soft Imaging System). To quantify axonal spheroids, cross-sections 2 mm caudal to the optic nerve head were analyzed and regularly distributed images over the cross-sectional area were taken at a fixed magnification. Using morphological criteria, identified abnormalities (spheroids) were counted and related to the total number of quantified axons. At least 10 images and more than 1,000 axons per animal were analyzed.

4.7 Immunoelectron microscopy

For immunoelectron microscopy, optic nerves and brains of perfusion fixed mice were embedded in 6% agarose after post-fixation over night. Vibratome sections (50 μm-thick) were cut and and free-floating sections were blocked with 1% BSA in PBS and incubated in 0.1M $NaIO_3$ in PBS and subsequently in 5% DMSO in PBS (Martini and Schachner, 1986). Immunohistochemistry against MHC-I on free-floating sections was performed using the same conditions as for fresh-frozen cryosections and chromogenic detection. After diaminobenzidine staining, the sections were osmificated and processed for light and electron microscopy as described above.

4.8 Flow cytometry

Leukocytes were isolated from spleen and brain as previously described (Ip et al., 2006b; Kroner et al., 2010). Splenocytes were extracted by passing the tissue through 70 μm cell strainers (BD Biosciences) and washed with PBS. Erythrocyte lysis was performed for 5 minutes at room temperature with a lysis buffer. Cells were then washed and stained.

CNS tissue was homogenized and cells were isolated from the interface of a 30 to 50% Percoll (GE Healthcare) gradient. Mononuclear cells were washed and T-lymphocytes were stained in FACS buffer using CD8-PE antibodies, gated and analyzed concerning expression of activation markers using CD62L-APC, CD44-PerCP and CD69-FITC antibodies and appropriate isotype controls (BD Biosciences). Cells were analyzed using a FACSCalibur with CellQuest software (BD Biosciences).

4.9 Bone marrow transplantation

Bone marrow from donor mice was isolated and transferred according to previously published protocols (Ip et al., 2006b). Briefly, bone marrow was isolated by flushing out femoral bone marrow with sterile PBS, washed and filtered through a 70 µm cell strainer to remove debris. Afterwards, cells were resuspended in 500 µl PBS and approximately 2×10^7 cells were injected intravenously into recipient mice. $Ppt1^{-/-}$ $Rag1^{-/-}$ and $Ppt1^{+/+}Rag1^{-/-}$ control mice were reconstituted at 1 month of age and sacrificed at 3 months of age. Successful chimerism was controlled by flow cytometry of splenocytes and imunohistochemistry on optic nerve sections. Importantly, engraftment of transplanted bone marrow led to a frequency of the respective T-lymphocyte types in the Rag1-deficient host spleen and CNS tissue that was similar to $Rag1$-positive mice.

In additional experiments bone marrow from 3-month-old $Ppt1^{-/-}$ or $Cln3^{-/-}$ mice was transplanted into $Ppt1^{+/+}Rag1^{-/-}$ mice to identify putative intrinsic detrimental alterations of bone-marrow derived cells caused by the lysosomal protein deficiencies. Recipient mice were sacrificed at 15 months of age showing no signs of neurological abnormalities.

4.10 Detection of autofluorescent storage material

To detect autofluorescent material in retinal ganglion cells or LGNd neurons, transverse sections of retinae or coronal brain sections were labeled using mouse anti-mouse NeuN primary antibodies and Cy3-conjugated secondary antibodies. Fluorescence microscopic images of the RGC layer or the LGNd in at least 3 non-adjacent sections per animal were acquired with identical settings. Using ImageJ, a

threshold analysis was performed for measuring the area of NeuN immunoreactivity and the area of autofluorescent signal with a GFP filter set. The ratio of autofluorescent area per NeuN+ area was determined in at least 10 neurons per image and related to the mean value obtained for wt mice.

4.11 Determination of myoclonic jerks

The frequency of myoclonic jerks was observed during the daylight cycle by placing mice individually in a clean cage in a quiet room for a 5 min observation period. During this period an observer unaware of the genotype documented all myoclonic jerks according to previously described criteria (Gupta et al., 2001). $Ppt1^{+/+}Rag1^{+/+}$ (wt) and $Ppt1^{+/+}Rag1^{-/-}$ control mice were observed until 15 months of age and did not show any myoclonic jerks until this age (data not shown). Similarly, $Sn^{-/-}$ mice did not display myoclonic jerks until the oldest age investigated (18 months).

4.12 Analysis of visual acuity

$Ppt1^{+/+}$, $Ppt1^{-/-}Rag1^{+/+}$ and $Ppt1^{-/-}Rag1^{-/-}$ mice at 6 months of age were analyzed using an optomotor testing apparatus and the corresponding software (Optomotry; Cerebral Mechanics, Inc.) as previously described (Prusky et al., 2000). Visual acuity was determined by increasing the spatial frequency of a virtual vertical sine wave grating at 100% contrast until an opto-kinetic response was no longer induced.

4.13 Total RNA and protein isolation

Snap frozen nervous tissue was homogenized (ART-MICCRA D-8, ART Labortechnik) in TRIzol® reagent (Invitrogen). Total RNA and proteins were isolated by Phenol-Chloroform extraction, phase separation and subsequent precipitation according to the guidelines of manufacturer.
Precipitated RNA was solubilized in DEPC-water and concentration and quality of RNA were measured using a BioPhotometer (Eppendorf). Proteins were precipitated from the phenolic phase using isopropanol. Protein pellets were washed three times with 0.3M guanidine hydrochloride in 95% ethanol and one time with ethanol for twenty minutes each and then dried. Proteins were solubilized in 1% SDS or RIPA

buffer containing protease inhibitor. Concentration of resulting protein samples were examined by a Lowry assay (Sigma Aldrich).

4.14 Semi-quantitative real-time PCR

After photometry, 1 µg of RNA was reverse transcribed in a 100 µl reaction using random hexamer primers (Applied Biosystems). Complementary DNA samples were subsequently analyzed as triplicates by semi-quantitative real-time polymerase chain reaction using previously developed TaqMan$^{®}$ assays (IL-1β: Mm00434228_m1; TNF-α: Mm00443258_m1; 18s: 4319413E) and TaqMan$^{®}$ universal PCR master mix (Applied Biosystems) according to the guidelines of manufacturers and previously published protocols (Groh et al., 2012).

4.15 Analysis of longevity

$Ppt1^{-/-}$ mice ($Ppt1^{-/-}Rag1^{+/+}$, $Ppt1^{-/-}Sn^{+/+}$), $Ppt1^{-/-}Rag1^{-/-}$ and $Ppt1^{-/-}Sn^{-/-}$ mice were allowed to age unmanipulated until death; mice in moribund condition (according to cumulative criteria, http://www.stabsstelleau.zv.uni-wuerzburg.de/?id=49517) were sacrificed. Kaplan-Meier analysis was used to measure cumulative survival and determine differences concerning lifespan. Wild-type, $Ppt1^{+/+}Rag1^{-/-}$ and $Ppt1^{+/+}Sn^{-/-}$ control mice were observed until 15 months of age and did not show premature death until this age (respective data is not shown).

4.16 Statistical analysis

All quantifications and functional/behavioral analyses were performed by investigators unaware of the genotypes of the respective mice. Shapiro-Wilk test was used to control for normal distribution of data sets. Normally distributed data were compared using the unpaired two-tailed Student's t-test. Statistical analyses of electron microscopic quantifications were performed by use of the non-parametric Mann-Whitney U-test. For multiple comparisons, one-way ANOVA followed by Tukey's *post hoc* tests were used. Longevity values were compared by Kaplan-Meier analysis. P-values considered as significant were indicated by asterisks according to the following discrimination: * $P < 0.05$; ** $P < 0.01$; *** $P < 0.001$. Significant

differences between $Ppt1^{+/+}$ and $Ppt1^{-/-}$ or $Cln3^{+/+}$ and $Cln3^{-/-}$ genotype groups are indicated above the corresponding bars.

5. Results

5.1 Mouse model of INCL (*Ppt1*$^{-/-}$ mice)

5.1.1 *Ppt1*$^{-/-}$ mice display progressive perturbation and loss of retinal ganglion cells

The neuropathological phenotype of the INCL model was analyzed from 1 to 7 months of age, i.e. at ages covering presymptomatic (1 month), symptomatic (3 and 5 months) and disease end stage (7 months) when the first 20-30% of mice are dying. Cresyl violet staining on flat mounted retinae was performed in wild-type (wt; *Ppt1*$^{+/+}$) and *Ppt1*-deficient mutants (*Ppt1*$^{-/-}$) at these ages and revealed a progressively decreased density of Nissl stained retinal ganglion cells (RGCs; Fig. 1A).

In addition, RGC counts were performed using immunohistochemistry against the transcription factor Brn3a which has a function in dendritic and cell soma-related stratification of RGCs that is not related to disease (Badea et al., 2009; Galindo-Romero et al., 2011). In 5-month-old mice the number of Brn3a+ cells in the ganglion cell layer of transverse sections through retinae from *Ppt1*$^{-/-}$ mice was significantly reduced (by 37% +/- 1%; n = 4 per group; $P < 0.001$) when compared with wt mice (Fig. 1B).

Next, the integrity of RGCs and their axons was investigated by retrograde labeling with fluorogold. In 5-month-old *Ppt1*$^{-/-}$ mice there were significantly fewer fluorogold-labeled RGCs after six days of retrograde transport (Fig. 1C,D), which could not be ameliorated by extending this survival time up to 12 days, demonstrating a complete block of retrograde transport (not shown). The reduction in retrogradely labeled RGCs (52% +/- 10%) was more pronounced than the loss of RGCs determined by cresyl violet staining at the same age (26% +/- 6%). This indicates that the impaired retrograde transport cannot solely be explained by loss of RGCs but also reflects perturbed axonal integrity, probably including axonal transection.

As an alternative axonopathic marker immunohistochemistry using antibodies against non-phosphorylated neurofilaments (SMI32) was performed. In optic nerve sections from *Ppt1*$^{-/-}$ mice, but barely in sections from wt mice, intensely labeled SMI32+ axonal spheroids could be detected (Fig. 1E). Counts revealed progressively

increased numbers of these axonal spheroids in *Ppt1*^{-/-} mice from 3 months onwards, reflecting on-going damage of RGC axons (Fig. 1F). The use of quantitative neurofilament-based immunofluorescence in cross-sections 2 mm caudal to the optic nerve head revealed that 43±5% (*n* = 4 per group; *P* < 0.01) of the axonal signal was lost in *Ppt1*^{-/-} mice (Figure 1G), supporting the finding of axonal loss in *Ppt1*^{-/-} mice.
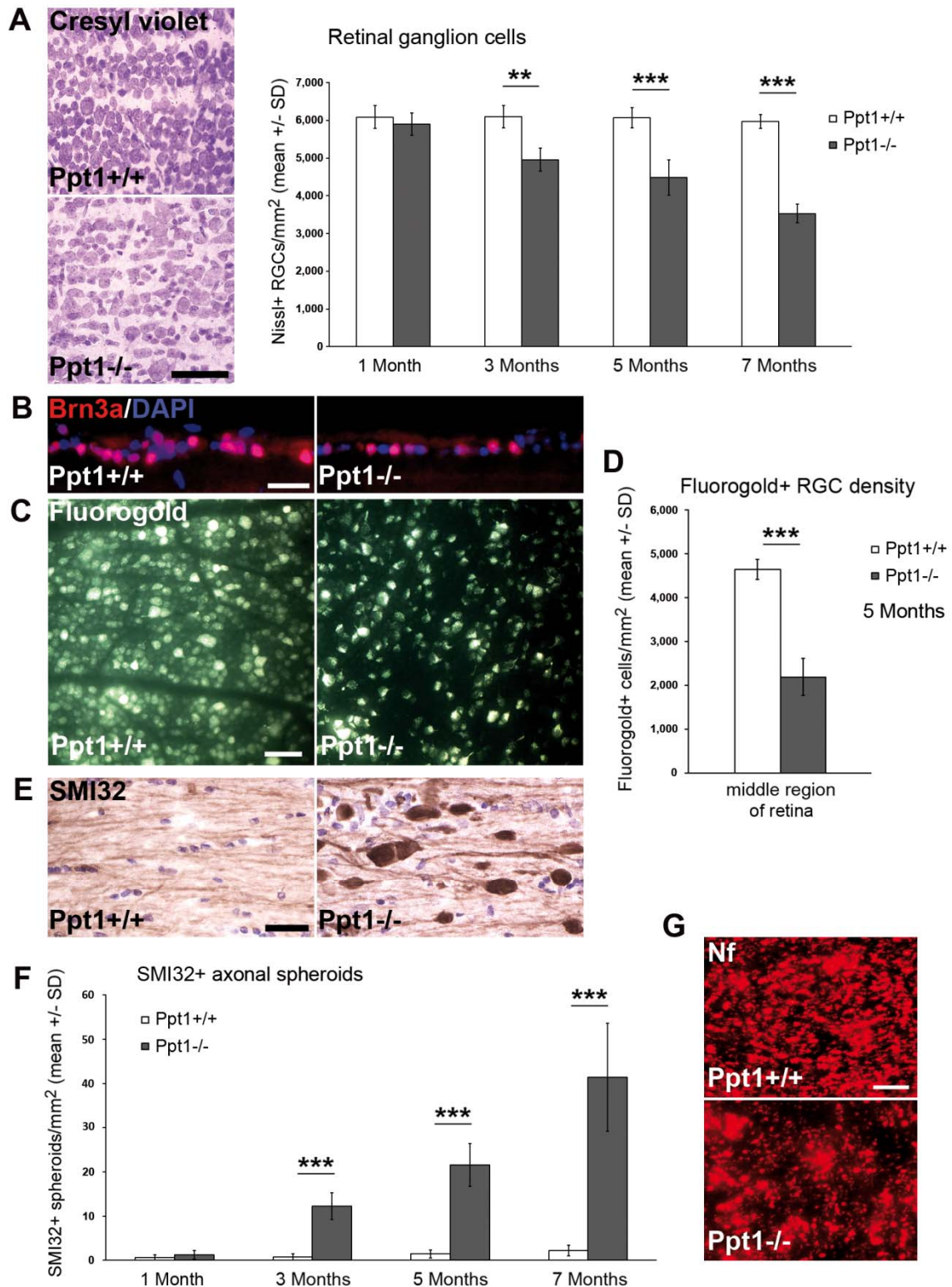
Figure 1 Progressive loss of retinal ganglion cells and axonal degeneration in $Ppt1^{-/-}$ mice. (**A**) Cresyl violet staining of retinal flat mount preparations (at 5 months) and quantification of Nissl+ retinal ganglion cells in 1, 3, 5 and 7-month-old $Ppt1^{+/+}$ and $Ppt1^{-/-}$ mice (n = 4-5 per group). Scale bar = 50 µm. (**B**) Brn3a immunohistochemistry on retinal sections from 5-month-old $Ppt1^{+/+}$ and $Ppt1^{-/-}$ mice. Scale bar = 30 µm. Numbers of Brn3a+ retinal ganglion cells in $Ppt1^{-/-}$ mice were reduced to 62.8±0.4% of $Ppt1^{+/+}$ mice (n = 4 per group). $P < 0.001$. (**C**) Fluorescence micrographs of retinal flat mount preparations 6 days after injection of fluorogold into the superior colliculus of 5-month-old $Ppt1^{+/+}$ and $Ppt1^{-/-}$ mice. Scale bar = 50 µm. (**D**) Quantification of fluorogold-labelled retinal ganglion cells revealed a significant cell loss in 5-month-old $Ppt1^{-/-}$ compared with $Ppt1^{+/+}$ mice (n = 3 per group). (**E**) Immunohistochemistry using antibodies against non-phosphorylated neurofilaments (SMI32; brownish precipitate) counterstained with haematoxylin (blue) in longitudinal optic nerve section of 7-month-old $Ppt1^{+/+}$ and $Ppt1^{-/-}$ mice. SMI32+ spheroids were often accompanied by numerous cell nuclei. Scale bar = 30 µm. (**F**) Quantification revealed that SMI32+ axonal spheroids are barely detectable in optic nerves of $Ppt1^{+/+}$ mice but accumulated in 3-,5- and 7-month-old $Ppt1^{-/-}$ mice (n = 4 per group). (**G**) Immunohistochemistry against neurofilaments on optic nerve cross-sections from 7-month-old $Ppt1^{-/-}$ mice demonstrated a reduction of signal to 57.3±4.8% of $Ppt1^{+/+}$ mice (n = 4 per group). $P < 0.01$. Scale bar = 20 µm. Significant differences were determined by Student's t-tests. ** $P < 0.01$; *** $P < 0.001$. RGC = retinal ganglion cell.

According to the investigations, the putative staging of axon damage might start with swelling and enhanced SMI32-immunoreactivity, followed by disintegration and degeneration (Fig. 2A,B). Electron microscopy of optic nerve sections additionally demonstrated an accumulation of disintegrating mitochondria and other organelles in axonal spheroids (Fig. 2C). Interestingly, the majority of developing axonal spheroids detected in 5-month-old $Ppt1^{-/-}$ mice was found in the juxtaparanodal domains of the nodes of Ranvier and showed a chiasm-directed orientation. This observation was confirmed by double immunohistochemistry against non-phosphorylated neurofilaments in combination with the juxtaparanodal marker Caspr2, showing that 75% (+/- 7%; n = 3) of the SMI32+ axonal spheroids co-localized with swollen juxtaparanodes and displayed again a chiasm-directed orientation (Fig. 2D).

Taken together, these data demonstrate a progressive degeneration of RGCs in $Ppt1^{-/-}$ mice, which seems to be preceded by axon dysfunction and degeneration. The progression of pathological changes in the $Ppt1$-deficient brain and especially in the thalamocortical system has previously been described in detail (Kielar *et al.*, 2007; Kielar *et al.*, 2009).
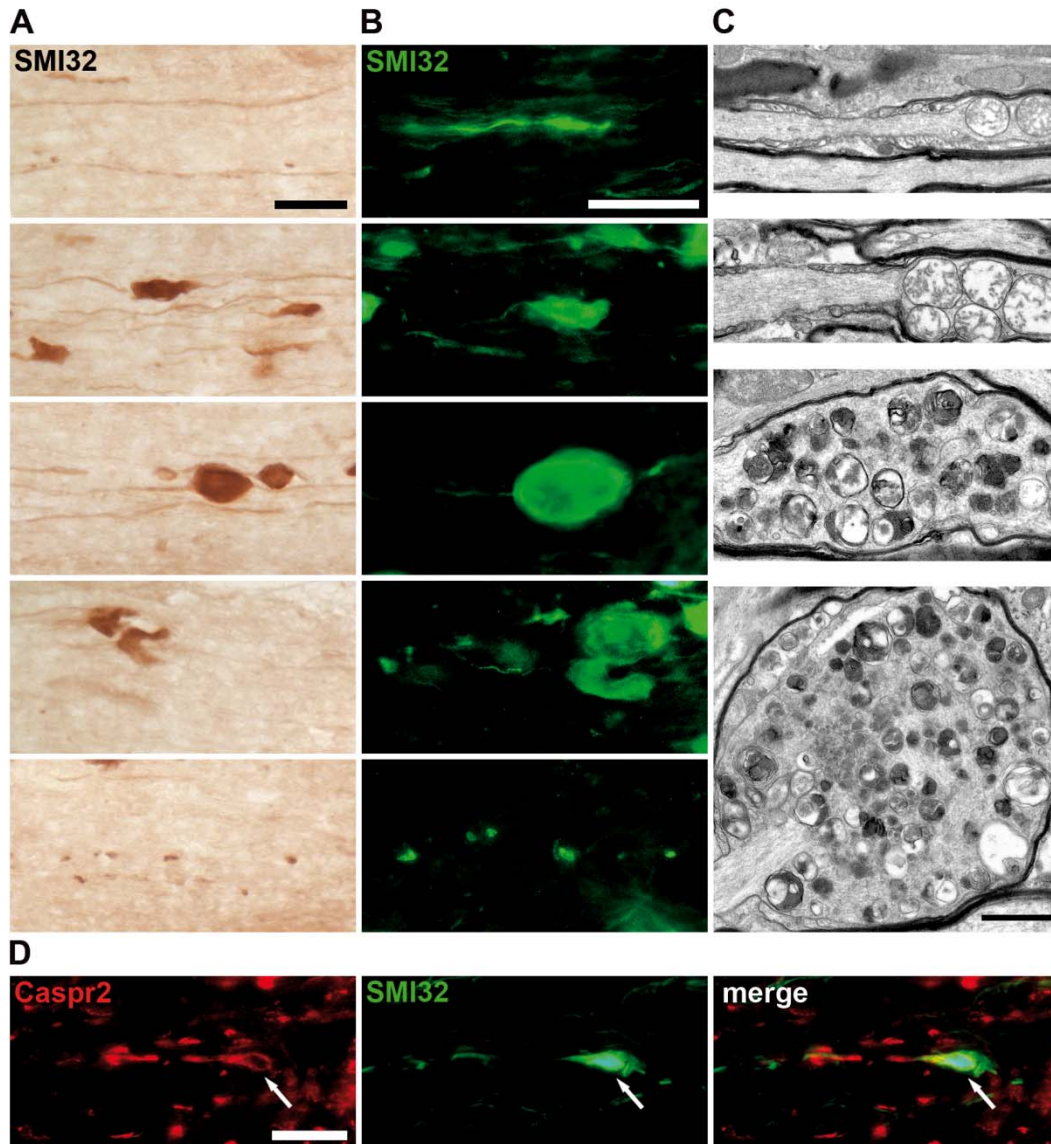
Figure 2 Putative stages of juxtaparanodal axon spheroid formation in *Ppt1*^{-/-} mice. (**A**) Light and (**B**) fluorescence micrographs of putative subsequent stages (top to bottom) of axonal swelling and degeneration revealed after immunohistochemistry using antibodies against non-phosphorylated neurofilaments on longitudinal optic nerve sections from 5-month-old *Ppt1*^{-/-} mice. Spheroid formation appeared to start with swelling and enhanced SMI32 immunoreactivity, progressively increasing in size and circularity. In some cases, multiple spheroids accumulated along single axons. Large spheroids sometimes appeared to show disintegration and fragmented small immunoreactive remnants oriented in rows might indicate transection, breakdown and degeneration of axons. Scale bars = 30 µm. (**C**) Electron microscopy of longitudinal optic nerve sections from 5-month-old *Ppt1*^{-/-} mice. Mitochondria accumulated in juxtaparanodal spheroids, appeared to disintegrate, and especially in larger spheroids mitochondria seemed to fuse with lysosomes. Other organelles as well as dense bodies also accumulated in axon spheroids. Scale bar = 1 µm. (**D**) Immunohistochemistry against Caspr2 and SMI32 on longitudinal optic nerve sections from 5-month-old *Ppt1*^{-/-} mice demonstrated that spheroids were predominantly (75%) located in the juxtaparanodal domains (arrows). Scale bar = 20 µm. All micrographs are oriented so that the retina is located to the left and the optic chiasm to the right.

5.1.2 CD8+ T-lymphocytes in the CNS of *Ppt1$^{-/-}$* mice are associated with axonal spheroids and carry markers of mature effector cells

To investigate cells of the adaptive immune system in the optic nerves of *Ppt1$^{-/-}$* and *Cln3$^{-/-}$* mice immunohistochemistry against CD3, CD8, CD4 and B220 was performed. At all ages investigated, the number of B220+ B-lymphocytes was very low in wt and *Ppt1$^{-/-}$* mice as well as *Cln3$^{-/-}$* mice. Additionally, immunohistochemical studies using antibodies against mouse IgGs failed to provide evidence for a significant auto-antibody binding to CNS neurons and axons in *Ppt1$^{-/-}$* mice (not shown). Moreover, CD4+ cells were very low in number (between 0.66 and 1.38 cells/mm^2 with no significant difference between genotype groups at 1, 3 and 5 months) and there was a small, but significant, increase in their number in *Ppt1$^{-/-}$* mice, but only at 7 months of age (*Ppt1$^{+/+}$* mice: 0.87±0.34 cells/mm^2; *Ppt1$^{-/-}$* mice: 1.87±0.66 cells/mm^2; *n* = 4 per group; *P* < 0.05). In contrast, the number of CD8+ cells was low in wt mice, but progressively increased in *Ppt1$^{-/-}$* mice from 3 months of age onwards (Fig. 3A,C). Notably, in 5-month-old *Ppt1$^{-/-}$* mice 30% (± 10%; *n* = 4) of CD8+ cells were attached to small SMI32+ axonal spheroids and some CD8+ cells showed expression of the major cytotoxic agents perforin and granzyme B (Fig. 3B,E-G). The additional immunoreactivity of these cells for CD3 in double labelings confirmed that the cells indeed were T-lymphocytes. Quantifications revealed that 78% (± 9%; *n* = 4 per group) of all T-lymphocytes in the optic nerves of *Ppt1$^{-/-}$* mice were CD8+ at all ages (Fig. 3D).
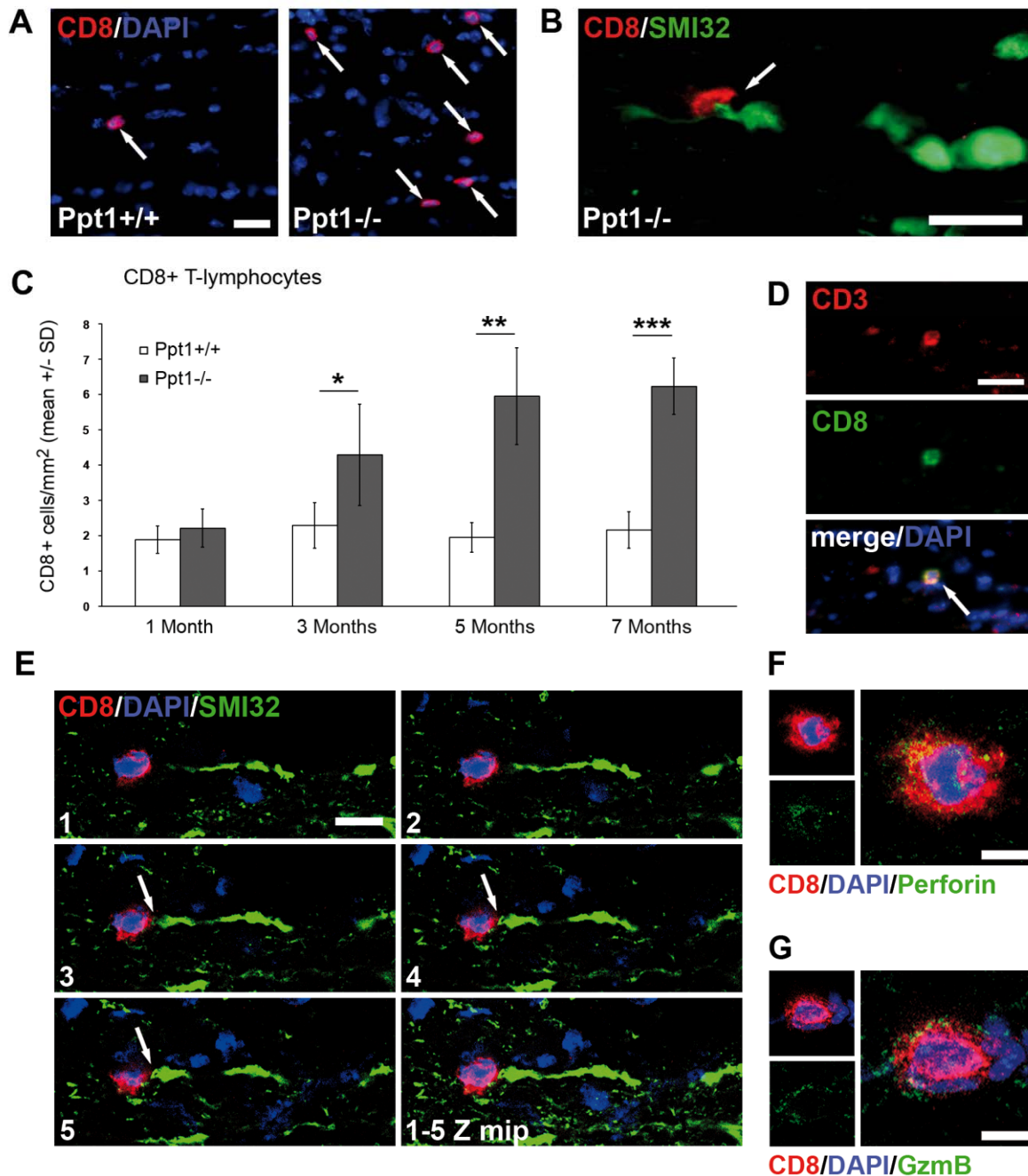
Figure 3 Progressive infiltration of CD8+ T-lymphocytes into the CNS of *Ppt1*^{-/-} mice. (**A**) Immunohistochemical detection of CD8+ cells (arrows) in longitudinal optic nerve sections from 5-month-old *Ppt1*^{+/+} and *Ppt1*^{-/-} mice. Scale bar = 30 μm. (**B**) Double immunohistochemistry revealed close contact (arrow) between CD8+ cells and SMI32+ axonal spheroids in *Ppt1*^{-/-} mice. Scale bar = 30 μm. (**C**) Counts of CD8+ cells revealed their significantly increased number in optic nerves of *Ppt1*^{-/-} mice compared with *Ppt1*^{+/+} mice at 3, 5 and 7 months of age (*n* = 4 per group). Student's *t*-test. (**D**) Double immunohistochemistry against CD8 and CD3 identified all CD8 + cells in optic nerve sections as T-lymphocytes (arrow). The large majority (~80%; *n* = 4 per group at each age) of CD3+ T-lymphocytes were also CD8+. Scale bar = 30 μm. (**E**) Confocal microscopy of CD8+ T-cells and SMI32+ damaged axons in longitudinal optic nerve sections from 5-month-old *Ppt1*^{-/-} mice revealed close apposition (arrows) of the scanned lymphocyte to an injured axon. Images 1-5 depict single optical slices at a distance of 0.5 μm to each other and a Z stack maximum intensity projection (1-5 Z mip) is shown in the lower right panel. Scale bar = 10

µm. (**F**) Confocal microscopy of CD8+ T-cells in longitudinal optic nerve sections from 5-month-old $Ppt1^{-/-}$ mice demonstrated expression of perforin and (**G**) granzyme B (GzmB) in cytoplasmic granular structures. * P < 0.05;** P < 0.01; *** P < 0.001.

Flow cytometric analyses of freshly isolated brain lymphocytes and splenocytes from 5-month-old $Ppt1^{-/-}$ and wt mice (n = 3) revealed that 65±9% of the CD8+ T-lymphocytes in the CNS of $Ppt1^{-/-}$ mice were CD44+ and CD62L- mature effector T-lymphocytes in contrast to only 12±2% in the spleen (Fig. 4A). While 54±3% of the CD8+ T-lymphocytes in the spleen showed a CD62L+ and CD44- immature phenotype and 29±2% were double-positive memory T-lymphocytes, CD62L+ T-cells were barely detectable in the brains of $Ppt1^{-/-}$ mice. Similar results were obtained using CD69 as another activation marker (Fig. 4C). In comparison, CD8+ cells in the brains of wt mice showed a lower expression of these activation markers (Fig. 4B,D). In conclusion, the majority of CD8+ T-lymphocytes in the CNS of $Ppt1^{-/-}$ mice were mature effector cells expressing markers of activation.
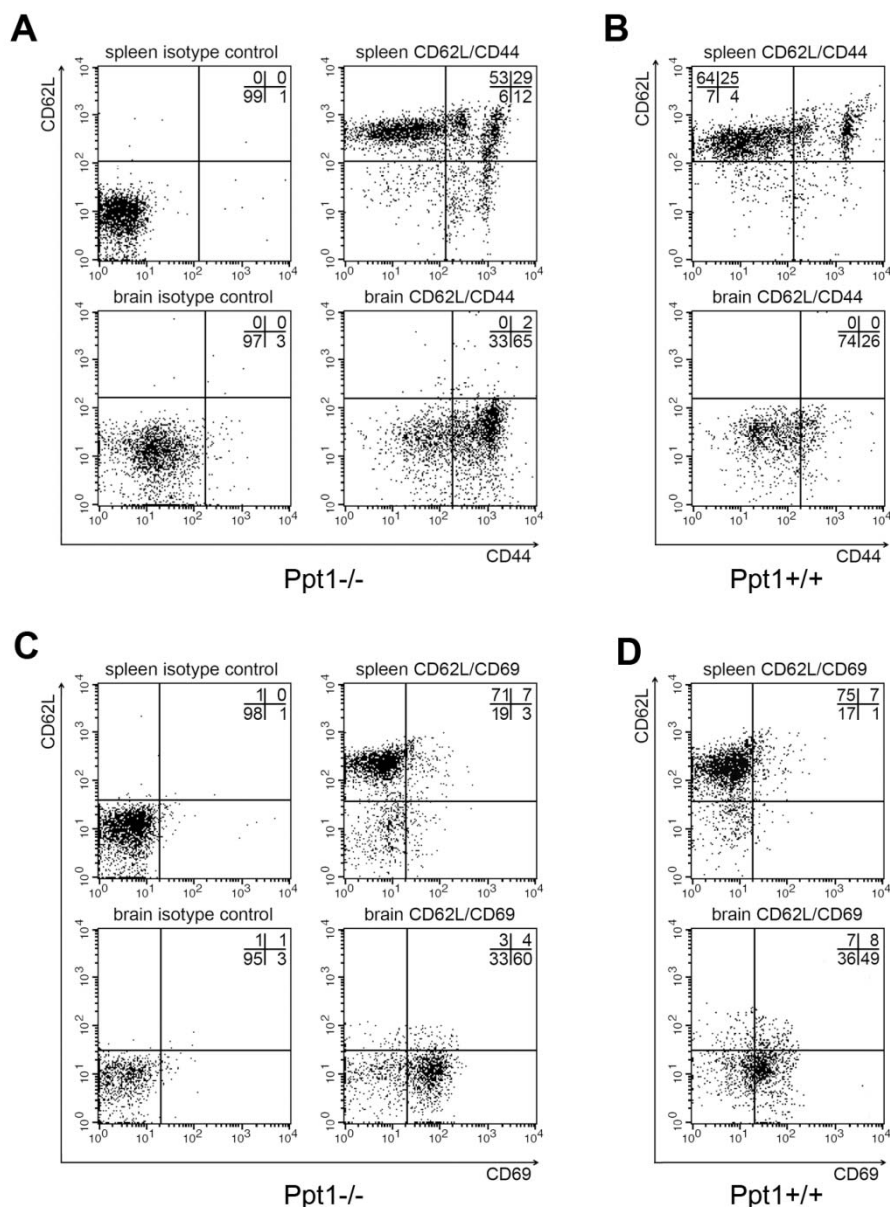
Figure 4 Expression of effector markers on CD8+ T-cells from *Ppt1^-/-^* and *Ppt1^+/+^* mice.
(**A**) Representative examples of flow cytometry of spleen (upper plots) and brain (lower plots) lymphocytes from *Ppt1^-/-^* mice gated for CD8 and analyzed for CD62L (marker for immature lymphocytes in this context) and the effector markers CD44 or (**C**) CD69. Left plots show appropriate isotype controls. (**B**) Representative examples of flow cytometry of spleen and brain lymphocytes from *Ppt1^+/+^* mice gated for CD8 and analyzed for CD62L and the effector markers CD44 or (**D**) CD69. Percentages of cells per quadrant are provided in each plot.

Additionally, the integrity of the blood-brain barrier was investigated. Consistent with a recent study (Saha et al., 2012), 7-month-old *Ppt1^-/-^* mice showed a disrupted blood-brain barrier integrity, as reflected by an increased extravasation of blood albumin (Fig. 5), whereas extravasation of blood albumin was not detectable in these mice at 5 months and earlier (not shown).

Figure 5 Impaired blood-brain barrier integrity in $Ppt1^{-/-}$ mice. Immunohistochemical detection of serum albumin and laminin on coronal brain sections of thalamic regions from 7-month-old $Ppt1^{+/+}$ and $Ppt1^{-/-}$ mice. Albumin reactivity (red) was mostly confined to the inside of blood vessels (green, a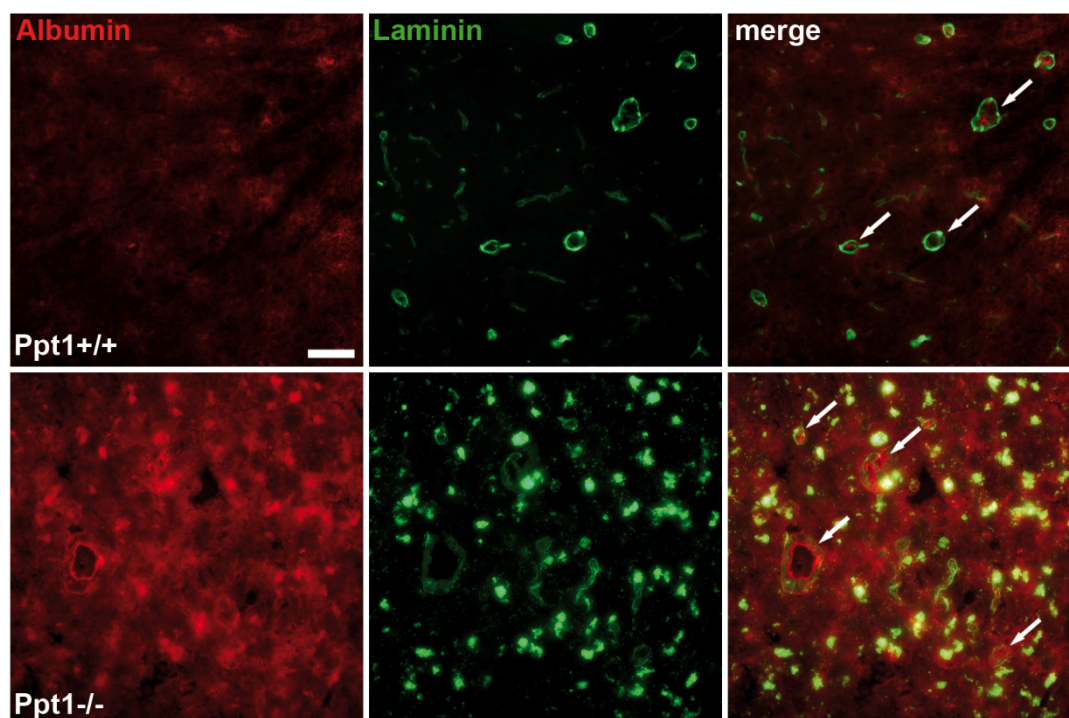rrows) in wt mice, but there was additional profound extravasation (diffuse red) in $Ppt1^{-/-}$ mice. Also note the accumulation of autofluorescent storage material (green/yellow in merge) in the parenchyma of $Ppt1^{-/-}$ mice. Scale bar = 50 µm.

Next, the expression of MHC-I, the cognate recognition molecule on target structures of CD8+ T-lymphocytes was investigated. In the retinal ganglion cell layer, as well as in the optic nerves and thalamocortical brain regions of $Ppt1^{-/-}$ mice there was a prominent upregulation of MHC-I immunoreactivity in comparison with wt mice, in which MHC-I expression was weak and restricted to perivascular areas (Fig. 6A-C). Double immunohistochemistry demonstrated that some SMI32+ axons in $Ppt1^{-/-}$ mice showed MHC-I expression. Neuronal MHC-I expression might be a functional prerequisite for being targeted by CD8+ T-lymphocytes (Fig. 6D). However, large SMI32+ axonal spheroids did not seem to show prominent MHC-I immunoreactivity.

To confirm increased surface expression of MHC-I on neurons in $Ppt1^{-/-}$ mice, immunostained and plastic embedded material was investigated by light microscopy (Fig. 6E) and electron microscopy (Fig. 6F-H). Semithin sections of thalamic brain regions revealed numerous MHC-I immunoreactive profiles in $Ppt1^{-/-}$ mice, which were virtually absent in wt mice (Fig. 6E). Using electron microscopy MHC-I expression was detected on the cell surface and in the endoplasmic reticulum of

neuronal somata (Fig. 6F), mostly on cells which contained large amounts of storage material. Moreover, some axons in the optic nerve and synapses in the superior colliculus showed expression of MHC-I in *Ppt1*^{-/-} mice (Fig 6G,H). In an individual case, an MHC-I-positive axon was found to be associated with a non-neuronal cell containing a lytic granule, most likely identifying the cell as an immune-related cell (Fig. 6G). Other cells in the CNS of *Ppt1*^{-/-} mice that showed increased MHC-I expression included endothelial cells and microglia/macrophage-like cells (Fig. 8A).
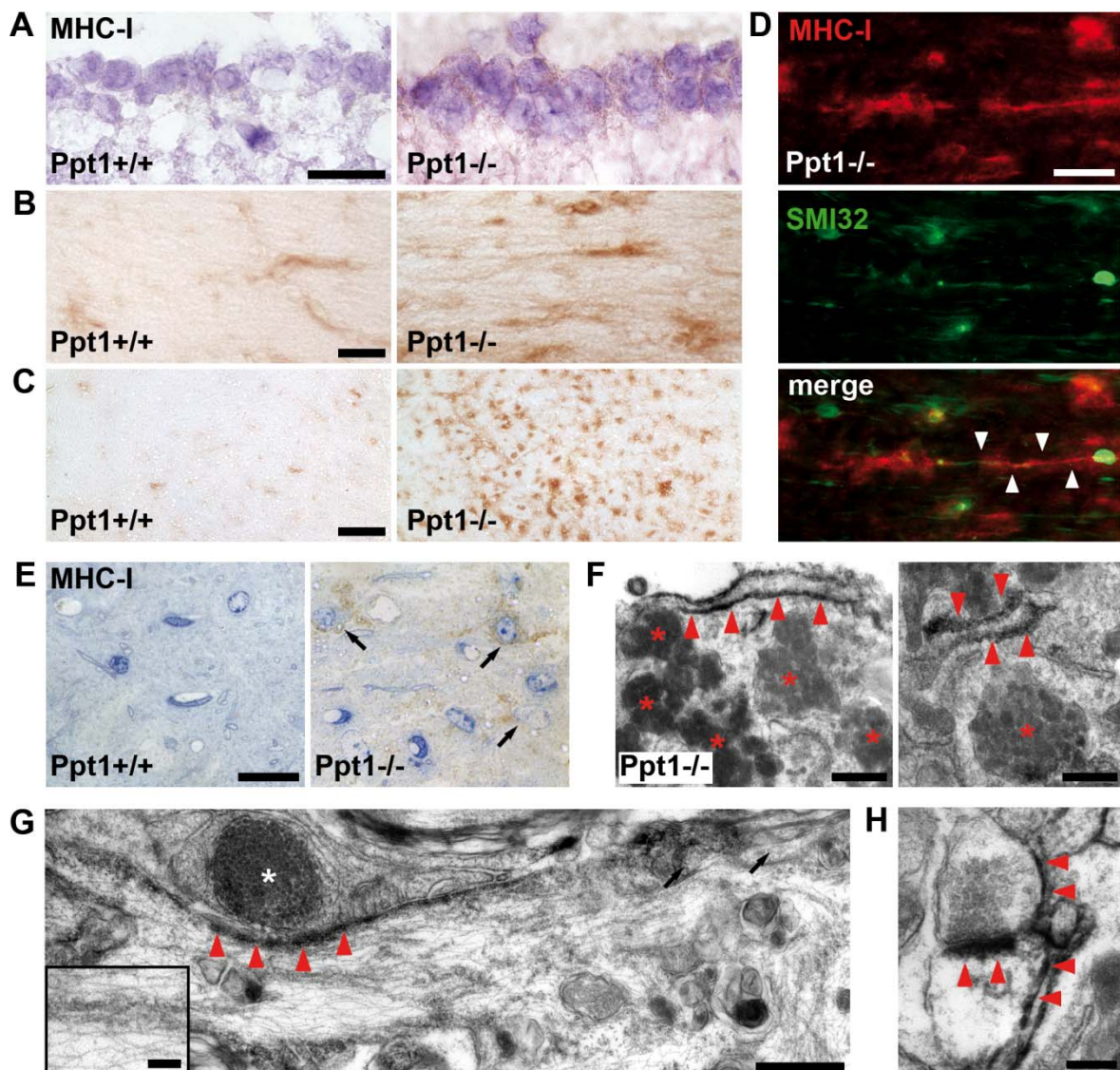
Figure 6 Increased surface expression of MHC-I on neurons in *Ppt1*^{-/-} mice. (**A**) Immunohistochemical detection of MHC-I (brownish precipitate) in the retinal ganglion cell layer of 5-month-old *Ppt1*^{+/+} and *Ppt1*^{-/-} mice counterstained with cresyl violet. Scale bar = 20 µm. (**B**) Immunohistochemical detection of MHC-I in longitudinal optic nerve sections (Scale bar = 30 µm) and (**C**) thalamic brain regions of 5-month-old *Ppt1*^{+/+} and *Ppt1*^{-/-} mice. Scale bar = 100 µm. MHC-I expression was weak in the CNS of *Ppt1*^{+/+} mice and increased in *Ppt1*^{-/-} mice. (**D**) Double immunohistochemistry using antibodies against MHC-I and SMI32 on

longitudinal optic nerve sections from 5-month-old *Ppt1*^{-/-} mice. Arrowheads demarcate an axon immunoreactive for MHC-I and non-phosphorylated neurofilaments. Scale bar = 30 µm. (**E**) Semi-thin sections of laterodorsal thalamic nucleus after immunolabelling and plastic embedding showed MHC-I+ cells (arrows) in 5-month-old *Ppt1*^{-/-}, but barely in *Ppt1*^{+/+} mice. Scale bar = 20 µm. (**F**) Electron microscopy demonstrated surface expression of MHC-I (dark precipitate; red arrowheads) on neuronal somata in *Ppt1*^{-/-} mice (left). Note the prominent accumulation of storage material in the MHC-I+ neuron (red asterisks). Membranes of the endoplasmic reticulum also showed immunoreactivity in some neurons (right). Scale bars = 0.5 µm. (**G**) Electron micrograph of an MHC-I+ axon in a longitudinal optic nerve section of a 5-month-old *Ppt1*^{-/-} mouse. Note that the axon is contacted by a cell containing a structure reminiscent of a lytic granule (white asterisk), suggestive for an immune-related cell. Neurofilaments and microtubules as seen at higher magnification (inset) and paranodal loops (arrows) of myelinating oligodendrocytes unequivocally identify the MHC-I+ structure as an axon. Note that this axon shows features of perturbation as reflected by spheroid formation and disturbed organelles. Scale bar = 0.5 µm; inset: 0.1 µm. (**H**) Some pre- and post-synaptic structures in the superior colliculus also showed MHC-I immunoreactivity in *Ppt1*^{-/-} mice. Scale bar = 0.2 µm.

5.1.3 Microglia/macrophage-like cells are increased in number and activated in the CNS of *Ppt1*^{-/-} mice

Previous studies demonstrated that microglia/macrophage-like cells show elevated expression of F4/80 and morphological signs of activation in the brain of *Ppt1*^{-/-} mice and *Cln3*^{-/-} mice when compared with wt mice (Pontikis et al., 2004; Kielar et al., 2007).

In this study, microglia/macrophages were investigated in the optic nerves of *Ppt1*^{-/-} mice and wt mice at different ages by immunohistochemistry against CD11b. In comparison with wt mice, microglia/macrophages in *Ppt1*^{-/-} mice showed increased expression of CD11b and "bushy" cell processes typical of activation (Fig. 7A,B). Quantification revealed significantly increased numbers of CD11b+ cells in optic nerves of *Ppt1*^{-/-} mice from 3 months of age onwards, correlating with the onset of the observed axonopathic changes (Fig. 7C). Similar to the histopathological alterations there was a progressive increase in the number of CD11b+ cells in *Ppt1*^{-/-} mice until the age of 7 months, the latest time point investigated. Moreover, expression levels of markers of microglial activation, including CD16/32 and CD86, were upregulated, as well as the neurotoxic cytokines IL-1β and TNF-α (Fig. 8B). The morphology and number of microglia/macrophages was similar when using other typical microglial markers like Iba1 or CD68 (Fig. 7D,E).
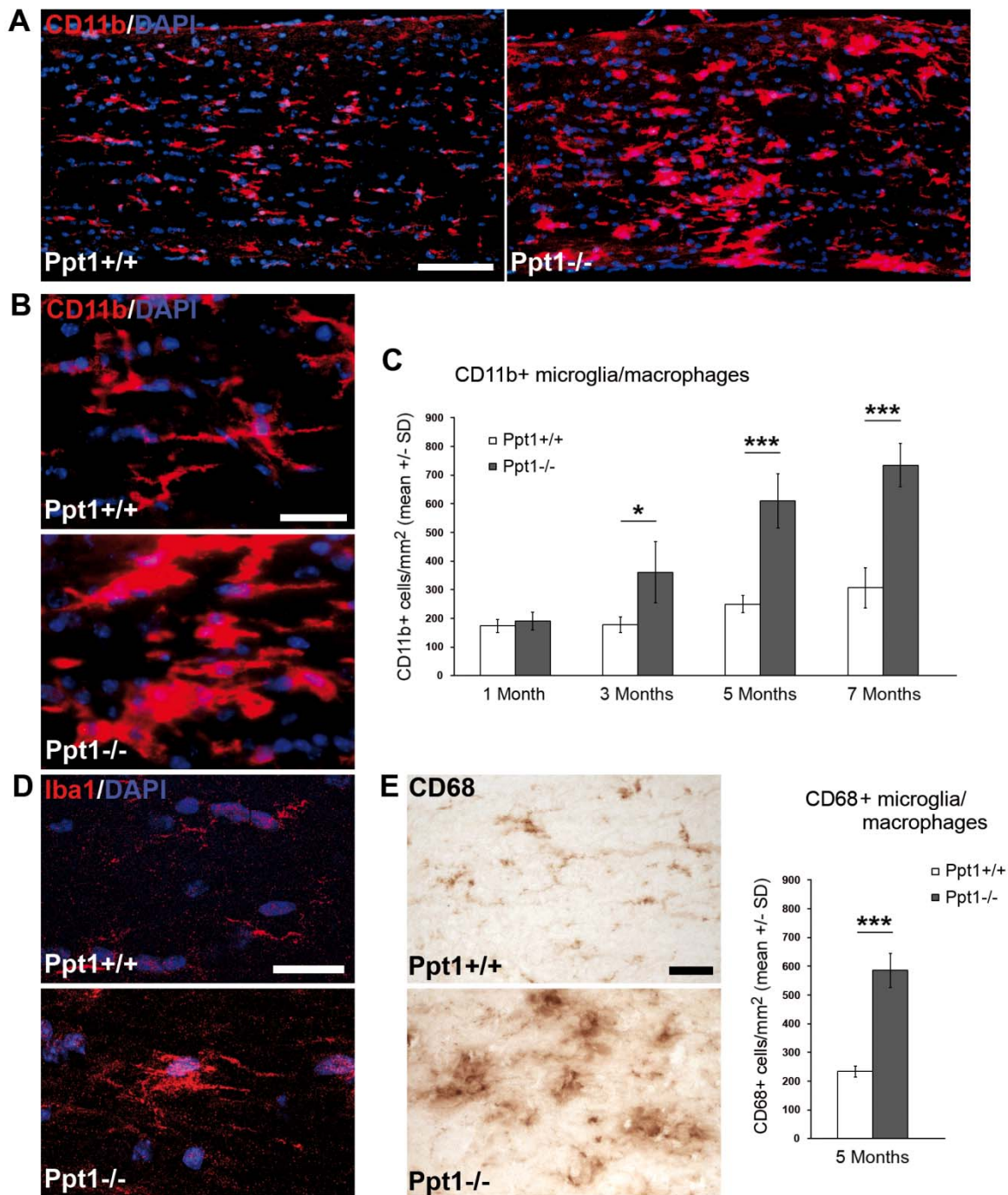
Figure 7 Increased numbers and activation of microglia/macrophage-like cells in the CNS of *Ppt1⁻/⁻* mice. (**A**) Immunohistochemical detection of CD11b+ microglia/macrophage-like cells in longitudinal optic nerve sections from 5-month-old *Ppt1⁺/⁺* and *Ppt1⁻/⁻* mice. Scale bar = 100 μm. (**B**) Higher magnification micrographs of CD11b + cell profiles demonstrate increased expression of CD11b and 'bushy' cell processes typical of activation. Scale bar = 30 μm. (**C**) Quantification of CD11b + cells revealed their significantly increased number in *Ppt1⁻/⁻* mice compared with *Ppt1⁺/⁺* mice at 3, 5 and 7 months of age (*n* = 4–5 per group). Student's *t*-test. (**D**) Confocal microscopic Z maximum intensity projections (Z mips; five image stack; distance 0.5 mm) of Iba1-labeled microglia/macrophage-like cells confirm 'bushy' morphology in *Ppt1⁻/⁻* mice. Scale bar = 20 μm. (**E**) Light microscopy and

quantification of CD68+ microglia/macrophage-like cells (chromogenic detection) in longitudinal optic nerve sections from 5-month-old $Ptt1^{+/+}$ and $Ptt1^{-/-}$ mice reveals comparable morphology and cell numbers as determined using immunofluorescence against CD11b. Scale bar = 30 μm. * $P < 0.05$; *** $P < 0.001$.
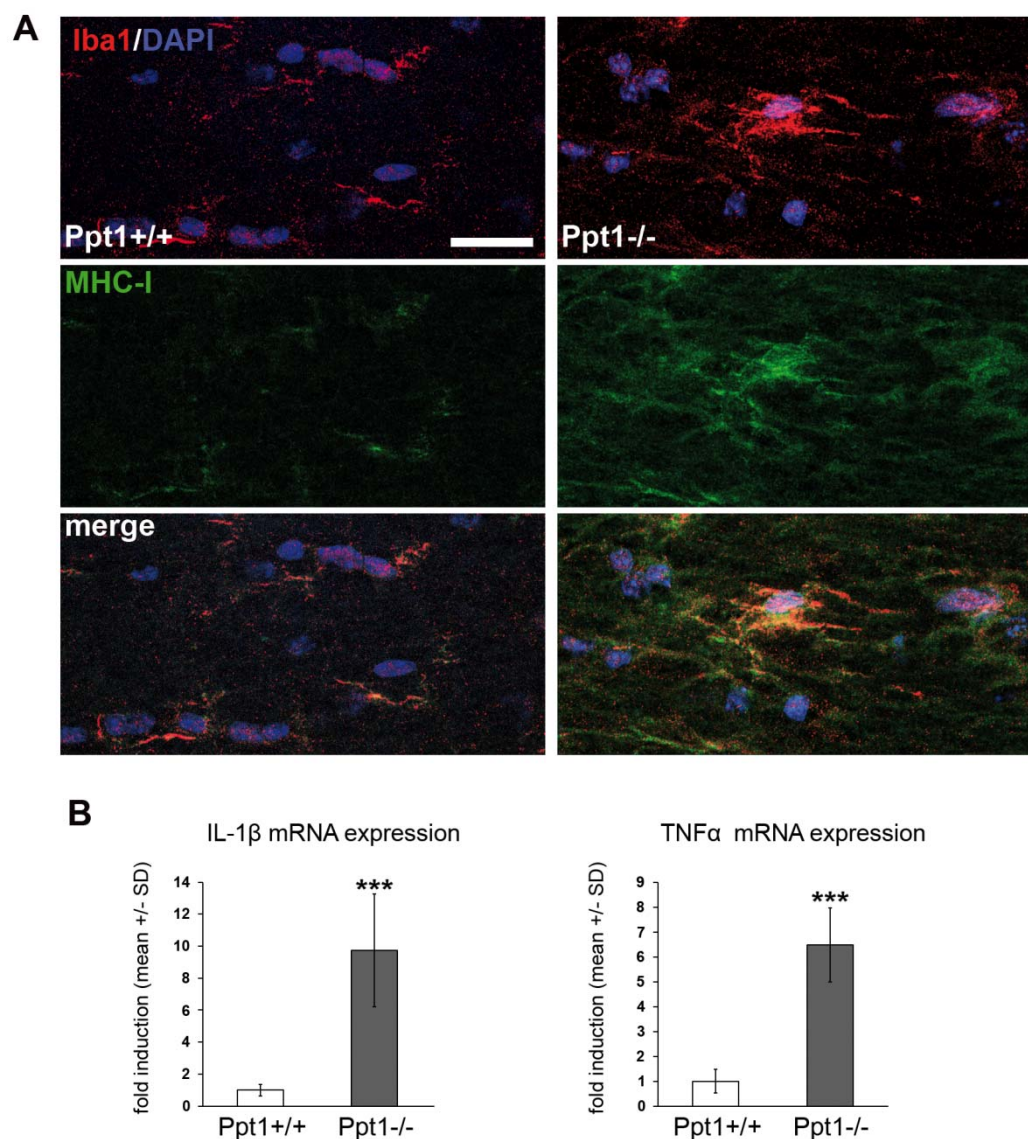
Figure 8 Increased expression of MHC-I by microglia/macrophages and neurotoxic cytokines in the CNS of $Ptt1^{-/-}$ mice. (**A**) Confocal microscopic Z maximum intensity projections (Z mips; 5 image stack; distance 0.5 μm) of Iba1+ microglia/macrophages in combination with MHC-I in the optic nerves of 5-month-old $Ptt1^{-/-}$ mice. Expression of MHC-I was increased on microglia/macrophages of $Ptt1^{-/-}$ mice, which also showed typical morphological signs of activation (images of Iba1 labelings are also shown in Figure 5). Scale bar = 20 μm. (**B**) mRNA expression of the neurotoxic cytokines IL-1β and TNF-α was significantly increased in optic nerves of 6-month-old $Ptt1^{-/-}$ mice in comparison with $Ptt1^{+/+}$ mice (n = 4 per group) as determined by semi-quantitative real-time PCR. Student's t-tests. *** $P < 0.001$.

For comparison, data from $Ptt1^{+/+}$ and $Ptt1^{-/-}Rag1^{+/+}$ mice, as shown in Figure 7 are presented here again.

5.1.4 Lymphocytes impair neuronal survival and axonal integrity in *Ppt1*^{-/-} mice

In order to investigate the putative pathogenic impact of lymphocytes in *Ppt1*-deficient mice, *Ppt1*^{-/-} mice were crossbred with *Rag1*-deficient mice lacking mature T- and B-lymphocytes (Mombaerts et al., 1992) and the neuropathological phenotypes in *Ppt1*^{-/-}*Rag1*^{-/-} mice were compared with those seen in single mutants (*Ppt1*^{-/-}*Rag1*^{+/+}). As expected, T-lymphocytes were completely absent in the CNS of *Ppt1*^{-/-}*Rag1*^{-/-} mice (not shown). Additionally, there were significantly fewer CD11b+ microglia/macrophage-like cells in optic nerves of 5-month-old *Ppt1*^{-/-}*Rag1*^{-/-} mice compared with *Ppt1*^{-/-}*Rag1*^{+/+} mice (Fig. 9), whereas the expression of MHC-I was not obviously different (Fig. 10).
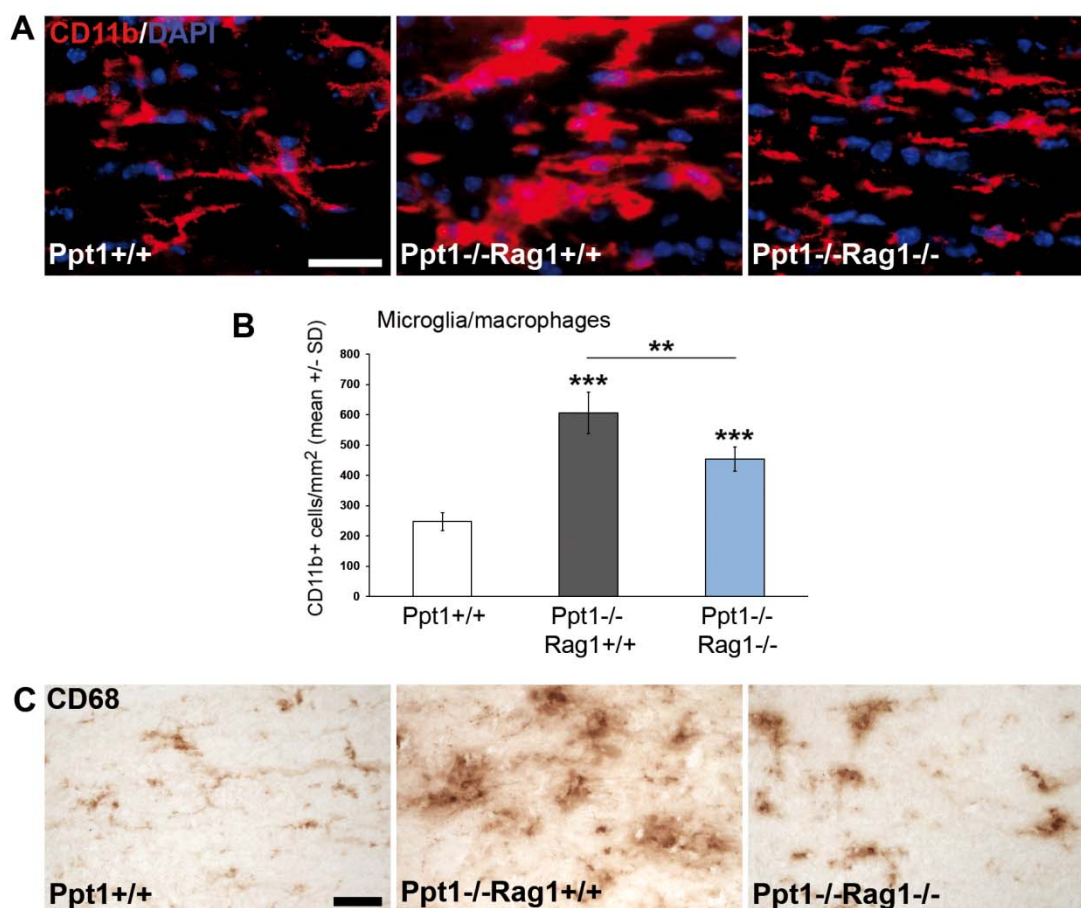
Figure 9 *Rag1* deficiency attenuates the increased numbers of microglia/macrophage-like cells in the optic nerves of *Ppt1*^{-/-} mice. (**A**) Immunohistochemical detection and (**B**) quantification of CD11b+ cells in longitudinal optic nerve sections from 5-month-old *Ppt1*^{+/+}, *Ppt1*^{-/-}*Rag1*^{+/+} and *Ppt1*^{-/-}*Rag1*^{-/-} mice (*n* = 4-5 per group). *Ppt1*^{-/-}*Rag1*^{-/-} mice presented with lower numbers of microglia/macrophages than *Ppt1*^{-/-}*Rag1*^{+/+} mice. One-way ANOVA and

Tukey's *post hoc* tests. (**C**) Immunohistochemical detection of microglia/macrophage-like cells using CD68 as marker demonstrated similar results. ** $P < 0.01$; *** $P < 0.001$.
For comparison, data from $Ppt1^{+/+}$ and $Ppt1^{-/-}Rag1^{+/+}$ mice, as shown in Figure 7 are presented here again.
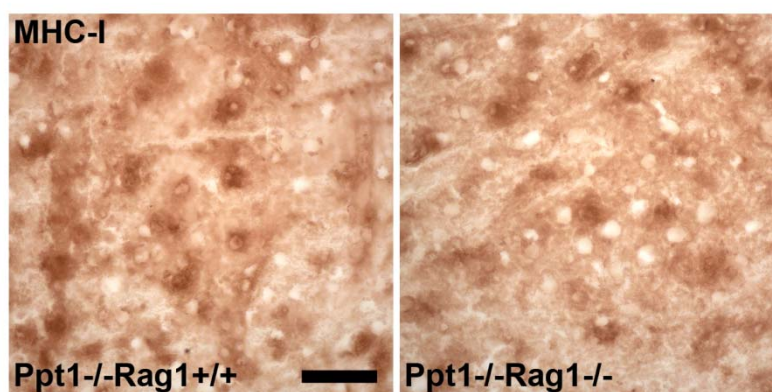
Figure 10 Increased expression of MHC-I in the CNS of $Ppt1^{-/-}Rag1^{-/-}$ mice. Immunohistochemical detection of MHC-I (brownish precipitate) in the laterodorsal thalamic nucleus of 5-month-old $Ppt1^{-/-}Rag1^{+/+}$ and $Ppt1^{-/-}Rag1^{-/-}$ mice. Expression of MHC-I did not appear obviously different in the absence of Rag1 and was clearly increased in comparison with $Ppt1^{+/+}$ mice (for comparison see Figure 6). Scale bar = 50 μm.

When the impact of immune cells on neuronal survival was analyzed by cresyl violet staining on retinal flat mount preparations, $Ppt1^{-/-}Rag1^{-/-}$ mice presented with a significant amelioration of RGC degeneration at 3, 5 and 7 months of age (Fig. 11A,C,D). Similarly, the loss of Brn3a+ RGCs was significantly attenuated (not shown). These findings were not confined to the retina, since a similar attenuation of neurodegeneration could be observed in the laterodorsal thalamic nucleus of $Ppt1^{-/-}Rag1^{-/-}$ mice (Fig. 11E).

To prove that it is the absence of lymphocytes that ameliorates these neurodegenerative phenotypes, bone-marrow reconstitution experiments using wt mice as donors were performed. The success of transplant engraftment was controlled by flow cytometry and immunohistochemistry to prove the presence of the respective lymphocyte populations in the spleen and CNS. This strategy has the advantage that the established mouse mutants with an impaired adaptive immune system ($Ppt1^{-/-}Rag1^{-/-}$ mice) are the common "baseline" for a series of experiments, making the different transplantation procedures directly comparable with each other. Via this approach, reconstitution of the $Ppt1^{-/-}Rag1^{-/-}$ mutants with wild-type bone

marrow reversed the *Rag1*-related amelioration at the level of neurodegeneration in the RGC layer and LGNd nucleus (Fig. 11B,F). Similarly, transplantation with bone marrow from *CD4$^{-/-}$* donor mice also reversed the *Rag1*-related amelioration. In contrast, bone marrow chimeras lacking only CD8+ T-lymphocytes presented with an ameliorated loss of RGCs and LGNd neurons similar to *Ppt1$^{-/-}$Rag1$^{-/-}$* mice (Fig. 11B,F).
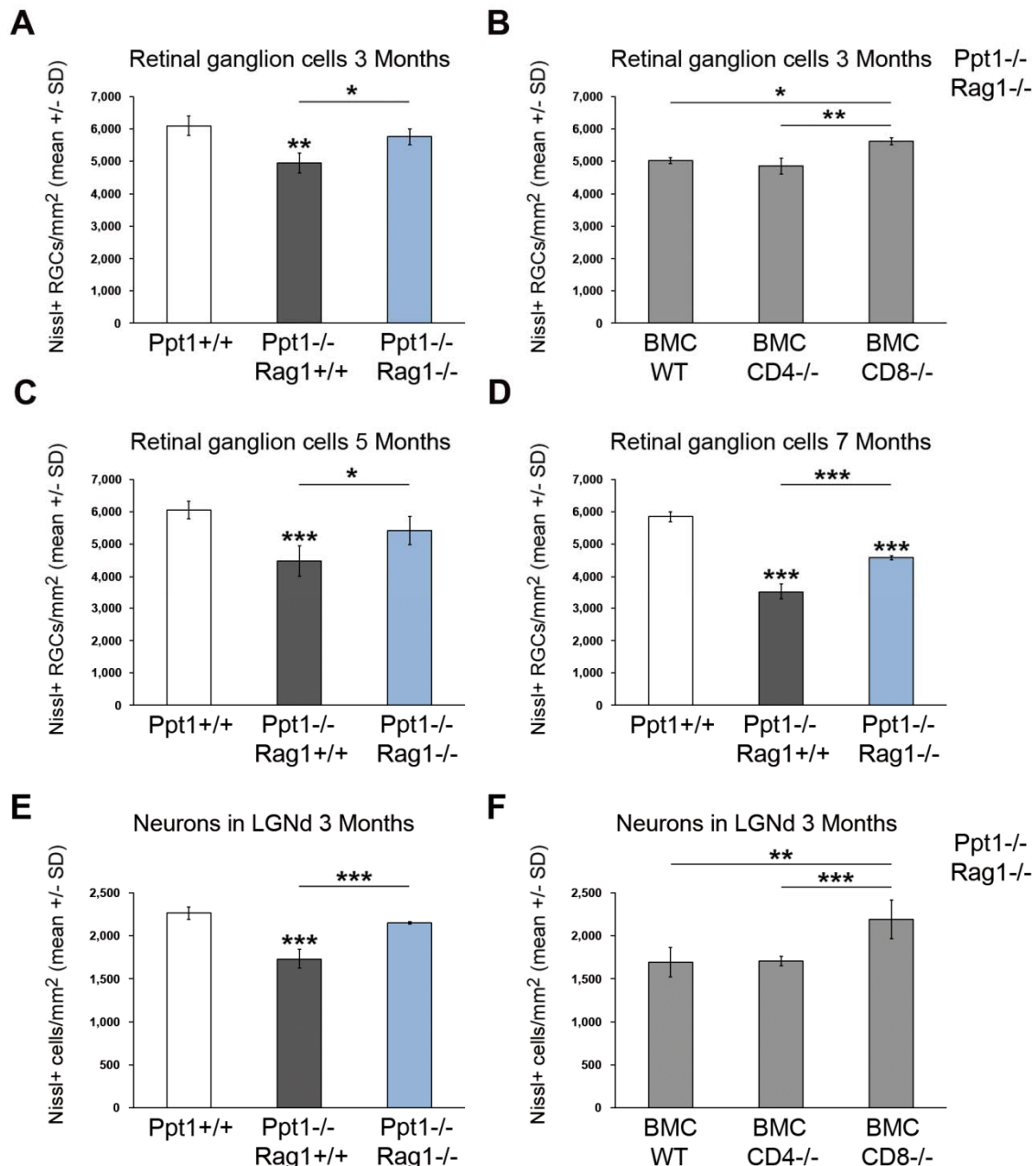
Figure 11 *Rag1* deficiency ameliorates loss of retinal ganglion cells and thalamic neurons in *Ppt1$^{-/-}$* mice and can be reverted by bone marrow cells from wild-type and *CD4$^{-/-}$* but not *CD8$^{-/-}$* mice. (**A**) Quantification of Nissl+ retinal ganglion cells after cresyl violet staining of retinal flat mount preparations from 3-month-old *Ppt1$^{+/+}$*, *Ppt1$^{-/-}$Rag1$^{+/+}$* and *Ppt1$^{-/-}$Rag1$^{-/-}$* mice (*n* = 4-5 per group) and (**B**) *Ppt1$^{-/-}$Rag1$^{-/-}$* bone marrow chimeras (BMCs) which received bone

marrow from wild-type, $CD4^{-/-}$ or $CD8^{-/-}$ donor mice (n = 4 per group). $Ppt1^{-/-}Rag1^{-/-}$ mice presented with preserved numbers of retinal ganglion cells compared with $Ppt1^{-/-}Rag1^{+/+}$ mice and this effect was abolished by bone marrow cells from wild-type and $CD4^{-/-}$ but not $CD8^{-/-}$ mice. Quantification of Nissl stained retinal ganglion cells after cresyl violet staining of retinal flat mount preparations from (**C**) 5-month-old and (**D**) 7-month-old $Ppt1^{+/+}$, $Ppt1^{-/-}$ $Rag1^{+/+}$ and $Ppt1^{-/-}Rag1^{-/-}$ mice (n = 4 per group). (**E**) Quantification of Nissl stained neurons after cresyl violet staining of coronal brain sections in the laterodorsal thalamic nucleus (LGNd) from 3-month-old $Ppt1^{+/+}$, $Ppt1^{-/-}Rag1^{+/+}$ and $Ppt1^{-/-}Rag1^{-/-}$ mice (n = 3 per group) and (**F**) $Ppt1^{-/-}Rag1^{-/-}$ bone marrow chimeras that received bone marrow from wild-type, $CD4^{-/-}$ or $CD8^{-/-}$ donor mice (n = 4 per group). Significant differences were determined by one-way ANOVA and Tukey's *post hoc* tests. * $P < 0.05$; ** $P < 0.01$; *** $P < 0.001$. For comparison, data from $Ppt1^{+/+}$ and $Ppt1^{-/-}Rag1^{+/+}$ mice, as shown in Figure 1 are presented here again.

Furthermore, the pronounced reduction in the number of retrogradely labeled RGCs in 3-month-old $Ppt1^{-/-}$ mice was almost completely prevented by $Rag1$ deficiency (Fig. 12A,B). Analysis of cleaved caspase 3, a typical apoptotic marker, demonstrated a localization of this marker in axonal spheroids rather than in the cell soma of RGCs, suggesting that the axonal compartment is one of the first targets of the cytotoxic immune cells (Fig. 12C). Cleaved caspase 3-positive axonal profiles were never seen in wt mice (not shown).
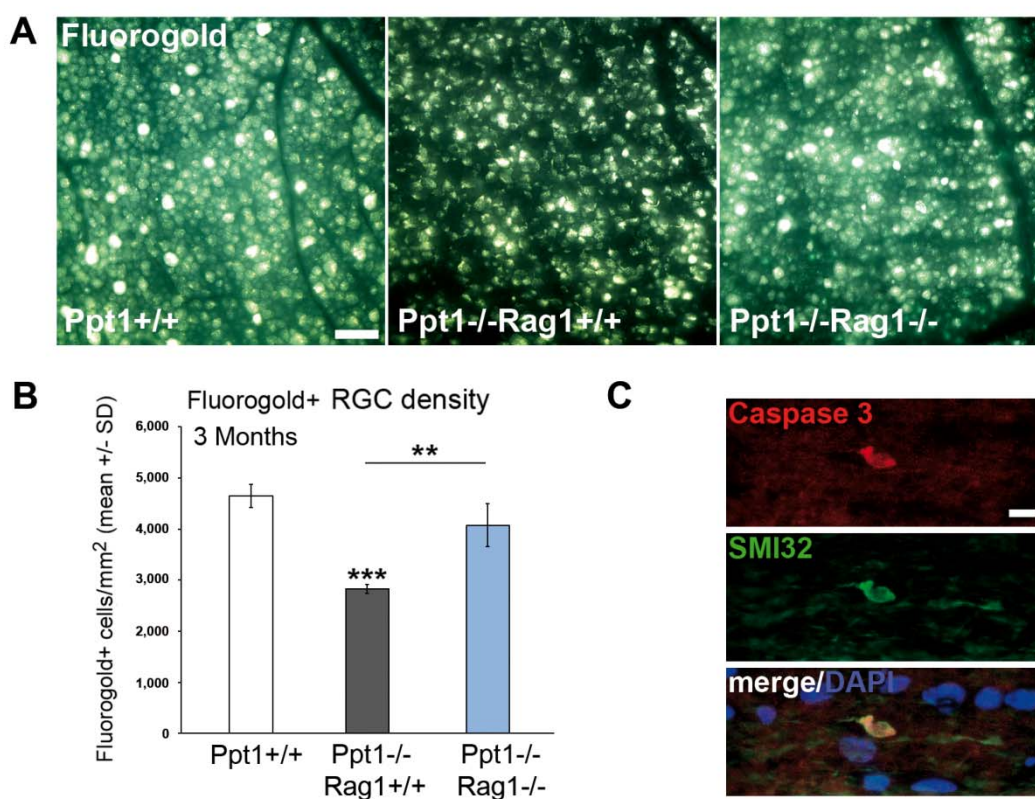
Figure 12 *Rag1* deficiency ameliorates perturbation of retinal ganglion cell axons in Ppt1-/- mice. (**A**) Fluorescence micrographs of retinal flat mount preparations 6 days after injection of fluorogold into the superior colliculus of 3-month-old *Ppt1$^{+/+}$, Ppt1$^{-/-}$Rag1$^{+/+}$* and *Ppt1$^{-/-}$ Rag1$^{-/-}$* mice. Scale bar = 50 µm. (**B**) Quantification of fluorogold-labelled retinal ganglion cells revealed a significant cell loss in 3-month-old *Ppt1$^{-/-}$Rag1$^{+/+}$* compared with *Ppt1$^{+/+}$* mice, but no difference in retinal ganglion cell numbers in *Ppt1$^{+/+}$* versus *Ppt1$^{-/-}$Rag1$^{-/-}$* mice (*n* = 3 per group). One-way ANOVA and Tukey's *post hoc* test. (**C**) Immunohistochemical detection of cleaved caspase 3 in combination with SMI32 in longitudinal optic nerve sections from 5-month-old *Ppt1-/-* mice reveals expression in axonal spheroids. Scale bar = 10 µm. ** *P* < 0.01; *** *P* < 0.001.

Electron microscopic investigation and quantification at 3, 5 and 7 months of age also revealed a significantly attenuated formation of axonal spheroids in optic nerve cross-sections from *Ppt1$^{-/-}$Rag1$^{-/-}$* mice in comparison with sections from *Ppt1$^{-/-}$Rag1$^{+/+}$* mice (Fig. 13A,D; Fig. 14A,B). Similarly, immunohistochemistry against non-phosphorylated neurofilaments on longitudinal sections confirmed significantly fewer SMI32+ axonal spheroids in the double mutants at 3, 5 and 7 months of age (Fig. 13C,F; Fig. 14C,D). Corroborating the findings concerning the pathogenic impact of CD8+ T-lymphocytes on neuronal loss, 3-month-old chimeras which received bone marrow from CD8-deficient donor mice showed no difference in the formation of axonal spheroids in comparison with wt or *Ppt1-/-Rag1-/-* mice. In contrast, transplantation of bone marrow from wt or CD4-deficient donor mice reversed the *Rag1*-related attenuation of spheroid formation (Fig. 13B,E,G).

Taken together, CD8+ T-lymphocytes were unequivocally demonstrated to play an important role in disease progression and substantially contribute to neurodegeneration and axon perturbation in *Ppt1*-deficient mice.
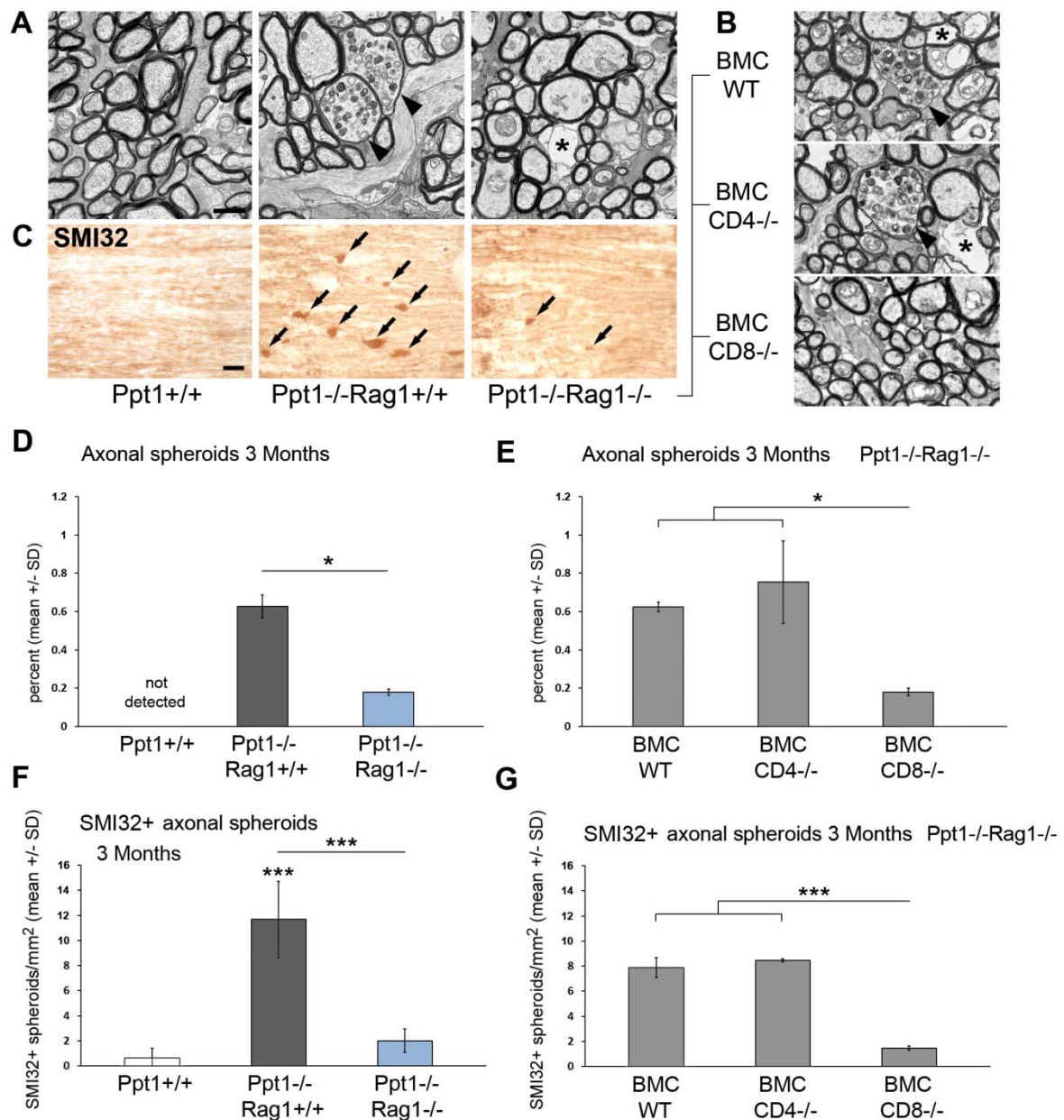
Figure 13 *Rag1*$^{-/-}$ deficiency ameliorates axonal spheroid formation in *Ppt1*$^{-/-}$ mice and can be reversed by bone marrow cells from wild-type and *CD4*$^{-/-}$ but not *CD8*$^{-/-}$ mice. (**A**) Electron micrographs of optic nerve cross-sections from 3-month-old *Ppt1*$^{+/+}$, *Ppt1*$^{-/-}$*Rag1*$^{+/+}$ and *Ppt1*$^{-/-}$*Rag1*$^{-/-}$ mice and (**B**) bone marrow chimeras (BMCs). Axonal spheroids are demarcated by arrowheads. Note the presence of vacuoles (asterisks) in the genotypes deficient for Ppt1, probably indicating storage material removed during the dehydration process. Scale bar = 1 µm. (**C**) Immunohistochemistry using antibodies against non-phosphorylated neurofilaments (SMI32) in longitudinal optic nerve sections from 3-month-old *Ppt1*$^{+/+}$, *Ppt1*$^{-/-}$*Rag1*$^{+/+}$ and *Ppt1*$^{-/-}$*Rag1*$^{-/-}$ mice. Axonal spheroids are marked by arrows. Scale bar = 30 µm. (**D**) Electron microscopic quantification of axonal spheroids in 3-month-old *Ppt1*$^{+/+}$, *Ppt1*$^{-/-}$*Rag1*$^{+/+}$ and *Ppt1*$^{-/-}$*Rag1*$^{-/-}$ mice (*n* = 4-5 per group) and (**E**) bone marrow chimeras (*n* = 4 per group). Percentages of axons with spheroids in relation to all quantified axons are shown. Spheroid formation was significantly attenuated by *Rag1* deficiency and this effect was abolished by bone marrow cells from wild-type (WT) and *CD4*$^{-/-}$, but not *CD8*$^{-/-}$ mice. Bonferroni-corrected Mann-Whitney *U*-tests. (**F**) Quantification of SMI32+ axonal spheroids in 3-month-old *Ppt1*$^{+/+}$,

Ppt1$^{-/-}$*Rag1*$^{+/+}$ and *Ppt1*$^{-/-}$*Rag1*$^{-/-}$ mice (*n* = 4-5 per group) and (**G**) bone marrow chimeras (*n* = 4 per group). One-way ANOVA and Tukey's *post hoc* tests. * *P* < 0.05; *** *P* < 0.001. For comparison, data from *Ppt1*$^{+/+}$ and *Ppt1*$^{-/-}$*Rag1*$^{+/+}$ mice, as shown in Figure 1 are presented here again.
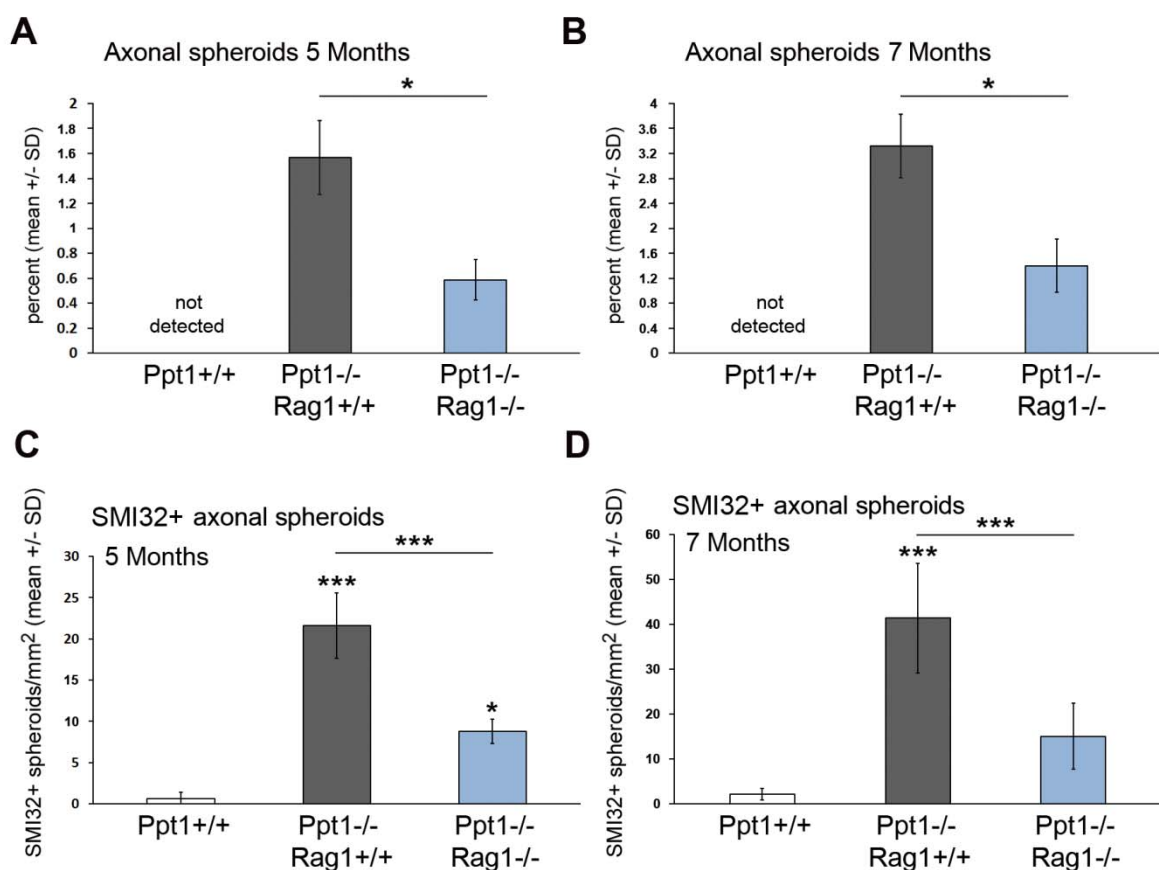
Figure 14 *Rag1* deficiency ameliorates axonal spheroid formation in symptomatic and late-stage *Ppt1*$^{-/-}$ mice. (**A**) Quantification of axonal spheroids in optic nerve cross-sections from 5-month-old and (**B**) 7-month-old *Ppt1*$^{+/+}$, *Ppt1*$^{-/-}$*Rag1*$^{+/+}$ and *Ppt1*$^{-/-}$*Rag1*$^{-/-}$ mice (*n* = 4 per group) by electron microscopy. Percentages of axons with spheroids in relation to all quantified axons are shown. Mann-Whitney *U*-test. (**C**) Quantification of axonal spheroids in longitudinal optic nerve sections from 5-month-old and (**D**) 7-month-old *Ppt1*$^{+/+}$, *Ppt1*$^{-/-}$*Rag1*$^{+/+}$ and *Ppt1*$^{-/-}$*Rag1*$^{-/-}$ mice (*n* = 3-4 per group) by immunohistochemistry (SMI32). Note the different scales of the y-axes at 5 and 7 months. One-way ANOVA and Tukey's *post hoc* tests. * *P* < 0.05; *** *P* < 0.001. For comparison, data from *Ppt1*$^{+/+}$ and *Ppt1*$^{-/-}$*Rag1*$^{+/+}$ mice, as shown in Figure 1 are presented here again.

Increased accumulation of autofluorescent storage material is a characteristic of INCL and has been suggested to result from lysosomal dysfunction (Seehafer and Pearce, 2006). To determine whether there was any impact of *Rag1* deficiency on the accumulation of storage material in neurons, threshold quantification of autofluorescence in NeuN labeled RGCs and LGNd neurons was performed.

Measuring the total autofluorescence would not be sufficient, since I) $Ppt1^{-/-}Rag1^{-/-}$ and $Ppt1^{-/-}Rag1^{+/+}$ mice show different densities of neurons due to their neurodegenerative phenotype and II) microglia/macrophages with large range of autofluorescence intensity (partially due to different phagocytic activities) would make interpretation of primary neuronal alterations difficult (see Fig. 15F). By restricting the measured signal to NeuN+ cells in the RGC layer and thalamic LGNd nucleus a more than 10-fold increase in autofluorescence was measured in 5-month-old $Ppt1^{-/-}$ mice in relation to wt mice (Fig. 15A-D). Importantly, no significant difference in autofluorescence was detected in neurons from $Ppt1^{-/-}Rag1^{-/-}$ mice, demonstrating that $Rag1$ deficiency does not alter the generation of the typical storage product in $Ppt1$-deficient neurons (Fig. 15C,D).
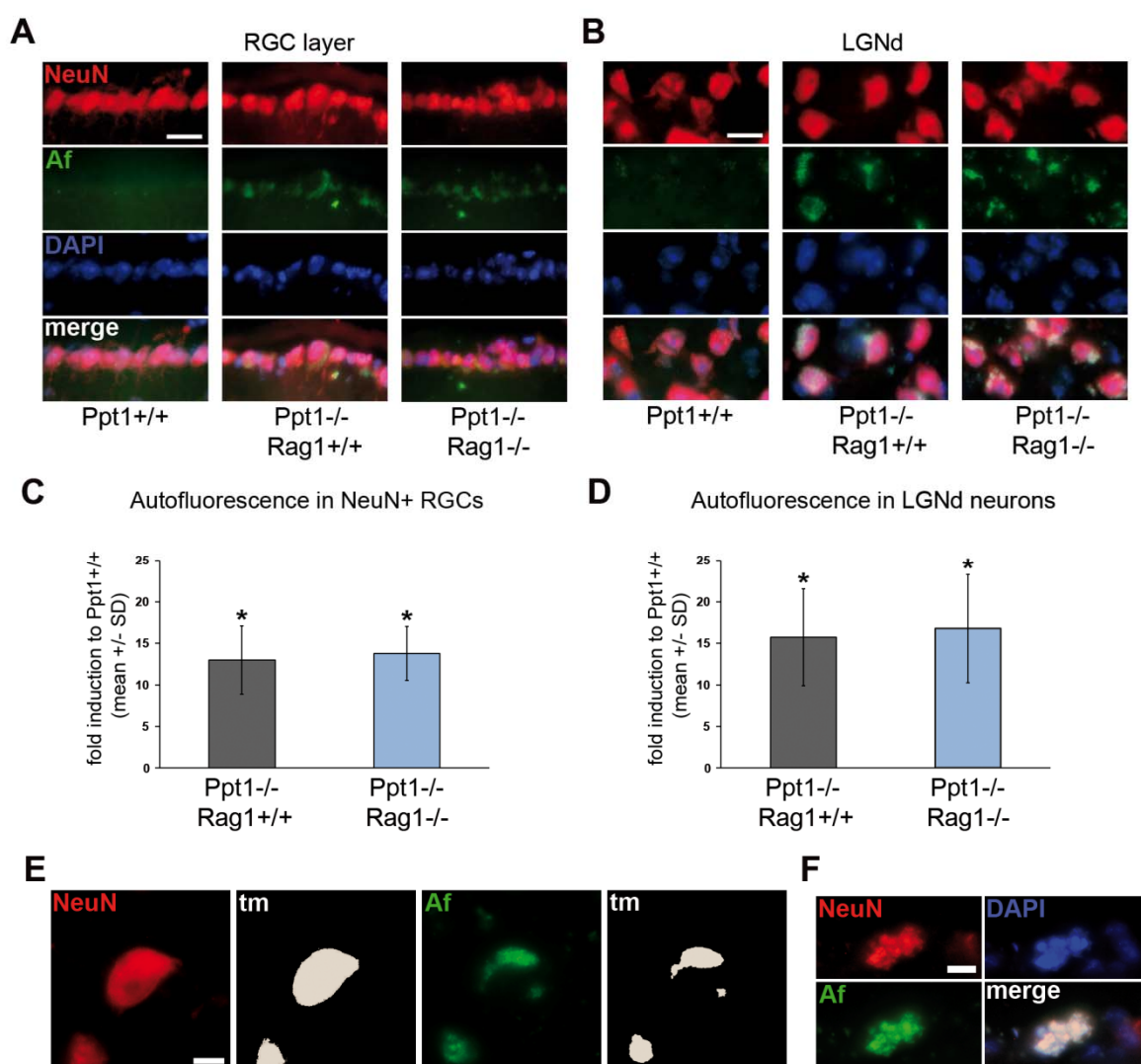

Figure 15 $Rag1$ deficiency does not affect the accumulation of autofluorescent storage material in neurons of $Ppt1^{-/-}$ mice. (**A**) Fluorescence micrographs of retinal ganglion cells

(RGCs) and (**B**) laterodorsal thalamic nucleus (LGNd) neurons from 5-month-old $Ppt1^{+/+}$, $Ppt1^{-/-}Rag1^{+/+}$ and $Ppt1^{-/-}Rag1^{-/-}$ mice labelled with antibodies against NeuN. Autofluorescence was detected using a GFP filter set. Af = autofluorescence. Scale bars = 30 µm. (**C**) Threshold analysis of autofluorescence in NeuN+ retinal ganglion cells and (**D**) laterodorsal thalamic nucleus neurons demonstrates ~13- to 16-fold increased accumulation in both $Ppt1^{-/-}Rag1^{+/+}$ and $Ppt1^{-/-}Rag1^{-/-}$ mice in comparison with wild-type mice (n = 3-4 per group). One-way ANOVA and Tukey's *post hoc* test. (**E**) Examples of thresholding analyses for NeuN and autofluorescence signals. Thresholding masks (tm) demarcate positive signals of which the areas were measured. Scale bar = 10 µm. (**F**) Other non-neuronal cells (NeuN negative; probably microglia/macrophage-like cells) also showed prominent accumulation of storage material, but were excluded from analysis. * $P < 0.05$.

5.1.5 Lack of lymphocytes leads to a substantial amelioration of the functional and clinical phenotype and improves longevity of $Ppt1^{-/-}$ mice

To clarify whether there was any functional improvement of the visual system by $Rag1$ deficiency, opto-kinetic measurements were performed. At 6 months of age, $Ppt1$-deficient mice showed a significantly decreased visual acuity compared with wt mice, consistent with the documented degeneration of RGCs. $Ppt1^{-/-}Rag1^{-/-}$ mice also showed a decreased visual acuity compared with wt mice, but a significantly higher visual acuity than $Ppt1^{-/-}Rag1^{+/+}$ mice, demonstrating an amelioration of this functional impairment (Fig. 16A).

More general effects of $Rag1$ deficiency on the clinical phenotype of $Ppt1^{-/-}$ mice were also investigated. Myoclonic jerks were significantly reduced in 5-month-old double mutants (Fig. 16B). Kaplan-Meier analysis of survival time ultimately demonstrated a significantly increased average lifespan of $Ppt1^{-/-}Rag1^{-/-}$ mice in comparison with $Ppt1^{-/-}Rag1^{+/+}$ mice. While the first $Ppt1^{-/-}Rag1^{+/+}$ mice died at postnatal day 185, $Ppt1^{-/-}Rag1^{-/-}$ mice did not die before day 242 (Fig. 16C). These observations strongly suggest that absence of mature T-lymphocytes leads to a general amelioration of the clinical phenotype and disease severity in $Ppt1^{-/-}$ mice.
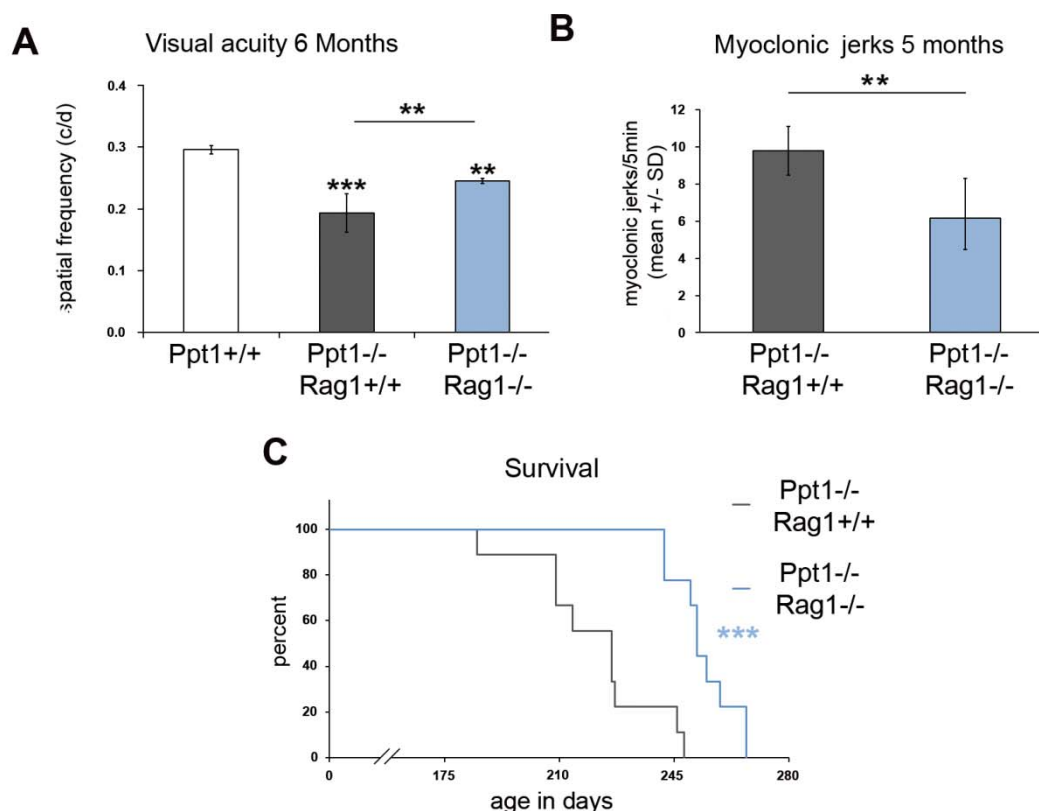
Figure 16 *Rag1* deficiency ameliorates the functional and clinical phenotypes, and improves longevity of *Ppt1⁻ᐟ⁻* mice. (**A**) Visual acuity measured by optokinetic responses of 6-month-old *Ppt1⁺ᐟ⁺*, *Ppt1⁻ᐟ⁻Rag1⁺ᐟ⁺* and *Ppt1⁻ᐟ⁻Rag1⁻ᐟ⁻* mice (*n* = 4 per group). *Rag1* deficiency significantly improved visual acuity in *Ppt1⁻ᐟ⁻* mice. One-way ANOVA and Tukey's *post hoc* test. (**B**) Myoclonic jerks during 5 min observation were significantly less frequent in 5-month-old *Ppt1⁻ᐟ⁻Rag1⁻ᐟ⁻* than in *Ppt1⁻ᐟ⁻Rag1⁺ᐟ⁺* mice. Student's *t*-test. (**C**) Kaplan-Meier survival analysis of *Ppt1⁻ᐟ⁻Rag1⁺ᐟ⁺* and *Ppt1⁻ᐟ⁻Rag1⁻ᐟ⁻* mice (*n* = 9 per group) demonstrated improved longevity in the absence of Rag1. ** $P < 0.01$; *** $P < 0.001$.

5.1.6 Microglia/macrophage-like cells in the CNS of *Ppt1⁻ᐟ⁻* mice show increased expression of sialoadhesin

In addition to an increased number, CD11b+ microglia/macrophage-like cells showed morphological signs of activation in the optic nerves of *Ppt1⁻ᐟ⁻* mice (see above). To further investigate their proinflammatory activation, the expression of sialoadhesin (Sn) was analyzed by immunohistochemistry. In wt mice, Sn expression was restricted to few perivascular cells and was not detected on parenchymal microglia/macrophages. In line with an increased activation, Sn expression was upregulated in optic nerves and thalamic brain regions of *Ppt1⁻ᐟ⁻* mice from 3 months of age onwards (Fig. 17). In addition, similar to CD8+ T-lymphocytes, CD11b+

microglia/macrophages and also Sn+ microglia/macrophages were often detected in close proximity or direct contact with SMI32+ axonal spheroids (Fig. 18).
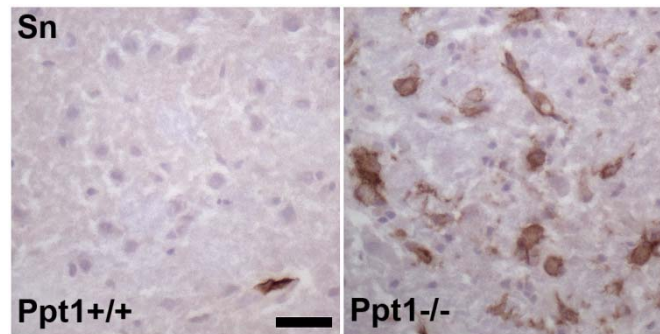
Figure 17 Increased expression of sialoadhesin (Sn) on microglia/macrophages in *Ppt1*$^{-/-}$ mice. Immunohistochemistry using antibodies against Sn (brownish precipitate) counterstained with haematoxylin (blue) in thalamic brain regions of 5-month-old *Ppt1*$^{+/+}$ and *Ppt1*$^{-/-}$ mice. Scale bar = 30 μm.
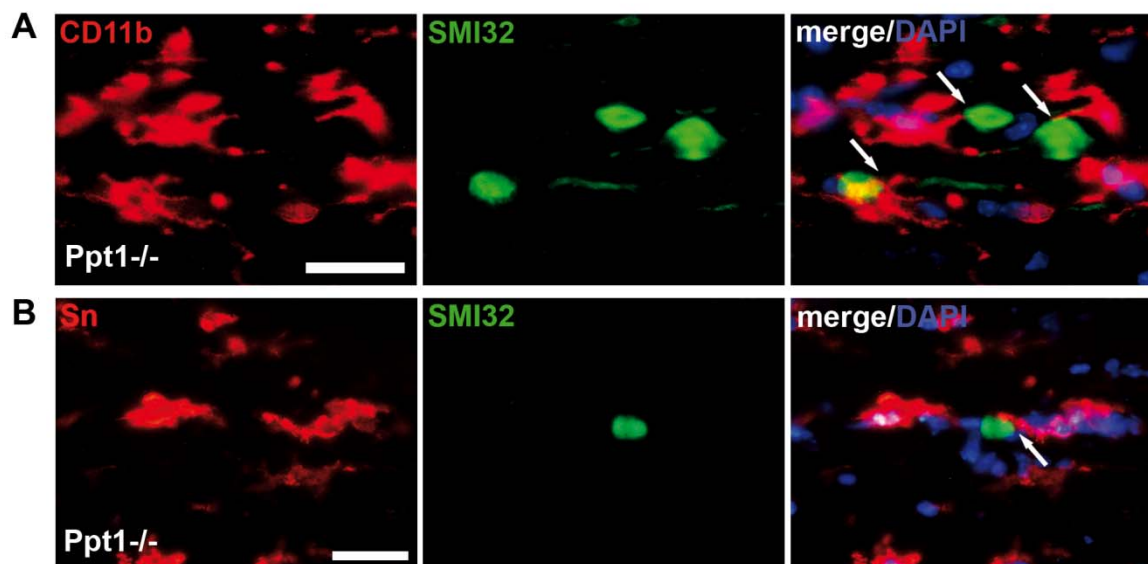
Figure 18 Close contact between Sn+ microglia/macrophages and SMI32+ axonal spheroids in the CNS of *Ppt1*$^{-/-}$ mice. (**A**) Double immunohistochemistry in longitudinal optic nerve sections from 5-month-old *Ppt1*$^{-/-}$ mice reveals close apposition (arrows) of CD11b+ cells to injured axons. Scale bar = 30 μm. (**B**) Microglia/macrophages in proximity to SMI32+ axonal spheroids often showed increased expression of Sn. Scale bar = 30 μm.

5.1.7 Absence of sialoadhesin ameliorates neural damage and improves longevity in *Ppt1*^{-/-} mice

To investigate whether there is a pathogenic impact of increased sialoadhesin expression on activated microglia/macrophage-like cells in the CNS of *Ppt1*^{-/-} mice, they were crossbred with *Sn*-deficient mice (Oetke et al., 2006) and the neuropathological phenotypes in *Ppt1*^{-/-}*Sn*^{-/-} mice were compared with those seen in single mutants (*Ppt1*^{-/-}*Sn*^{+/+}). As expected, Sn expression was completely absent in the CNS of *Ppt1*^{-/-}*Sn*^{-/-} mice (not shown). Additionally, there were significantly fewer CD11b+ microglia/macrophage-like cells in optic nerves of 5-month-old *Ppt1*^{-/-}*Sn*^{-/-} mice compared with *Ppt1*^{-/-}*Sn*^{+/+} mice (Fig. 19).
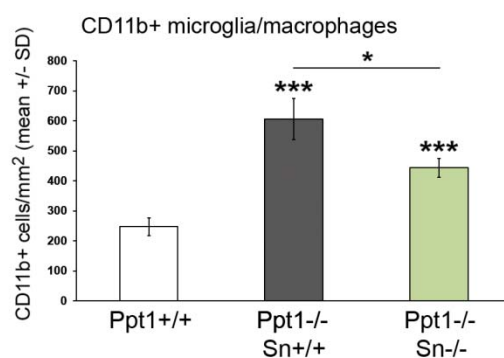
Figure 19 *Sn* deficiency attenuates the increase in numbers of microglia/macrophage-like cells in the optic nerves of *Ppt1*^{-/-} mice. Quantification of CD11b+ cells in longitudinal optic nerve sections from 5-month-old *Ppt1*^{+/+}, *Ppt1*^{-/-}*Sn*^{+/+} and *Ppt1*^{-/-}*Sn*^{-/-} mice (n = 4-5 per group). One-way ANOVA and Tukey's *post hoc* test. * $P < 0.05$; *** $P < 0.001$. For comparison, data from *Ppt1*^{+/+} and *Ppt1*^{-/-}*Sn*^{+/+} mice, as shown in Figure 7 are presented here again.

When the impact of Sn expression on neuronal survival was analyzed by cresyl violet staining on retinal flat mount preparations, *Ppt1*^{-/-}*Sn*^{-/-} mice presented with a significant attenuation of RGC degeneration at 5 months of age (Fig. 20A). Electron microscopic quantification at 5 months of age also revealed a significantly attenuated formation of axonal spheroids in optic nerve cross-sections from *Ppt1*^{-/-}*Sn*^{-/-} mice in comparison with sections from *Ppt1*^{-/-}*Sn*^{+/+} mice (Fig. 20B). Similarly, immunohistochemistry against non-phosphorylated neurofilaments on longitudinal sections identified significantly fewer SMI32+ axonal spheroids in the double mutants compared with single mutants (Fig. 20C).
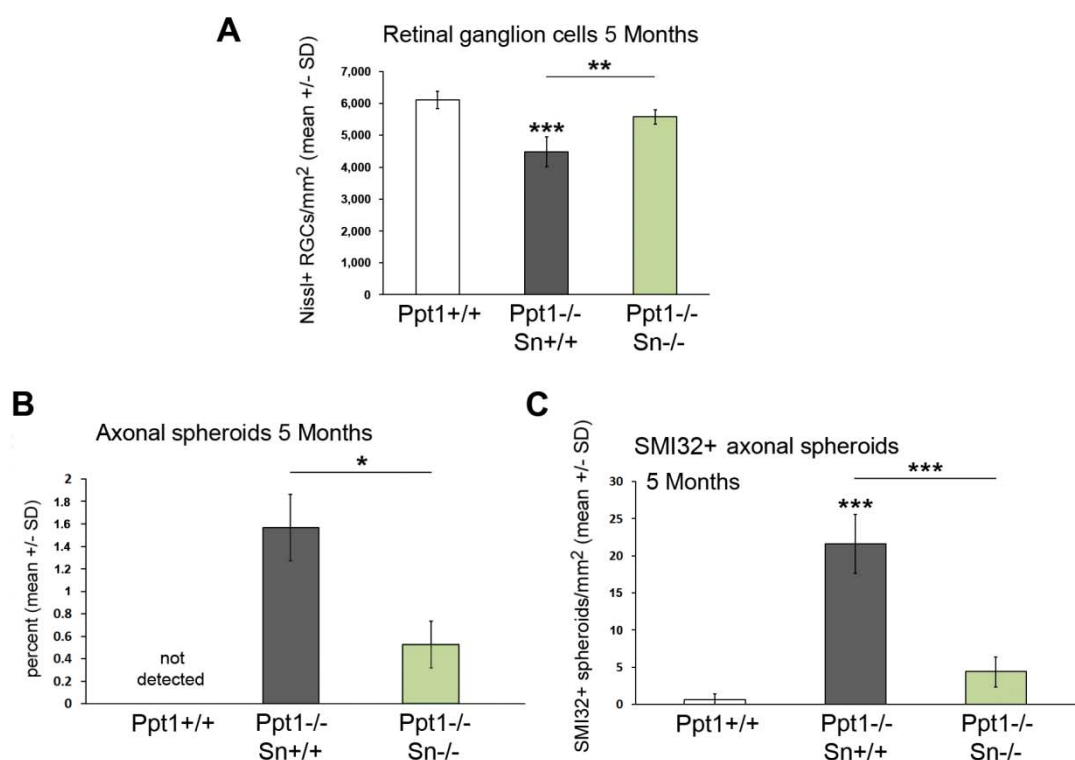
Figure 20 *Sn* deficiency ameliorates loss of retinal ganglion cells and axonal spheroid formation in *Ppt1*$^{-/-}$ mice. (**A**) Quantification of Nissl+ retinal ganglion cells after cresyl violet staining of retinal flat mount preparations from 5-month-old *Ppt1*$^{+/+}$, *Ppt1*$^{-/-}$*Sn*$^{+/+}$ and *Ppt1*$^{-/-}$*Sn*$^{-/-}$ mice (*n* = 4 per group). One-way ANOVA and Tukey's *post hoc* tests. (**B**) Quantification of axonal spheroids in optic nerve cross-sections from 5-month-old *Ppt1*$^{+/+}$, *Ppt1*$^{-/-}$*Sn*$^{+/+}$ and *Ppt1*$^{-/-}$*Sn*$^{-/-}$ mice (*n* = 4 per group) by electron microscopy. Percentages of axons with spheroids in relation to all quantified axons are shown. Mann-Whitney *U*-test. (**C**) Quantification of SMI32+ axonal spheroids in 5-month-old *Ppt1*$^{+/+}$, *Ppt1*$^{-/-}$*Sn*$^{+/+}$ and *Ppt1*$^{-/-}$*Sn*$^{-/-}$ mice (*n* = 4 per group). One-way ANOVA and Tukey's *post hoc* tests. * $P < 0.05$; ** $P < 0.01$; *** $P < 0.001$. For comparison, data from *Ppt1*$^{+/+}$ and *Ppt1*$^{-/-}$*Sn*$^{+/+}$ mice, as shown in Figure 14 are presented here again.

Again, along with the amelioration of neurodegeneration, myoclonic jerks were also significantly reduced in 5-month-old double mutants lacking Sn expression (Fig. 21A). Kaplan-Meier analysis of survival time demonstrated a significantly increased average survival time of *Ppt1*$^{-/-}$*Sn*$^{-/-}$ mice in comparison with *Ppt1*$^{-/-}$*Sn*$^{+/+}$ mice (Fig. 21B).
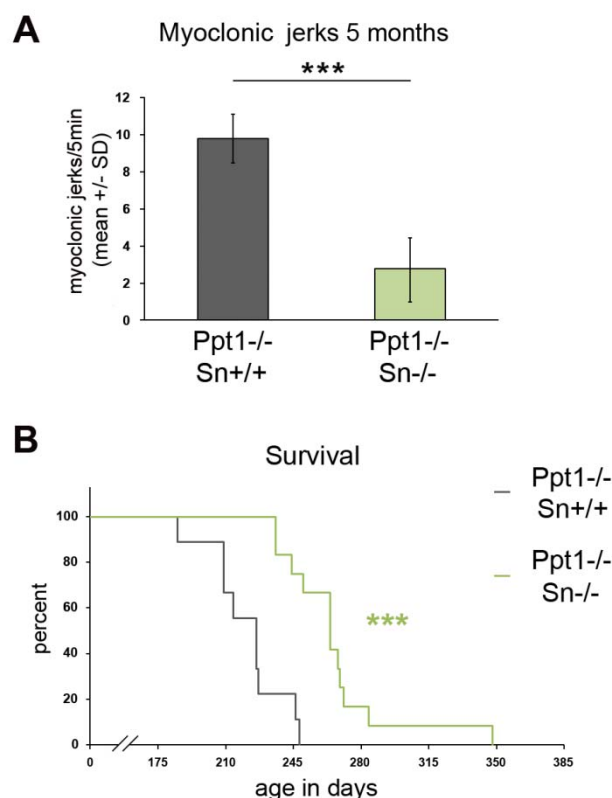
Figure 21 *Sn* deficiency ameliorates myoclonic jerks and improves longevity of *Ppt1*$^{-/-}$ mice. (**A**) Myoclonic jerks during 5 min observation were significantly less frequent in 5-month-old *Ppt1*$^{-/-}$*Sn*$^{-/-}$ than in *Ppt1*$^{-/-}$*Sn*$^{+/+}$ mice. Student's *t*-test. (**C**) Kaplan-Meier survival analysis of *Ppt1*$^{-/-}$*Sn*$^{+/+}$ and *Ppt1*$^{-/-}$*Sn1*$^{-/-}$ mice (*n* = 9-12 per group) demonstrated improved longevity in the absence of Sn. *** *P* < 0.001. For comparison, data from *Ppt1*$^{+/+}$ and *Ppt1*$^{-/-}$*Sn*$^{+/+}$ mice, as shown in Figure 16 are presented here again.

5.2 Mouse model of JNCL (*Cln3*$^{-/-}$ mice)

5.2.1 *Cln3*$^{-/-}$ mice show late-onset perturbation and loss of retinal ganglion cells

Having shown that there is progressive degeneration of RGCs and their axons in *Ppt1*$^{-/-}$ mice, the *Cln3*$^{-/-}$ model of JNCL was analyzed accordingly. In line with the later onset of the juvenile form of the disease, a decreased density of Nissl stained RGCs was not detected before an age of 18 months (Fig. 22A).

Electron microscopic investigation of optic nerves and immunohistochemistry also revealed the presence of axonal spheroids in *Cln3*$^{-/-}$ mice from an age of 15 months onwards. Morphologically, these axonal spheroids were not distinguishable to those observed in *Ppt1*$^{-/-}$ mice. Quantification of SMI32+ spheroids at 18 months of age revealed significantly increased numbers of spheroids in comparison with wt mice (Fig. 22B-D).

The degree of neuronal impairment detected by these methods in 18-month-old $Cln3^{-/-}$ mice was similar to that detected in 3- to 5-month-old $Ppt1^{-/-}$ mice, reflecting a later onset of neuronal impairment in the model of JNCL.
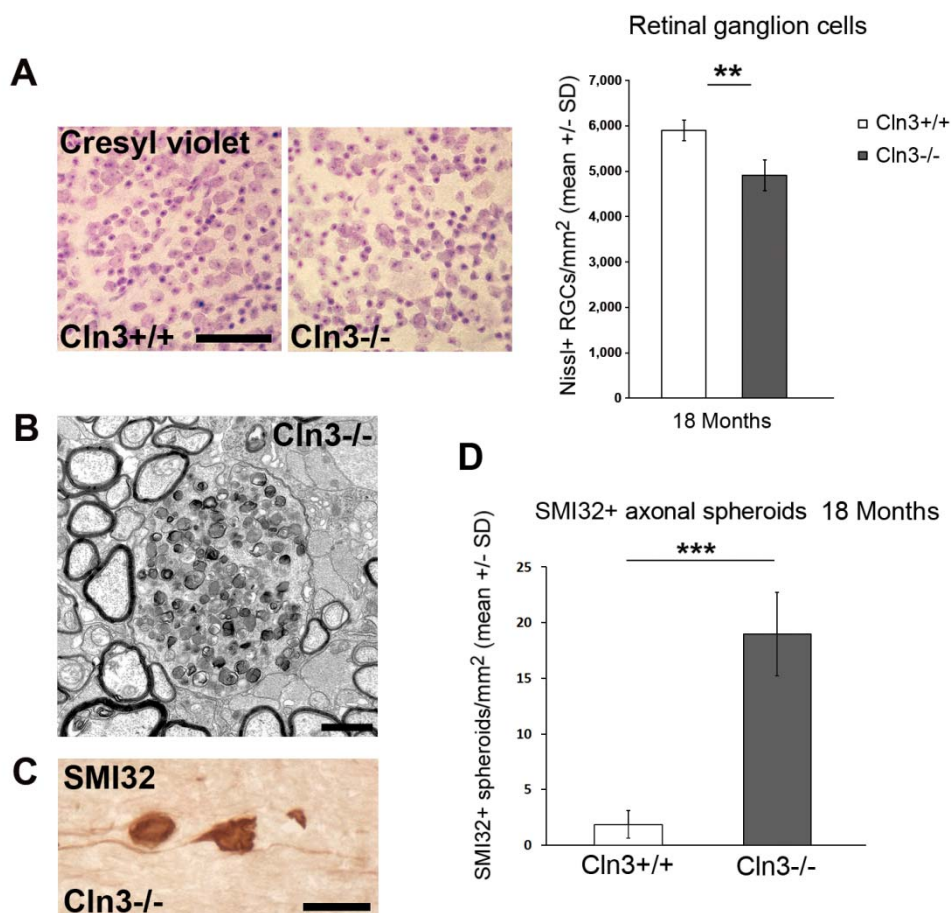
Figure 22 Loss of retinal ganglion cells and axonal degeneration in $Cln3^{-/-}$ mice. (**A**) Cresyl violet staining of retinal flat mount preparations and quantification of Nissl+ retinal ganglion cells in 18-month-old $Cln3^{+/+}$ and $Cln3^{-/-}$ mice (n = 4 per group). Scale bar = 50 µm. (**B**) Electron microscopy of optic nerve cross-sections from 15-month-old $Cln3^{-/-}$ mice. Organelles as well as dense bodies accumulated in axonal spheroids. Scale bar = 1 µm. (**C**) Immunohistochemistry using antibodies against non-phosphorylated neurofilaments (SMI32; brownish precipitate) in longitudinal optic nerve section of 18-month-old $Cln3^{-/-}$ mice. Scale bar = 30 µm. (**F**) Quantification revealed that SMI32+ axonal spheroids are rare in optic nerves of $Cln3^{+/+}$ mice but abundant in 18-month-old $Cln3^{-/-}$ mice (n = 4 per group). Significant differences were determined by Student's t-tests. ** $P < 0.01$; *** $P < 0.001$.

5.2.2 Numbers of CD8+ T-lymphocytes and expression of MHC-I are increased in the CNS of $Cln3^{-/-}$ mice

Similar to neuronal perturbation, increased numbers of T-lymphocytes were detected at an advanced age in the JNCL model. At 18 months of age, there were significantly

more CD8+ T-lymphocytes in the optic nerves of $Cln3^{-/-}$ mice compared with age-matched wt mice (Fig. 23A). Similar to $Ppt1^{-/-}$ mice, CD8+ T-lymphocytes comprised about 80% of all CD3+ T-lymphocytes and there was also a small, but significant, increase in the number of CD4+ T-lymphocytes ($Cln3^{+/+}$ mice: 0.98±0.44 cells/mm^2; $Cln3^{-/-}$ mice: 2.00±0.57 cells/mm^2; n = 4 per group; P < 0.05).

In addition to increased numbers of T-lymphocytes, there also was an increased expression of MHC-I in 18-month-old $Cln3^{-/-}$ mice compared with wt mice (Fig. 23B). An impairment of blood-brain barrier integrity has previously been described in $Cln3^{-/-}$ mice (Lim et al., 2007).
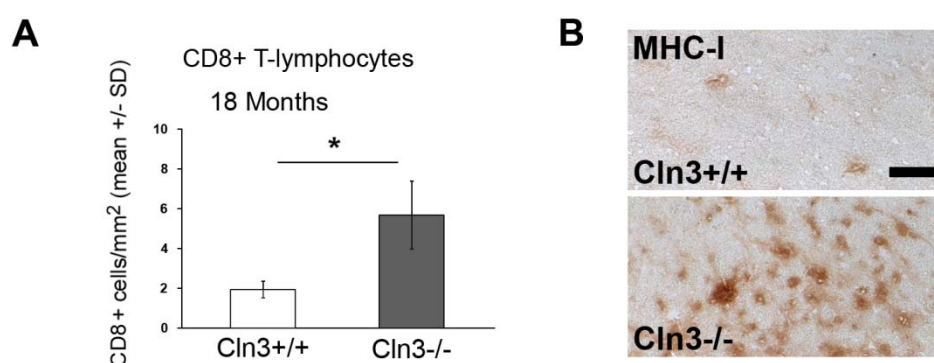
Figure 23 Increased numbers of CD8+ T-lymphocytes and expression of MHC-I in the CNS of $Cln3^{-/-}$ mice. (**A**) Counts of CD8+ cells revealed significantly increased numbers in optic nerves of $Cln3^{-/-}$ mice compared with $Cln3^{+/+}$ mice at 18 months of age (n = 4 per group). Student's t-test. (**B**) Immunohistochemical detection of MHC-I in thalamic brain regions of 5-month-old $Cln3^{+/+}$ and $Cln3^{-/-}$ mice. Scale bar = 100 μm. * P < 0.05.

To analyze the impact of lymphocytes in $Cln3^{-/-}$ mice, crossbreeding with $Rag1^{-/-}$ mice would be necessary for a proof of principle. However, $Cln3^{-/-}$ mice were not crossbred with $Rag1^{-/-}$ mice for this study since I) some evidence for a detrimental contribution of adaptive immune reactions has recently already been reported in this mouse model (Seehafer et al., 2011) and II) different groups of investigators had already generated $Cln3^{-/-}Rag1^{-/-}$ double mutant mice at the time of this study, possibly compromising the novelty of results (Cooper et al., unpublished). Since such crossbreeding experiments are very time-consuming and elaborate, the present study focused on the role of sialoadhesin in $Cln3^{-/-}$ mice.

5.2.3 Microglia/macrophage-like cells in the CNS of *Cln3$^{-/-}$* mice are increased in number and show increased expression of sialoadhesin

CD11b+ microglia/macrophages in the optic nerves of *Cln3$^{-/-}$* mice showed morphological signs of activation from 15 months of age onwards and were significantly increased in number at 18 months of age in comparison with wt mice (Fig. 24A,B). In addition, part of the microglia/macrophage-like cells in *Cln3$^{-/-}$* mice showed increased expression of sialoadhesin and were in close proximity to SMI32+ injured axons (Fig. 24C).
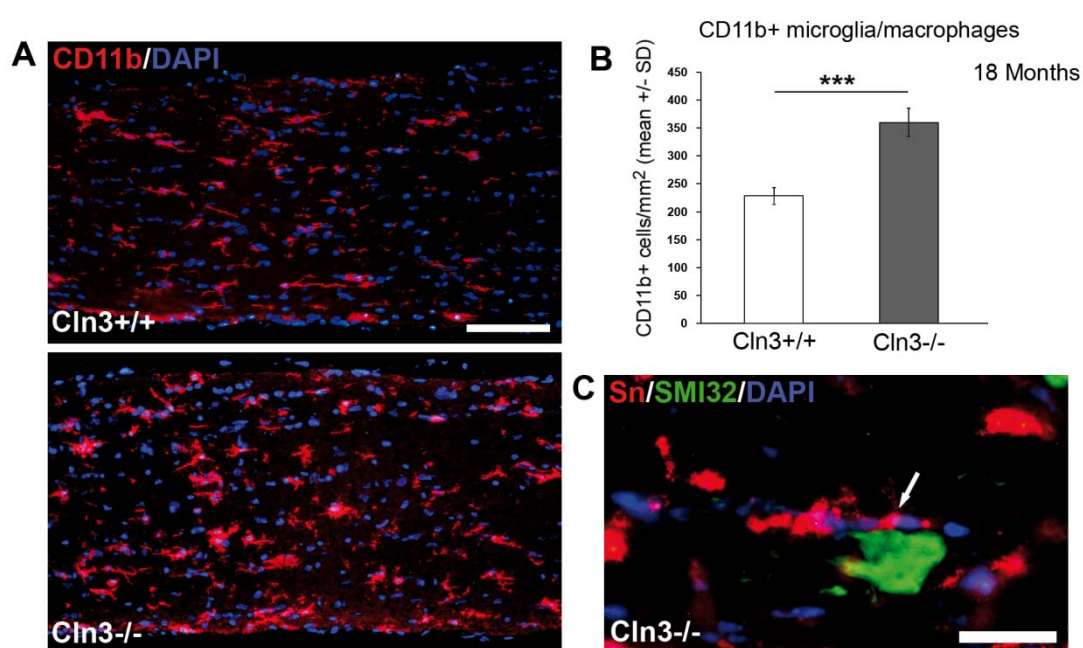
Figure 24 Increased numbers of microglia/macrophage-like cells and expression of Sn in the CNS of *Cln3$^{-/-}$* mice. (**A**) Immunohistochemical detection of CD11b+ microglia/macrophage-like cells in longitudinal optic nerve sections from 18-month-old *Cln3$^{+/+}$* and *Cln3$^{-/-}$* mice. Scale bar = 100 µm. (**B**) Quantification of CD11b + cells revealed their significantly increased number in *Cln3$^{-/-}$* mice compared with *Cln3$^{+/+}$* mice at 18 months of age (*n* = 4 per group). Student's *t*-test. *** *P* < 0.001. (**C**) Microglia/macrophages in proximity to SMI32+ axonal spheroids often showed increased expression of Sn (arrow). Scale bar = 30 µm.

5.2.4 Absence of sialoadhesin ameliorates neural damage in the CNS of *Cln3$^{-/-}$* mice

Similar to *Ppt1$^{-/-}$* mice, *Cln3$^{-/-}$* mice were crossbred with *Sn*-deficient mice and the neuropathological phenotypes of *Cln3$^{-/-}$Sn$^{-/-}$* mice were compared with those seen in single mutants (*Cln3$^{-/-}$Sn$^{+/+}$*) at 18 months of age.

Again, in addition to the expected lack of Sn expression, there were significantly fewer CD11b+ microglia/macrophage-like cells in optic nerves of $Cln3^{-/-}Sn^{-/-}$ mice compared with $Cln3^{-/-}Sn^{+/+}$ mice (Fig. 25).
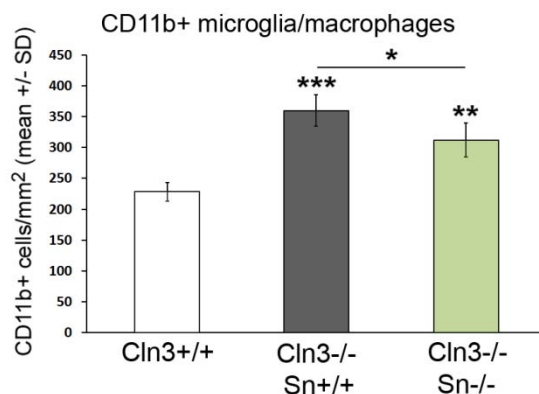
Figure 25 *Sn* deficiency attenuates the increase in numbers of microglia/macrophage-like cells in the optic nerves of $Cln3^{-/-}$ mice. Quantification of CD11b+ cells in longitudinal optic nerve sections from 18-month-old $Cln3^{+/+}$, $Cln3^{-/-}Sn^{+/+}$ and $Cln3^{-/-}Sn^{-/-}$ mice ($n = 4$ per group). One-way ANOVA and Tukey's *post hoc* tests. $*$ $P < 0.05$; $**$ $P < 0.01$; $***$ $P < 0.001$. For comparison, data from $Cln3^{+/+}$ and $Cln3^{-/-}Sn^{+/+}$ mice, as shown in Figure 24 are presented here again.

Neuronal survival was analyzed by cresyl violet staining on retinal flat mount preparations and $Cln3^{-/-}Sn^{-/-}$ mice presented with a significant attenuation of RGC degeneration compared with $Cln3^{-/-}Sn^{+/+}$ mice (Fig. 26A). The formation of axonal spheroids was also significantly reduced in the absence of Sn as assessed by electron microscopic quantification and immunohistochemistry against non-phosphorylated neurofilaments (Fig. 26B,C).

Taken together, the absence of sialoadhesin on microglia/macrophage-like cells in $Cln3^{-/-}$ mice significantly ameliorated the severity of the disease, further demonstrating a pathogenic contribution of immune reactions.
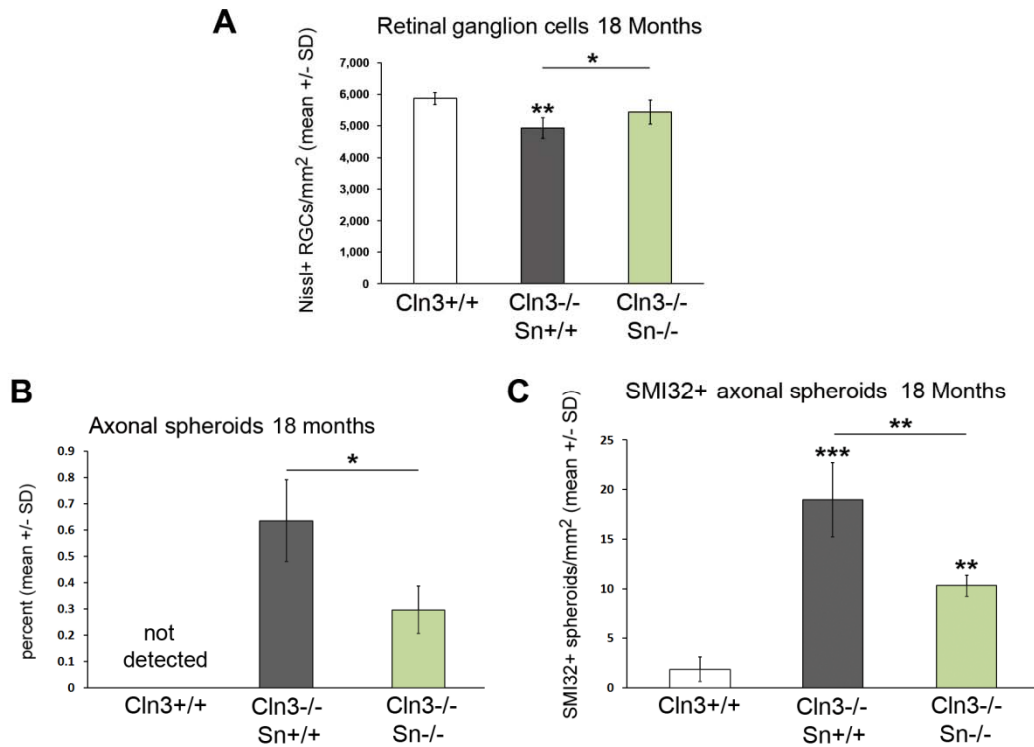
Figure 26 *Sn* deficiency ameliorates loss of retinal ganglion cells and axonal spheroid formation in *Cln3*$^{-/-}$ mice. (**A**) Quantification of Nissl+ retinal ganglion cells after cresyl violet staining of retinal flat mount preparations from 18-month-old *Cln3*$^{+/+}$, *Cln3*$^{-/-}$*Sn*$^{+/+}$ and *Cln3*$^{-/-}$*Sn*$^{-/-}$ mice (*n* = 4 per group). One-way ANOVA and Tukey's *post hoc* tests. (**B**) Quantification of axonal spheroids in optic nerve cross-sections from 18-month-old *Cln3*$^{+/+}$, *Cln3*$^{-/-}$*Sn*$^{+/+}$ and *Cln3*$^{-/-}$*Sn*$^{-/-}$ mice (*n* = 4 per group) by electron microscopy. Percentages of axons with spheroids in relation to all quantified axons are shown. Mann-Whitney *U*-test. (**C**) Quantification of SMI32+ axonal spheroids in 18-month-old *Cln3*$^{+/+}$, *Cln3*$^{-/-}$*Sn*$^{+/+}$ and *Cln3*$^{-/-}$*Sn*$^{-/-}$ mice (*n* = 4 per group). One-way ANOVA and Tukey's *post hoc* tests. * *P* < 0.05; ** *P* < 0.01; *** *P* < 0.001. For comparison, data from *Cln3*$^{+/+}$ and *Cln3*$^{-/-}$*Sn*$^{+/+}$ mice, as shown in Figure 22 are presented here again.

6. Discussion

6.1 Immune cells are pathogenic mediators in mouse models of NCL

In this study, a robust amelioration of axonopathic changes and neuron loss is shown for the first time in an animal model of INCL by genetically inactivating the adaptive immune system or the expression of a cell adhesion molecule of the innate immune system. Moreover, by reconstitution of the *Rag1*-deficient mutants with bone marrow from distinct lymphocytic mutants, CD8+ T-lymphocytes were identified as important pathogenic mediators. The absence of these T-lymphocytes led not only to an amelioration of axonal and neuronal degeneration, but this neuronal preservation was also reflected by improved visual acuity, reduced frequency of myoclonic jerks and extended longevity, demonstrating a positive clinical effect of immune cell inactivation.

A previous study in a model of Sandhoff disease, another lysosomal storage disorder, has demonstrated that the chemokine macrophage inflammatory protein-1 (MIP-1) alpha contributes to the severity of neurodegeneration, most likely by mediating monocytic infiltration (Wu and Proia, 2004). Moreover, a recent study demonstrated that genetically attenuated astrocyte activation by combined GFAP and vimentin deficiency in $Ppt1^{-/-}$ mice resulted in an aggravated disease phenotype and the proposed mechanisms included increased immune cell infiltration into the CNS and cytokine upregulation (Macauley et al., 2011).

Indeed the present study could show that ablation of lymphocytes substantially attenuates the disease and clearly identified immune cells as pathogenic mediators. Moreover, inhibition of Sn expression on microglia/macrophage-like cells additionally showed that innate immune reactions also contribute to pathomechanistic processes of the disease.

There were also previous observations indicating that immune components might contribute to the juvenile form of NCL, as pharmacological and genetic suppression of the immune system moderately improved motor performance in the corresponding $Cln3^{-/-}$ mouse model (Seehafer et al., 2011). Despite the fact that we did not crossbreed $Cln3^{-/-}$ mice with *Rag1*-deficient mutants, several observations indicate that lymphocytes probably play a similar pathogenic role as in $Ppt1^{-/-}$ mice. First, there was a similar temporal and spatial association between increased numbers of

T-lymphocytes and the occurrence of axonal damage in both mouse models. Second, similar to *Ppt1*^{-/-} mice, we observed a profoundly increased expression of MHC-I in the CNS of *Cln3*^{-/-} mice, a functional prerequisite for target recognition by CD8+ T-lymphocytes. Finally, the morphological appearance of axonal spheroids, including the preferential development in juxtaparanodal compartments, as well as the types of immune cells associated with impaired axons appeared similar in both models, except for the later onset of pathology in *Cln3*^{-/-} mice.

Concerning the impact of increased Sn expression on microglia/macrophage-like cells in *Cln3*^{-/-} mice, the results of the crossbreeding experiments clearly demonstrated a pathogenic contribution to disease progression, further arguing for a similar role of inflammatory reactions in two distinct models of NCL. Thus, two models of NCL with mutations in different genes share secondary immune reactions as an important similarity and common modulator of disease.

There is increasing knowledge available of the pathogenic link of other neurodegenerative disorders to inflammation. For example, in Alzheimer's disease, microglial cells appear to play both neuroprotective roles by removing antibody-decorated β-amyloid, but have also aggravating activities due to detrimental consequences of cytokine release (Fuhrmann et al., 2010; Glass et al., 2010). Previous studies have also demonstrated that secondary inflammation contributes to disease outcome in mouse models with myelin-related mutations in the CNS (Ip et al., 2006b) as well as in the PNS (Fischer et al., 2008b; Kohl et al., 2010a; Groh et al., 2012). Thus, secondary inflammation emerges as a common pathogenetically relevant feature in a wide variety of inherited and spontaneous neurological disorders.

6.2 Visual impairment and degeneration of retinal ganglion cells in mouse models of NCL

This study was focused upon the visual system for two reasons: First, ophthalmological abnormalities are usually the first clinical signs of the NCLs (Haltia, 2006). Second, the visual system is an ideal structure to investigate disease progression due to its simple and easily accessible neural components, comprising

ganglionic cell bodies in the retina, a myelinated pathway (optic nerve) and a well defined synaptic projection domain in the colliculus superior.

The findings in this system faithfully reflected the impact of the immune system onto different levels of the diseased nervous system, including axon damage, neuronal cell body loss and visual dysfunction in a spatio-temporal manner. By revealing an early morphological and functional impairment of RGCs, the study substantially extends the observations made in the $Ppt1^{-/-}$ mutants concerning the cause of visual impairment in INCL using histopathology and ERG measurements (Griffey et al., 2006).

Furthermore, the results focusing on axonal transport demonstrate that axonal damage occurs before substantial loss of neuronal cell bodies. Accordingly, cleaved caspase 3, a typical marker of apoptosis was found in the swellings of degenerating axons. Previous studies in $Cln3^{-/-}$ mice also indicated degenerative changes in the optic nerve and thalamic projection nuclei rather than in the retina (Weimer et al., 2006). These observations were corroborated by the results of this study, showing that also in $Cln3^{-/-}$ mice RGC degeneration appears to be preceded by impaired axonal integrity. In line with these findings, several studies demonstrated that axonal and synaptic alterations precede the selective loss of neurons, not only in multiple models of NCL (Kim et al., 2008; Partanen et al., 2008; Kielar et al., 2009) but also in other forms of neurological diseases such as multiple sclerosis (Trapp et al., 1998), Alzheimer's disease (Selkoe, 2002), amyotrophic lateral sclerosis (Fischer et al., 2004) and, as a representative of ophthalmic disorders, glaucoma (Buckingham et al., 2008).

Thus, the analyis of the retino-tectal system identified axon damage as an early, neurodegenerative event, adding to the concept of early axonal damage in many neurodegenerative disorders (Coleman, 2005). It remains to be seen whether it will emerge as a general feature of neurodegenerative disorders that early axonal damage is mediated or amplified by components of the immune system.

6.3 CD8+ T-lymphocytes promote neuronal damage in $Ppt1^{-/-}$ mice

Of note, similar to previous studies in other mouse models (Ip et al., 2006b; Kroner et al., 2010), CD8+ T-lymphocytes were identified as major pathogenic effector cells of

the adaptive immune system. Although experimental proof of a substantial implication of CD8+ T-cells has been provided specifically in 3-month-old *Ppt1* mutants, there is strong evidence that the pathogenic effect of lymphocytes is also caused by CD8+ cells at older ages. These cells are not only the predominant lymphocyte population in the CNS, but they steadily increase in number and predominance with disease progression. Moreover, at ages older than 3 months, the investigations clearly demonstrated that CD8+ cells are preferentially in close contact to damaged axonal structures, which were strongly reduced in number in the absence of lymphocytes. Lastly, the immunohistochemical studies also showed that, at older ages, some of these CD8+ cells express the major cytotoxic agents perforin and granzyme B.

In contrast to previous studies in myelin mutant mice, *Ppt1*-deficient neurons rather than oligodendrocytes might be the targets of CD8+ T-lymphocytes. This hypothesis is supported by the increased expression of MHC-I on RGC neurons and the observation that CD8+ T-cells were spatially associated with small SMI32+ axonal spheroids. Granzyme B employed by cytotoxic T-lymphocytes has been shown to activate caspase 3 in target cells. Therefore, the localization of cleaved caspase 3 in axonal spheroids further points towards an early attack of axonal structures. Interestingly, apoptotic processes promoted by granzyme B have also been shown to rely on disruption of mitochondria in addition to cleavage of caspase 3 (Goping et al., 2003). This is in line with the observation of disintegrating mitochondria in juxtaparanodal axonal spheroids of *Ppt1*$^{-/-}$ mice. Findings that also support pro-apoptotic processes in axonal swellings come from studies in other neurodegenerative disorders. In many models, axonal spheroids have been shown to accumulate amyloid precursor protein (APP), which is used as a marker of disturbed axonal transport and axon damage (Coleman, 2005). Importantly, during apoptosis APP is directly and efficiently cleaved by activated caspase 3 (Gervais et al., 1999), which was detected in axonal spherods in this study. The fact that early damage was predominantly located at the juxtaparanodal domains of the node of Ranvier defines this region as a new "hot spot" of immune-mediated axonopathy.

How mutations in genes encoding for lysosomal enzymes lead to recruitment of inflammatory cells is currently not clear. The accumulation of storage material may cause distinct forms of cellular stress (Zhang et al., 2006; Ahtiainen et al., 2007; Wei et al., 2008), possibly resulting in the increased expression of MHC-I molecules on

prospective target cells and the upregulation of proinflammatory cytokines as shown in this study and in cultured astrocytes from *Ppt1*^{-/-} mice (Saha et al., 2008). Importantly, this study showed that the accumulation of storage material alone does not stringently cause immediate neurodegeneration, as demonstrated in the retino-tectal system, where neuronal integrity and function can be preserved for a significant time period by silencing the immune system.

In addition, the exact identities of putative antigens recognized by T-lymphocytes remain unknown. One important observation is that MHC-I expression was primarily found on cells with profound accumulation of storage material, indicating that components of the intracellular storage material might be recognized and presented as antigens. One could speculate that in healthy mice such components would be degraded by the functional lysosomal enzymes. Moreover, synaptic structures showed increased expression of MHC-I in the mutant mice. Previous studies have demonstrated that MHC-I molecules play a role in synaptic remodeling (Glynn et al., 2011). A direct role of Ppt1 for synaptic function has also been demonstrated previously (Kim et al., 2008). Synaptic function might be altered due to the lack of lysosomal enzymes and synapses might be preferentially attacked by T-lymphocytes. As mentioned, synaptic alterations have been shown to occur early in several NCL models (Partanen et al., 2008; Kielar et al., 2009).

Another open question concerns the exact mechanisms by which CD8+ T-lymphocytes contribute to axonal damage and neurodegeneration. The observation of lytic granules in cells contacting perturbed axons and the activation of caspase 3 and disintegration of mitochondria indicate that damage might be transmitted via the cytotoxic effector molecules perforin and granzyme B. Indeed, expression of these factors in CD8+ T-lymphocytes could be observed. However, the proof of principle that there is an MHC-I-dependent cytotoxic reaction of CD8+ T-lymphocytes against neuronal structures comprising these molecules remains to be acquired.

Importantly, the results show that the beneficial effects of immune depletion do not only occur in the retino-tectal system, but also in other brain regions like the laterodorsal thalamic nucleus, primary visual and somatosensory barrel field cortex (Groh et al., 2013). These observations not only reflect the prominent pathogenic role of the immune system in the CNS of INCL mice, but also point to the possiblity that the retino-tectal system may be viewed as a reliable surrogate tissue for evaluating

disease progression and possible therapeutic effects in future treatment approaches by using modern imaging techniques, such as optic coherence tomography.

6.4 Sialoadhesin+ microglia/macrophage-like cells promote neuronal damage in mouse models of NCL

Sialoadhesin, also designated siglec-1 or CD169, is a member of the siglec family of sialic acid binding Ig-like lectins (Crocker et al., 1994). The structure of Sn is highly conserved and contains 17 Ig-like domains. Based on its molecular architecture Sn is suggested to have a function in cell-cell interaction (Munday et al., 1999). Sn expression has been found on macrophage-like cells in various tissues including secondary lymphoid organs, liver (Crocker and Gordon, 1989), peripheral nerve (Kobsar et al., 2006) and in the lesioned brain (Perry et al., 1992) as well as under inflammatory conditions in CNS tissue during EAE (Wu et al., 2009) or models of leukodystrophy (Ip et al., 2007). Moreover, a role for Sn expression in disease progression and axonal damage as well as demyelination has been demonstrated at least in some disease models. Recently, it has also been shown to enable receptor-mediated internalization of pathogens carrying sialic acids into Sn-expressing macrophages, thus mediating endocytosis (Chen et al., 2012).

The present study demonstrated that Sn+ microglia/macrophage-like cells are also substantially involved in neurodegenerative processes mediated by the immune system in distinct mouse models of two lysosomal storage disorders. The beneficial effect of the absence of Sn might be explained by different scenarios or a combination of these possibilities.

On the one hand, it is known that classically activated so-called M1 type macrophages and microglial cells can secrete neurotoxic factors like reactive oxygen species, nitric oxide or cytokines like IL-1β or TNF-α (Sica and Mantovani, 2012). Interestingly, these reactions have also been associated with juxtaparanodal axonal swelling and mitochondrial damage in a MOG-EAE model (Nikic et al., 2011), which appears similar as the early stages of spheroid formation found in this study. As sialoadhesin is expressed specifically on activated microglia/macrophage-like cells there might be a direct role for the surface protein in the secretion of these factors or in other detrimental functions leading to neurotoxic properties of Sn+ cells.

Alternatively, there might be modified interactions of microglia with T-lymphocytes in the absence of Sn which consequently lead to an altered activation state of microglia. These scenarios imply a direct role of activated microglia/macrophages in axonal damage.

On the other hand, an altered interaction of microglia with T-lymphocytes could also change the activation state or expansion of distinct subtypes of T-lymphocytes. Previous studies have shown that antigen presentation by Sn expressing macrophages is important for the generation of cytotoxic responses of CD8+ T-lymphocytes in a graft-versus-leukemia model (Muerkoster et al., 1999). A direct interaction of T-lymphocytes and microglia/macrophage-like cells might also explain the observation that both CD8+ cells and Sn+ cells were preferentially localized at juxtaparanodal axonal spheroids. Here they might directly interact with each other and promote cytotoxic activation. Moreover, it has been demonstrated in EAE that Sn expression on microglia negatively regulates the expansion of CD4+ FoxP3+ regulatory T-lymphocytes (Wu et al., 2009). These regulatory CD4+ T-cells can suppress inflammatory reactions in the CNS and thus inhibit neurotoxic processes of immune reactions. While these CD4+ FoxP3+ regulatory T-lymphocytes can ameliorate pathology in a CD4+ T-cell dependent EAE model, it remains to be determined if similar expansions of FoxP3+ cells in the absence of Sn occur in the NCL models, where CD8+ T-lymphocytes appear to be promoters of neuronal pathology. Absence of Sn in $Ppt1^{-/-}$ or $Cln3^{-/-}$ mice might also lead to an expansion of other regulatory T-cells. For example, regulatory CD8+ CD122+ T-cells have been shown to ameliorate disease in a different EAE model, which is also characterized by an important contribution of pathogenic CD8+ T-cells (Mangalam et al., 2012).

Thus, induction of Sn on microglia/macrophage-like cells in the CNS might induce a detrimental proinflammatory cascade by direct effects and/or by inhibition of the expansion of regulatory T-lymphocytes, favoring a cytotoxic T-lymphocyte population. Future experiments should clarify if these scenarios explain the findings in the mouse models analyzed in this study. Regardless of a direct or indirect effect of Sn inactivation, the results demonstrate that activated microglia/macrophages and their interaction with other immune cells negatively impact neuronal survival in models of NCL, also linking innate immune reactions with neuronal impairment.

6.5 Conclusions for putative therapeutic approaches

This study shows that ablation of CNS-infiltrating T-lymphocytes or inhibition of sialoadhesin expression on microglia/macrophage-like cells ameliorates all investigated disease phenotypes in mouse models for INCL and JNCL, non-treatable fatal genetic diseases, in the unchanged presence of neuronal storage product. Considering that cytotoxic T-lymphocytes are identified as potent contributors to neurodegeneration in models of INCL, there is emerging hope that novel treatment approaches might be designed to foster neuronal survival and improve clinical outcome by attenuating lymphocytic inflammation in various forms of NCL. Alternatively, preventing microglial activation and Sn expression or function might provide a potential treatment option. Ideally, suppression or modulation of both innate and adaptive reactions could provide a synergistic therapeutic effect without negatively impacting the physiological functions fulfilled by the immune system.

Of note, in the present model, for most of the disease progression, the integrity of the BBB appears to remain preserved in $Ppt1^{-/-}$ mice, as has been observed in other neuroinflammatory conditions including some leukodystrophic models (Ip et al., 2008) and chronic progressive MS (Lassmann et al., 2012). This may have substantial implications, not only for disease mechanisms, but also for assessing putative therapeutic interventions with regard to the BBB permeability of the proposed drugs.

A promising approach to attenuate inflammation might be the inhibition of the infiltration of T-lymphocytes into the CNS using antibodies against alpha4-integrin, which is part of the very late antigen VLA-4 expressed on lymphocytes. Under inflammatory conditions alpha4-integrin interacts with the vascular cell adhesion molecule V-CAM on CNS endothelial cells, which is an important prerequisite for transmigration of lymphocytes across the blood-brain barrier (Coisne et al., 2009). Binding of antibodies can block the function and inhibit the transmigration of lymphocytes and a humanized form of the antibody (natalizumab, Tysabri) is used as an effective treatment for aggressive and basic therapy-resistant relapsing forms of multiple sclerosis (Wiendl et al., 2008). It remains to be determined if application of such antibodies to models of NCL alleviates disease in a similar way as $Rag1$ deficiency. Moreover, few patients in clinical trials with natalizumab were diagnosed with progressive multifocal leukoencephalopathy (PML) or other opportunistic infections. The currently restricted approval label represents a compromise between

the expected benefits and the potential risks of this therapy, which have to be carefully considered before assessing its efficacy in NCL.

Alternatively, keeping the contribution of CNS inflammation to neuronal damage in mind, it might turn out useful to test treatment approaches that combine anti-inflammatory and neuroprotective properties. For example, fumaric acid and Fingolimod are both therapeutic agents reported to attenuate CNS inflammation and also act neuroprotective (Linker et al., 2011; Pelletier and Hafler, 2012). Future studies could address the feasibility of therapeutic approaches with these agents in animal models of NCL.

In addition, there is increasing evidence that also in mouse models of NCL the combination of distinct treatment approaches can lead to synergistic effects that surpass the effects of individual approaches (Macauley et al., 2012). Suppression or modulation of specific immune reactions might emerge as one of such synergistic approaches and might turn out useful for a variety of neurological disorders.

6.6. Synopsis
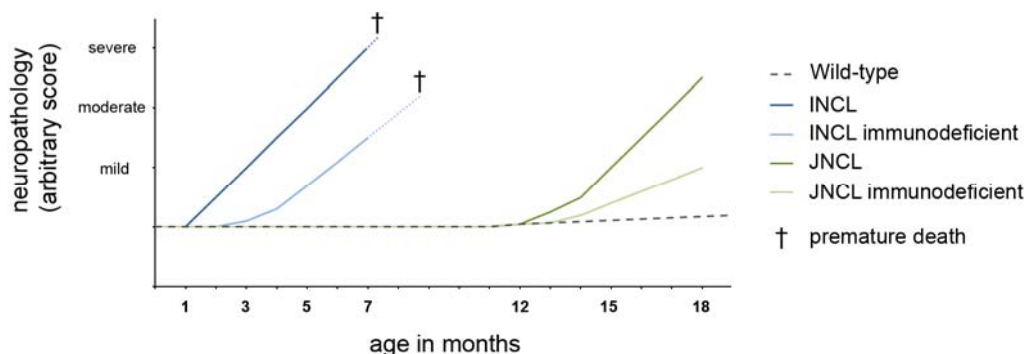
Figure 27 Synoptic view of onset and progression of neuropathology in the CNS of the studied models of INCL (blue) and JNCL (green). The main difference between the infantile and juvenile forms was age of onset of axonal and neuronal degeneration. In immunodeficient models of NCL (light blue and light green) onset and progression of neuropathological alterations was attenuated and premature death (†) was delayed.

7. References

Aguzzi A, Barres BA, Bennett ML (2013) Microglia: scapegoat, saboteur, or something else? Science 339:156-161.

Ahtiainen L, Kolikova J, Mutka AL, Luiro K, Gentile M, Ikonen E, Khiroug L, Jalanko A, Kopra O (2007) Palmitoyl protein thioesterase 1 (Ppt1)-deficient mouse neurons show alterations in cholesterol metabolism and calcium homeostasis prior to synaptic dysfunction. Neurobiol Dis 28:52-64.

Ajami B, Bennett JL, Krieger C, McNagny KM, Rossi FM (2011) Infiltrating monocytes trigger EAE progression, but do not contribute to the resident microglia pool. Nat Neurosci 14:1142-1149.

Armati P, Mathey E (2010) The Biology of Oligodendrocytes: Cambridge University Press.

Attwell D, Buchan AM, Charpak S, Lauritzen M, Macvicar BA, Newman EA (2010) Glial and neuronal control of brain blood flow. Nature 468:232-243.

Badea TC, Cahill H, Ecker J, Hattar S, Nathans J (2009) Distinct roles of transcription factors brn3a and brn3b in controlling the development, morphology, and function of retinal ganglion cells. Neuron 61:852-864.

Ballabio A, Gieselmann V (2009) Lysosomal disorders: from storage to cellular damage. Biochim Biophys Acta 1793:684-696.

Bellettato CM, Scarpa M (2010) Pathophysiology of neuropathic lysosomal storage disorders. J Inherit Metab Dis 33:347-362.

Berghoff M, Samsam M, Muller M, Kobsar I, Toyka KV, Kiefer R, Maurer M, Martini R (2005) Neuroprotective effect of the immune system in a mouse model of severe dysmyelinating hereditary neuropathy: enhanced axonal degeneration following disruption of the RAG-1 gene. Mol Cell Neurosci 28:118-127.

Block ML, Zecca L, Hong JS (2007) Microglia-mediated neurotoxicity: uncovering the molecular mechanisms. Nat Rev Neurosci 8:57-69.

Brinkmann BG, Agarwal A, Sereda MW, Garratt AN, Muller T, Wende H, Stassart RM, Nawaz S, Humml C, Velanac V, Radyushkin K, Goebbels S, Fischer TM, Franklin RJ, Lai C, Ehrenreich H, Birchmeier C, Schwab MH, Nave KA (2008) Neuregulin-1/ErbB signaling serves distinct functions in myelination of the peripheral and central nervous system. Neuron 59:581-595.

Buckingham BP, Inman DM, Lambert W, Oglesby E, Calkins DJ, Steele MR, Vetter ML, Marsh-Armstrong N, Horner PJ (2008) Progressive ganglion cell degeneration precedes neuronal loss in a mouse model of glaucoma. J Neurosci 28:2735-2744.

Camp LA, Verkruyse LA, Afendis SJ, Slaughter CA, Hofmann SL (1994) Molecular cloning and expression of palmitoyl-protein thioesterase. J Biol Chem 269:23212-23219.

Cantor H, Shen FW, Boyse EA (1976) Separation of helper T cells from suppressor T cells expressing different Ly components. II. Activation by antigen: after immunization, antigen-specific suppressor and helper activities are mediated by distinct T-cell subclasses. J Exp Med 143:1391-1340.

Carenini S, Maurer M, Werner A, Blazyca H, Toyka KV, Schmid CD, Raivich G, Martini R (2001) The role of macrophages in demyelinating peripheral nervous system of mice heterozygously deficient in p0. J Cell Biol 152:301-308.

Caroni P, Donato F, Muller D (2012) Structural plasticity upon learning: regulation and functions. Nat Rev Neurosci 13:478-490.

Chen SK, Tvrdik P, Peden E, Cho S, Wu S, Spangrude G, Capecchi MR (2010) Hematopoietic origin of pathological grooming in Hoxb8 mutant mice. Cell 141:775-785.

Chen WC, Kawasaki N, Nycholat CM, Han S, Pilotte J, Crocker PR, Paulson JC (2012) Antigen delivery to macrophages using liposomal nanoparticles targeting sialoadhesin/CD169. PLoS One 7:e39039.

Coisne C, Mao W, Engelhardt B (2009) Cutting edge: Natalizumab blocks adhesion but not initial contact of human T cells to the blood-brain barrier in vivo in an animal model of multiple sclerosis. J Immunol 182:5909-5913.

Coleman M (2005) Axon degeneration mechanisms: commonality amid diversity. Nat Rev Neurosci 6:889-898.

Cooper JD (2008) Moving towards therapies for juvenile Batten disease? Exp Neurol 211:329-331.

Cooper JD (2010) The neuronal ceroid lipofuscinoses: the same, but different? Biochem Soc Trans 38:1448-1452.

Cooper JD, Russell C, Mitchison HM (2006) Progress towards understanding disease mechanisms in small vertebrate models of neuronal ceroid lipofuscinosis. Biochim Biophys Acta 1762:873-889.

Cosmi L, Liotta F, Lazzeri E, Francalanci M, Angeli R, Mazzinghi B, Santarlasci V, Manetti R, Vanini V, Romagnani P, Maggi E, Romagnani S, Annunziato F (2003) Human CD8+CD25+ thymocytes share phenotypic and functional features with CD4+CD25+ regulatory thymocytes. Blood 102:4107-4114.

Cotman SL, Vrbanac V, Lebel LA, Lee RL, Johnson KA, Donahue LR, Teed AM, Antonellis K, Bronson RT, Lerner TJ, MacDonald ME (2002) Cln3(Deltaex7/8) knock-in mice with the common JNCL mutation exhibit progressive neurologic disease that begins before birth. Hum Mol Genet 11:2709-2721.

Crocker PR, Gordon S (1989) Mouse macrophage hemagglutinin (sheep erythrocyte receptor) with specificity for sialylated glycoconjugates characterized by a monoclonal antibody. J Exp Med 169:1333-1346.

Crocker PR, Mucklow S, Bouckson V, McWilliam A, Willis AC, Gordon S, Milon G, Kelm S, Bradfield P (1994) Sialoadhesin, a macrophage sialic acid binding receptor for haemopoietic cells with 17 immunoglobulin-like domains. EMBO J 13:4490-4503.

Cunningham C (2013) Microglia and neurodegeneration: The role of systemic inflammation. Glia 61:71-90.

Desnick RJ, Schuchman EH (2012) Enzyme replacement therapy for lysosomal diseases: lessons from 20 years of experience and remaining challenges. Annu Rev Genomics Hum Genet 13:307-335.

Di Filippo M, Sarchielli P, Picconi B, Calabresi P (2008) Neuroinflammation and synaptic plasticity: theoretical basis for a novel, immune-centred, therapeutic approach to neurological disorders. Trends Pharmacol Sci 29:402-412.

Drager UC, Olsen JF (1981) Ganglion cell distribution in the retina of the mouse. Invest Ophthalmol Vis Sci 20:285-293.

Edgar JM, McLaughlin M, Werner HB, McCulloch MC, Barrie JA, Brown A, Faichney AB, Snaidero N, Nave KA, Griffiths IR (2009) Early ultrastructural defects of axons and axon-glia junctions in mice lacking expression of Cnp1. Glia 57:1815-1824.

Fischer LR, Culver DG, Tennant P, Davis AA, Wang M, Castellano-Sanchez A, Khan J, Polak MA, Glass JD (2004) Amyotrophic lateral sclerosis is a distal axonopathy: evidence in mice and man. Exp Neurol 185:232-240.

Fischer S, Weishaupt A, Troppmair J, Martini R (2008a) Increase of MCP-1 (CCL2) in myelin mutant Schwann cells is mediated by MEK-ERK signaling pathway. Glia 56:836-843.

Fischer S, Kleinschnitz C, Muller M, Kobsar I, Ip CW, Rollins B, Martini R (2008b) Monocyte chemoattractant protein-1 is a pathogenic component in a model for a hereditary peripheral neuropathy. Mol Cell Neurosci 37:359-366.

Fuhrmann M, Bittner T, Jung CK, Burgold S, Page RM, Mitteregger G, Haass C, LaFerla FM, Kretzschmar H, Herms J (2010) Microglial Cx3cr1 knockout prevents neuron loss in a mouse model of Alzheimer's disease. Nat Neurosci 13:411-413.

Funfschilling U, Supplie LM, Mahad D, Boretius S, Saab AS, Edgar J, Brinkmann BG, Kassmann CM, Tzvetanova ID, Mobius W, Diaz F, Meijer D, Suter U, Hamprecht B, Sereda MW, Moraes CT, Frahm J, Goebbels S, Nave KA (2012) Glycolytic oligodendrocytes maintain myelin and long-term axonal integrity. Nature 485:517-521.

Fung-Leung WP, Schilham MW, Rahemtulla A, Kundig TM, Vollenweider M, Potter J, van Ewijk W, Mak TW (1991) CD8 is needed for development of cytotoxic T cells but not helper T cells. Cell 65:443-449.

Galindo-Romero C, Aviles-Trigueros M, Jimenez-Lopez M, Valiente-Soriano FJ, Salinas-Navarro M, Nadal-Nicolas F, Villegas-Perez MP, Vidal-Sanz M, Agudo-Barriuso M (2011) Axotomy-induced retinal ganglion cell death in adult mice: quantitative and topographic time course analyses. Exp Eye Res 92:377-387.

Gervais FG, Xu D, Robertson GS, Vaillancourt JP, Zhu Y, Huang J, LeBlanc A, Smith D, Rigby M, Shearman MS, Clarke EE, Zheng H, Van Der Ploeg LH, Ruffolo SC, Thornberry NA, Xanthoudakis S, Zamboni RJ, Roy S, Nicholson DW (1999) Involvement of caspases in proteolytic cleavage of Alzheimer's amyloid-beta precursor protein and amyloidogenic A beta peptide formation. Cell 97:395-406.

Ginhoux F, Greter M, Leboeuf M, Nandi S, See P, Gokhan S, Mehler MF, Conway SJ, Ng LG, Stanley ER, Samokhvalov IM, Merad M (2010) Fate mapping analysis reveals that adult microglia derive from primitive macrophages. Science 330:841-845.

Glass CK, Saijo K, Winner B, Marchetto MC, Gage FH (2010) Mechanisms underlying inflammation in neurodegeneration. Cell 140:918-934.

Glynn MW, Elmer BM, Garay PA, Liu XB, Needleman LA, El-Sabeawy F, McAllister AK (2011) MHCI negatively regulates synapse density during the establishment of cortical connections. Nat Neurosci 14:442-451.

Goping IS, Barry M, Liston P, Sawchuk T, Constantinescu G, Michalak KM, Shostak I, Roberts DL, Hunter AM, Korneluk R, Bleackley RC (2003) Granzyme B-induced apoptosis requires both direct caspase activation and relief of caspase inhibition. Immunity 18:355-365.

Griffey MA, Wozniak D, Wong M, Bible E, Johnson K, Rothman SM, Wentz AE, Cooper JD, Sands MS (2006) CNS-directed AAV2-mediated gene therapy ameliorates functional deficits in a murine model of infantile neuronal ceroid lipofuscinosis. Mol Ther 13:538-547.

Griffiths I, Klugmann M, Anderson T, Yool D, Thomson C, Schwab MH, Schneider A, Zimmermann F, McCulloch M, Nadon N, Nave KA (1998) Axonal swellings

and degeneration in mice lacking the major proteolipid of myelin. Science 280:1610-1613.

Groh J, Weis J, Zieger H, Stanley ER, Heuer H, Martini R (2012) Colony-stimulating factor-1 mediates macrophage-related neural damage in a model for Charcot-Marie-Tooth disease type 1X. Brain 135:88-104.

Groh J, Heinl K, Kohl B, Wessig C, Greeske J, Fischer S, Martini R (2010) Attenuation of MCP-1/CCL2 expression ameliorates neuropathy in a mouse model for Charcot-Marie-Tooth 1X. Hum Mol Genet 19:3530-3543.

Groh J, Kuhl TG, Ip CW, Nelvagal HR, Sri S, Duckett S, Mirza M, Langmann T, Cooper JD, Martini R (2013) Immune cells perturb axons and impair neuronal survival in a mouse model of infantile neuronal ceroid lipofuscinosis. Brain 136:1083-1101.

Gupta P, Soyombo AA, Atashband A, Wisniewski KE, Shelton JM, Richardson JA, Hammer RE, Hofmann SL (2001) Disruption of PPT1 or PPT2 causes neuronal ceroid lipofuscinosis in knockout mice. Proc Natl Acad Sci U S A 98:13566-13571.

Haltia M (2003) The neuronal ceroid-lipofuscinoses. J Neuropathol Exp Neurol 62:1-13.

Haltia M (2006) The neuronal ceroid-lipofuscinoses: from past to present. Biochim Biophys Acta 1762:850-856.

Hickey WF (2001) Basic principles of immunological surveillance of the normal central nervous system. Glia 36:118-124.

Ip CW, Kroner A, Crocker PR, Nave KA, Martini R (2007) Sialoadhesin deficiency ameliorates myelin degeneration and axonopathic changes in the CNS of PLP overexpressing mice. Neurobiol Dis 25:105-111.

Ip CW, Kroner A, Fischer S, Berghoff M, Kobsar I, Maurer M, Martini R (2006a) Role of immune cells in animal models for inherited peripheral neuropathies. Neuromolecular Med 8:175-190.

Ip CW, Kohl B, Kleinschnitz C, Reuss B, Nave KA, Kroner A, Martini R (2008) Origin of CD11b+ macrophage-like cells in the CNS of PLP-overexpressing mice: low influx of haematogenous macrophages and unchanged blood-brain-barrier in the optic nerve. Mol Cell Neurosci 38:489-494.

Ip CW, Kroner A, Bendszus M, Leder C, Kobsar I, Fischer S, Wiendl H, Nave KA, Martini R (2006b) Immune cells contribute to myelin degeneration and axonopathic changes in mice overexpressing proteolipid protein in oligodendrocytes. J Neurosci 26:8206-8216.

Ip CW, Kroner A, Groh J, Huber M, Klein D, Spahn I, Diem R, Williams SK, Nave KA, Edgar JM, Martini R (2012) Neuroinflammation by cytotoxic T-lymphocytes impairs retrograde axonal transport in an oligodendrocyte mutant mouse. PLoS One 7:e42554.

Jalanko A, Braulke T (2009) Neuronal ceroid lipofuscinoses. Biochim Biophys Acta 1793:697-709.

Jalanko A, Vesa J, Manninen T, von Schantz C, Minye H, Fabritius AL, Salonen T, Rapola J, Gentile M, Kopra O, Peltonen L (2005) Mice with Ppt1Deltaex4 mutation replicate the INCL phenotype and show an inflammation-associated loss of interneurons. Neurobiol Dis 18:226-241.

Jarvela I, Lehtovirta M, Tikkanen R, Kyttala A, Jalanko A (1999) Defective intracellular transport of CLN3 is the molecular basis of Batten disease (JNCL). Hum Mol Genet 8:1091-1098.

Kandel E, Schwartz J, Jessell T (2000) Principles of Neural Science, 4th Edition: McGraw-Hill.

Katz ML, Shibuya H, Liu PC, Kaur S, Gao CL, Johnson GS (1999) A mouse gene knockout model for juvenile ceroid-lipofuscinosis (Batten disease). J Neurosci Res 57:551-556.

Kettenmann H, Ransom B (2005) Neuroglia, 2nd Edition: Oxford University Press.

Kielar C, Maddox L, Bible E, Pontikis CC, Macauley SL, Griffey MA, Wong M, Sands MS, Cooper JD (2007) Successive neuron loss in the thalamus and cortex in a

mouse model of infantile neuronal ceroid lipofuscinosis. Neurobiol Dis 25:150-162.

Kielar C, Wishart TM, Palmer A, Dihanich S, Wong AM, Macauley SL, Chan CH, Sands MS, Pearce DA, Cooper JD, Gillingwater TH (2009) Molecular correlates of axonal and synaptic pathology in mouse models of Batten disease. Hum Mol Genet 18:4066-4080.

Kierdorf K et al. (2013) Microglia emerge from erythromyeloid precursors via Pu.1- and Irf8-dependent pathways. Nat Neurosci 16:273-280.

Kim SJ, Zhang Z, Sarkar C, Tsai PC, Lee YC, Dye L, Mukherjee AB (2008) Palmitoyl protein thioesterase-1 deficiency impairs synaptic vesicle recycling at nerve terminals, contributing to neuropathology in humans and mice. J Clin Invest 118:3075-3086.

Kiselyov K, Yamaguchi S, Lyons CW, Muallem S (2010) Aberrant Ca2+ handling in lysosomal storage disorders. Cell Calcium 47:103-111.

Kobsar I, Maurer M, Ott T, Martini R (2002) Macrophage-related demyelination in peripheral nerves of mice deficient in the gap junction protein connexin 32. Neurosci Lett 320:17-20.

Kobsar I, Hasenpusch-Theil K, Wessig C, Muller HW, Martini R (2005) Evidence for macrophage-mediated myelin disruption in an animal model for Charcot-Marie-Tooth neuropathy type 1A. J Neurosci Res 81:857-864.

Kobsar I, Oetke C, Kroner A, Wessig C, Crocker P, Martini R (2006) Attenuated demyelination in the absence of the macrophage-restricted adhesion molecule sialoadhesin (Siglec-1) in mice heterozygously deficient in P0. Mol Cell Neurosci 31:685-691.

Kobsar I, Berghoff M, Samsam M, Wessig C, Maurer M, Toyka KV, Martini R (2003) Preserved myelin integrity and reduced axonopathy in connexin32-deficient mice lacking the recombination activating gene-1. Brain 126:804-813.

Kohl B, Fischer S, Groh J, Wessig C, Martini R (2010a) MCP-1/CCL2 modifies axon properties in a PMP22-overexpressing mouse model for Charcot-Marie-tooth 1A neuropathy. Am J Pathol 176:1390-1399.

Kohl B, Groh J, Wessig C, Wiendl H, Kroner A, Martini R (2010b) Lack of evidence for a pathogenic role of T-lymphocytes in an animal model for Charcot-Marie-Tooth disease 1A. Neurobiol Dis 38:78-84.

Kohlschutter A, Gardiner RM, Goebel HH (1993) Human forms of neuronal ceroid-lipofuscinosis (Batten disease): consensus on diagnostic criteria, Hamburg 1992. J Inherit Metab Dis 16:241-244.

Kondo Y, Adams JM, Vanier MT, Duncan ID (2011) Macrophages counteract demyelination in a mouse model of globoid cell leukodystrophy. J Neurosci 31:3610-3624.

Kroner A, Ip CW, Thalhammer J, Nave KA, Martini R (2010) Ectopic T-cell specificity and absence of perforin and granzyme B alleviate neural damage in oligodendrocyte mutant mice. Am J Pathol 176:549-555.

Lassmann H (2010) Axonal and neuronal pathology in multiple sclerosis: what have we learnt from animal models. Exp Neurol 225:2-8.

Lassmann H, van Horssen J, Mahad D (2012) Progressive multiple sclerosis: pathology and pathogenesis. Nat Rev Neurol 8:647-656.

Leder C, Schwab N, Ip CW, Kroner A, Nave KA, Dornmair K, Martini R, Wiendl H (2007) Clonal expansions of pathogenic CD8+ effector cells in the CNS of myelin mutant mice. Mol Cell Neurosci 36:416-424.

Lim MJ, Alexander N, Benedict JW, Chattopadhyay S, Shemilt SJ, Guerin CJ, Cooper JD, Pearce DA (2007) IgG entry and deposition are components of the neuroimmune response in Batten disease. Neurobiol Dis 25:239-251.

Linker RA, Lee DH, Ryan S, van Dam AM, Conrad R, Bista P, Zeng W, Hronowsky X, Buko A, Chollate S, Ellrichmann G, Bruck W, Dawson K, Goelz S, Wiese S, Scannevin RH, Lukashev M, Gold R (2011) Fumaric acid esters exert

neuroprotective effects in neuroinflammation via activation of the Nrf2 antioxidant pathway. Brain 134:678-692.

Macauley SL, Pekny M, Sands MS (2011) The role of attenuated astrocyte activation in infantile neuronal ceroid lipofuscinosis. J Neurosci 31:15575-15585.

Macauley SL, Roberts MS, Wong AM, McSloy F, Reddy AS, Cooper JD, Sands MS (2012) Synergistic effects of central nervous system-directed gene therapy and bone marrow transplantation in the murine model of infantile neuronal ceroid lipofuscinosis. Ann Neurol 71:797-804.

Mangalam AK, Luckey D, Giri S, Smart M, Pease LR, Rodriguez M, David CS (2012) Two discreet subsets of CD8 T cells modulate PLP(91-110) induced experimental autoimmune encephalomyelitis in HLA-DR3 transgenic mice. J Autoimmun 38:344-353.

Martini R (2001) The effect of myelinating Schwann cells on axons. Muscle Nerve 24:456-466.

Martini R, Schachner M (1986) Immunoelectron microscopic localization of neural cell adhesion molecules (L1, N-CAM, and MAG) and their shared carbohydrate epitope and myelin basic protein in developing sciatic nerve. J Cell Biol 103:2439-2448.

Mitchison HM, Bernard DJ, Greene ND, Cooper JD, Junaid MA, Pullarkat RK, de Vos N, Breuning MH, Owens JW, Mobley WC, Gardiner RM, Lake BD, Taschner PE, Nussbaum RL (1999) Targeted disruption of the Cln3 gene provides a mouse model for Batten disease. The Batten Mouse Model Consortium [corrected]. Neurobiol Dis 6:321-334.

Mombaerts P, Iacomini J, Johnson RS, Herrup K, Tonegawa S, Papaioannou VE (1992) RAG-1-deficient mice have no mature B and T lymphocytes. Cell 68:869-877.

Mueller K (2013) Inflammation. Inflammation's yin-yang. Introduction. Science 339:155.

Muerkoster S, Rocha M, Crocker PR, Schirrmacher V, Umansky V (1999) Sialoadhesin-positive host macrophages play an essential role in graft-versus-leukemia reactivity in mice. Blood 93:4375-4386.

Munday J, Floyd H, Crocker PR (1999) Sialic acid binding receptors (siglecs) expressed by macrophages. J Leukoc Biol 66:705-711.

Murphy K, Travers P, Walport M (2007) Janeway's Immunobiology, 7th Edition: Garland Science.

Nave KA (2010) Myelination and the trophic support of long axons. Nat Rev Neurosci 11:275-283.

Nave KA, Salzer JL (2006) Axonal regulation of myelination by neuregulin 1. Curr Opin Neurobiol 16:492-500.

Nave KA, Trapp BD (2008) Axon-glial signaling and the glial support of axon function. Annu Rev Neurosci 31:535-561.

Nedergaard M, Verkhratsky A (2012) Artifact versus reality--how astrocytes contribute to synaptic events. Glia 60:1013-1023.

Neumann H (2001) Control of glial immune function by neurons. Glia 36:191-199.

Nikic I, Merkler D, Sorbara C, Brinkoetter M, Kreutzfeldt M, Bareyre FM, Bruck W, Bishop D, Misgeld T, Kerschensteiner M (2011) A reversible form of axon damage in experimental autoimmune encephalomyelitis and multiple sclerosis. Nat Med 17:495-499.

Nimmerjahn A, Kirchhoff F, Helmchen F (2005) Resting microglial cells are highly dynamic surveillants of brain parenchyma in vivo. Science 308:1314-1318.

Oetke C, Vinson MC, Jones C, Crocker PR (2006) Sialoadhesin-deficient mice exhibit subtle changes in B- and T-cell populations and reduced immunoglobulin M levels. Mol Cell Biol 26:1549-1557.

Ousman SS, Kubes P (2012) Immune surveillance in the central nervous system. Nat Neurosci 15:1096-1101.

Partanen S, Haapanen A, Kielar C, Pontikis C, Alexander N, Inkinen T, Saftig P, Gillingwater TH, Cooper JD, Tyynela J (2008) Synaptic changes in the thalamocortical system of cathepsin D-deficient mice: a model of human congenital neuronal ceroid-lipofuscinosis. J Neuropathol Exp Neurol 67:16-29.

Pelletier D, Hafler DA (2012) Fingolimod for multiple sclerosis. N Engl J Med 366:339-347.

Perry VH, Crocker PR, Gordon S (1992) The blood-brain barrier regulates the expression of a macrophage sialic acid-binding receptor on microglia. J Cell Sci 101 (Pt 1):201-207.

Pontikis CC, Cella CV, Parihar N, Lim MJ, Chakrabarti S, Mitchison HM, Mobley WC, Rezaie P, Pearce DA, Cooper JD (2004) Late onset neurodegeneration in the Cln3-/- mouse model of juvenile neuronal ceroid lipofuscinosis is preceded by low level glial activation. Brain Res 1023:231-242.

Prusky GT, West PW, Douglas RM (2000) Behavioral assessment of visual acuity in mice and rats. Vision Res 40:2201-2209.

Quaegebeur A, Lange C, Carmeliet P (2011) The neurovascular link in health and disease: molecular mechanisms and therapeutic implications. Neuron 71:406-424.

Rademakers R et al. (2012) Mutations in the colony stimulating factor 1 receptor (CSF1R) gene cause hereditary diffuse leukoencephalopathy with spheroids. Nat Genet 44:200-205.

Rahemtulla A, Fung-Leung WP, Schilham MW, Kundig TM, Sambhara SR, Narendran A, Arabian A, Wakeham A, Paige CJ, Zinkernagel RM, et al. (1991) Normal development and function of CD8+ cells but markedly decreased helper cell activity in mice lacking CD4. Nature 353:180-184.

Raivich G (2005) Like cops on the beat: the active role of resting microglia. Trends Neurosci 28:571-573.

Ransohoff RM (2011) Microglia and monocytes: 'tis plain the twain meet in the brain. Nat Neurosci 14:1098-1100.

Ransohoff RM, Kivisakk P, Kidd G (2003) Three or more routes for leukocyte migration into the central nervous system. Nat Rev Immunol 3:569-581.

Rasband MN (2011) Composition, assembly, and maintenance of excitable membrane domains in myelinated axons. Semin Cell Dev Biol 22:178-184.

Rifa'i M, Kawamoto Y, Nakashima I, Suzuki H (2004) Essential roles of CD8+CD122+ regulatory T cells in the maintenance of T cell homeostasis. J Exp Med 200:1123-1134.

Rousse I, Robitaille R (2006) Calcium signaling in Schwann cells at synaptic and extra-synaptic sites: active glial modulation of neuronal activity. Glia 54:691-699.

Saha A, Kim SJ, Zhang Z, Lee YC, Sarkar C, Tsai PC, Mukherjee AB (2008) RAGE signaling contributes to neuroinflammation in infantile neuronal ceroid lipofuscinosis. FEBS Lett 582:3823-3831.

Saha A, Sarkar C, Singh SP, Zhang Z, Munasinghe J, Peng S, Chandra G, Kong E, Mukherjee AB (2012) The blood-brain barrier is disrupted in a mouse model of infantile neuronal ceroid lipofuscinosis: amelioration by resveratrol. Hum Mol Genet 21:2233-2244.

Salzer JL, Brophy PJ, Peles E (2008) Molecular domains of myelinated axons in the peripheral nervous system. Glia 56:1532-1540.

Santavuori P, Haltia M, Rapola J (1974) Infantile type of so-called neuronal ceroid-lipofuscinosis. Dev Med Child Neurol 16:644-653.

Santavuori P, Haltia M, Rapola J, Raitta C (1973) Infantile type of so-called neuronal ceroid-lipofuscinosis. 1. A clinical study of 15 patients. J Neurol Sci 18:257-267.

Schafer DP, Lehrman EK, Kautzman AG, Koyama R, Mardinly AR, Yamasaki R, Ransohoff RM, Greenberg ME, Barres BA, Stevens B (2012) Microglia sculpt postnatal neural circuits in an activity and complement-dependent manner. Neuron 74:691-705.

Schmid CD, Stienekemeier M, Oehen S, Bootz F, Zielasek J, Gold R, Toyka KV, Schachner M, Martini R (2000) Immune deficiency in mouse models for inherited peripheral neuropathies leads to improved myelin maintenance. J Neurosci 20:729-735.

Schultz ML, Tecedor L, Chang M, Davidson BL (2011) Clarifying lysosomal storage diseases. Trends Neurosci 34:401-410.

Seehafer SS, Pearce DA (2006) You say lipofuscin, we say ceroid: defining autofluorescent storage material. Neurobiol Aging 27:576-588.

Seehafer SS, Ramirez-Montealegre D, Wong AM, Chan CH, Castaneda J, Horak M, Ahmadi SM, Lim MJ, Cooper JD, Pearce DA (2011) Immunosuppression alters disease severity in juvenile Batten disease mice. J Neuroimmunol 230:169-172.

Selkoe DJ (2002) Alzheimer's disease is a synaptic failure. Science 298:789-791.

Shi Z, Okuno Y, Rifa'i M, Endharti AT, Akane K, Isobe K, Suzuki H (2009) Human CD8+CXCR3+ T cells have the same function as murine CD8+CD122+ Treg. Eur J Immunol 39:2106-2119.

Sica A, Mantovani A (2012) Macrophage plasticity and polarization: in vivo veritas. J Clin Invest 122:787-795.

Trapp BD, Peterson J, Ransohoff RM, Rudick R, Mork S, Bo L (1998) Axonal transection in the lesions of multiple sclerosis. N Engl J Med 338:278-285.

Ueda M, Kusunoki S (2011) [Autoimmune neuropathies: diagnosis, treatment, and recent topics]. Brain Nerve 63:549-555.

Vitner EB, Platt FM, Futerman AH (2010) Common and uncommon pathogenic cascades in lysosomal storage diseases. J Biol Chem 285:20423-20427.

Wake H, Moorhouse AJ, Jinno S, Kohsaka S, Nabekura J (2009) Resting microglia directly monitor the functional state of synapses in vivo and determine the fate of ischemic terminals. J Neurosci 29:3974-3980.

Wei H, Kim SJ, Zhang Z, Tsai PC, Wisniewski KE, Mukherjee AB (2008) ER and oxidative stresses are common mediators of apoptosis in both neurodegenerative and non-neurodegenerative lysosomal storage disorders and are alleviated by chemical chaperones. Hum Mol Genet 17:469-477.

Weimer JM, Custer AW, Benedict JW, Alexander NA, Kingsley E, Federoff HJ, Cooper JD, Pearce DA (2006) Visual deficits in a mouse model of Batten disease are the result of optic nerve degeneration and loss of dorsal lateral geniculate thalamic neurons. Neurobiol Dis 22:284-293.

Wiendl H, Toyka KV, Rieckmann P, Gold R, Hartung HP, Hohlfeld R (2008) Basic and escalating immunomodulatory treatments in multiple sclerosis: current therapeutic recommendations. J Neurol 255:1449-1463.

Williams RE, Mole SE (2012) New nomenclature and classification scheme for the neuronal ceroid lipofuscinoses. Neurology 79:183-191.

Wong AM, Rahim AA, Waddington SN, Cooper JD (2010) Current therapies for the soluble lysosomal forms of neuronal ceroid lipofuscinosis. Biochem Soc Trans 38:1484-1488.

Wu C, Rauch U, Korpos E, Song J, Loser K, Crocker PR, Sorokin LM (2009) Sialoadhesin-positive macrophages bind regulatory T cells, negatively controlling their expansion and autoimmune disease progression. J Immunol 182:6508-6516.

Wu YP, Proia RL (2004) Deletion of macrophage-inflammatory protein 1 alpha retards neurodegeneration in Sandhoff disease mice. Proc Natl Acad Sci U S A 101:8425-8430.

Zhang Z, Lee YC, Kim SJ, Choi MS, Tsai PC, Xu Y, Xiao YJ, Zhang P, Heffer A, Mukherjee AB (2006) Palmitoyl-protein thioesterase-1 deficiency mediates the activation of the unfolded protein response and neuronal apoptosis in INCL. Hum Mol Genet 15:337-346.

8. Appendices

8.1 Technical equipment

BioPhotometer 6131		Eppendorf (Hamburg, Germany)
Centrifuges	Biofuge 15R	Heraeus (Hanau, Germany)
	Biofuge Pico	Heraeus (Hanau, Germany)
	Centrifuge 5810R	Eppendorf (Hamburg, Germany)
	Centrifuge 5415C	Eppendorf (Hamburg, Germany)
	Rotofix 32	Hettich (Tuttlingen, Germany)
Cryostats	CM 1900	Leica (Wetzlar, Germany)
	CM 3050S	Leica (Wetzlar, Germany)
Dry block thermostat TDB-120		Hartenstein (Würzburg, Germany)
ELISA reader Original Multiskan		EX Labsystems (Helsinki, Finland)
FACSCalibur		BD Biosciences (San Jose, USA)
Freezer		Liebherr (Biberach, Germany)
Gel chambers	Horizontal	PeqLab (Erlangen, Germany)
	Vertical: Mini Protean	Bio-Rad (München, Germany)
	Mini Trans Blot	Bio-Rad (München, Germany)
Hamilton syringes		Hamilton (Höchst, Germany)
Homogenizer	MICCRA D-8	ART (Mühlheim, Germany)
Microscopes	CX31	Olympus (Hamburg, Germany)
	BH2	Olympus (Hamburg, Germany)
	CKX41	Olympus (Hamburg, Germany)
	FluoView FV1000	Olympus (Hamburg, Germany)
	Axiophot 2	Zeiss (Oberkochen, Germany)
	LEO 906 E	Zeiss (Oberkochen, Germany)
Micro drill		FST (Heidelberg, Germany)
Micropump		Stoelting (Dublin, Ireland)
Microtome		Reichert-Jung (Heidelberg, Germany)
OptoMotry		CerebralMechanics Inc (London, UK)
Perfusion pump Reglo		Ismatec (Glattbrugg, Switzerland)
ProScan Slow Scan CCD camera		Pro Scan (Lagerlechfeld, Germany)
Pipettes		Abimed (Berlin, Germany)
		Eppendorf (Hamburg, Germany)

		Gilson (Bad Camberg, Germany)
Sonication device Sonoplus HD60		Bandelin Electronic (Berlin, Germany)
Stereotactic frame		Stoelting (Dublin, Ireland)
Thermocycler	Mastercycler gradient	Eppendorf (Hamburg, Germany)
	Primus96 advanced	Peqlab (Erlangen, Germany)
Vibratome	VT 1000S	Leica (Wetzlar, Germany)

Software

Adobe Photoshop	Adobe (San Jose, USA)
CellQuest Pro	BD Biosciences (San Jose, USA)
FluoView	Olympus (Hamburg, Germany)
iTEM	Olympus (Hamburg, Germany)
OptoMotry software	CerebralMechanics Inc (London, UK)
ImageJ	NIH (Bethesda, USA)
Office	Microsoft (Redmond, USA)
SPSS	IBM (Ehningen, Germany)

8.2 Buffers and solutions

Anaesthetic	1.2% Ketamin
	0.08% Rompun
	0.9% NaCl
Cresyl violet solution	0.1% cresyl violet
	1% acetic acid
DABCO	25% PBS
	75% Glycerol
	25 mg/ml 1,4-diazabicyclo[2.2.2]octane
Erythrocyte lysis buffer	0.15 M NH_4Cl
	1 mM $KHCO_3$
	0.1 mM Na_2EDTA
	pH 7.4
	sterile filtration
FACS buffer	1% BSA
	0.1% NaAzide
	in PBS
	sterile filtration
Haematoxylin	50 mg/ml $KAl(SO_4)_2$
	1 mg/ml Haematoxylin
	0.2 mg/ml $NaIO_3$
	2% acetic acid
Methylene blue	1% Methylene blue
	1% Azure II
	40% Saccharose
	pH9.2
1 x PBS	137 mM NaCl
	2.7 mM KCl
	1.5 mM KH_2PO_4
	8.1 mM Na_2HPO_4
	pH 7.4

1 x PBST	0.1% Tween 20
	in PBS
RIPA lysis buffer	25 mM Tris pH 8
	10 mM Hepes pH 4.4
	150mM NaCl
	5mM MgCl2
	145 mM KCl
	0.4 % EDTA
	0.1 % SDS
	1% Nonidet P40
	10 % Glycerol
Spurr's medium	10 g Vinyl/ERL
	6 g DER 736
	26 g NSA 26g
	0.4 g DMAE

8.3 Antibodies

Primary antibodies

Reactivity	Company	Clone	Host	Dilution	Fixation	Additives
Albumin	ICN Cappel	Polyclonal	Rabbit	1:500	4% PFA	0.1% Triton
B220	BD	RA3-6B2	Rat	1:100	Acetone	none
Brn3a	Santa Cruz	Polyclonal	Goat	1:100	4% PFA	0.3% Triton
Caspase 3	Abcam	Polyclonal	Rabbit	1:100	4% PFA	0.3% Triton
Caspr2	Millipore	Polyclonal	Rabbit	1:1000	Acetone	0.3% Triton
CD3	Serotec	CD3-12	Rat	1:100	4% PFA	none
CD4	Serotec	YTS191.1	Rat	1:1000	Acetone	none
CD8	Chemicon	IBL-3/25	Rat	1:1000	Acetone	none
CD11b	Serotec	M1/70.15	Rat	1:100	4% PFA	0.3% Triton
CD44-PerCP	BD	IM7	Rat	1:50	none	none
CD62L-APC	BD	MEL-14	Rat	1:50	none	none
CD69-FITC	BD	H1.2F3	Hamster	1:50	none	none
CD169	Serotec	3D6.112	Rat	1:300	Acetone	none
Granzyme B	Abcam	Polyclonal	Rabbit	1:100	Acetone	0.3% Triton
Laminin	Chemicon	AL-4	Rat	1:300	4% PFA	0.1% Triton
MBP	MBL	Polyclonal	Rabbit	1:500	4% PFA	0.3% Triton
MHC-I	Dianova	ER-HR 52	Rat	1:300	Acetone	none
NeuN	Millipore	A60	Mouse	1:1000	4% PFA	none
Neurofilament	Sigma	NR4	Mouse	1:150	4% PFA	none
Perforin	Santa Cruz	Polyclonal	Rabbit	1:100	Acetone	0.3% Triton
SMI32	Covance	SMI-32	Mouse	1:2000	4% PFA	none

Secondary antibodies

Reactivity	Company	Host	Dilution	Conjugation
Rat IgG	Dianova	Goat	1:300	Cy3
Mouse IgG	Dianova	Donkey	1:300	Cy3
Rabbit IgG	Dianova	Goat	1:300	Cy3
Goat IgG	Dianova	Donkey	1:300	Cy3
Rat IgG	Dianova	Goat	1:300	Cy2
Mouse IgG	Dianova	Goat	1:300	Cy2
Rat IgG	Vector	Rabbit	1:100	Biotin
Mouse IgG	Vector	Goat	1:100	Biotin

Isotype controls

Reactivity	Company	Host	Dilution	Conjugation
none	BD	Hamster	1:50	FITC
none	BD	Rat	1:50	APC
none	BD	Rat	1:50	PerCP

8.4 Primer sequences for genotyping

Cln1

      PG59   5' GTACATAGTTCATGCTCAGCC 3'

      PG60   5' CTGCTAGGTACCTCTAGAGGG 3'

      S175   5' GATTGGGAAGACAATAGCAGGCATGC 3'

Cln3

      Ex1F   5' TGTATAGCAGACAGCGGAACC 3'

      M6R   5' CACTCCGACTATCCAACCGA 3'

      Neo Fo   5' TCGCCTTCTTGACGAGTTCT 3'

Rag1

      RAG-1F1   5' GAGGTTCCGCTACGACTCTG 3'

      RAG-1F2   5' CCGGACAAGTTTTTCATCGT 3'

      RAG-1R   5' TGGATGTGGAATTGTTGCGAG 3'

Sn

      Siglec-1   5' GGCCATATGTAGGGTCGTCT 3'

      Siglec-2   5' CACCACGGTCACTGTGACAA 3'

CD4

      CD4-F   5' CCTCTTGGTTAATGGGGGAT 3'

      CD4-R   5' TTTTTCTGGTCCAGGGTCAC 3'

      CD4-NEO   5' GTGTTGGGTCGTTTGTTCG 3'

CD8

      oIMR1098 5' GACCTGGTATGTGAAGTGTTGG 3'

      oIMR1099 5' ACATCACCGAGTTGCTGATG 3'

      oIMR1100 5' GCTATCAGGACATAGCGTTGG 3'

9. Acknowledgements

First, I would like to thank Prof. Dr. Rudolf Martini for giving me the opportunity to do my PhD thesis in his laboratory. I am grateful for his excellent supervision, permanent support and advice.

Many thanks go to Dr. Jonathan D Cooper and Dr. Thomas Kühl as well as Dr. Thomas Langmann and Myriam Mirza and their groups, with whom we had a fruitful collaboration on the topics investigated during this thesis.

Furthermore, I would like to thank Prof. Dr. Jens Volkmann and Prof. Dr. Klaus Toyka, the present and former directors of the Department of Neurology and Prof. Dr. Erich Buchner for the second assessment of the thesis.

I am also indebted to the NCL foundation (Hamburg) and the R+W foundation (Klingenberg) for funding me during my PhD thesis.

In addition, I would like to thank the current and former members of the Martini laboratory for their help and discussions, especially Henryk Blazyca, Dr. Stefan Fischer, Dr. Chi Wang Ip, Dennis Klein, Dr. Bianca Kohl, Dr. Antje Kroner, Silke Loserth, Bettina Meyer and Dr. Agnes Patzko.

Many thanks also go to Helga Brünner, Jacqueline Schreiber and Anja Weidner for attentive and sophisticated care of animals, and especially Karl-Heinz Aulenbach, who sadly passed away in March.

Last but not least, I thank my family and friends for their constant support.

10. Abbreviations

Af	Autofluorescence
APC	Allophycocyanin
BBB	Blood-brain barrier
BMC	Bone marrow chimera
Brn3a	Brain-specific homeobox/POU domain protein 3A
BSA	Bovine serum albumine
CD	Cluster of differentiation
CIDP	Chronic inflammatory demyelinating polyneuropathy
CLN3	Ceroid lipofuscinosis, neuronal 3
CMT	Charcot-Marie-Tooth disease
CNS	Central nervous system
Cx32	Connexin 32
Cy	Cyanine
DABCO	1,4-Diazabicyclo[2.2.2]octane
DNA	Deoxyribonucleic acid
DAPI	4',6-Diamidino-2-phenylindole
DEPC	Diethylpyrocarbonate
DMSO	Dimethyl sulfoxide
DSS	Dejerine-Sottas syndrome
EAE	Experimental autoimmune encephalomyelitis
ERG	Electroretinogram
ERK	Extracellular signal-regulated kinase
FACS	Fluorescence activated cell sorting
FITC	Fluorescein isothiocyanate
GA	Glutaraldehyde
GBS	Guillain-Barré syndrome
GFAP	Glial fibrillary acidic protein
GFP	Green fluorescent protein
GzmB	Granzyme B
Iba1	Ionized calcium-binding adapter molecule 1
Ig	Immunoglobulin
IL-1β	Interleukin-1 beta
INCL	Infantile neuronal ceroid lipofuscinosis

JNCL	Juvenile neuronal ceroid lipofuscinosis
LGNd	Laterodorsal thalamic nucleus
MBP	Myelin basic protein
MCP-1	Monocyte chemoattractant protein-1
MEK	MAPK/ERK kinase
MHC-I	Major histocompatibility complex class I
MIP-1	Macrophage inflammatory protein-1
MOG	Myelin oligodendrocyte glycoprotein
NCL	Neuronal ceroid lipofuscinosis
NeuN	Neuronal nuclei
Nf	Neurofilament
OCT	Optic coherence tomography
P0	Myelin protein zero
PBS	Phosphate buffered saline
PCR	Polymerase chain reaction
PE	Phycoerythrin
PerCP	Peridinin-Chlorophyll
PFA	Paraformaldehyde
PLP	Proteolipid protein
PMP22	Peripheral myelin protein 22
PNS	Peripheral nervous system
Ppt1	Palmitoyl protein thioesterase 1
Rag1	Recombination activating gene 1
RGC	Retinal ganglion cell
RIPA	Radioimmunoprecipitation assay
RNA	Ribonucleic acid
Sn	Sialoadhesin
TNF-α	Tumor necrosis factor-alpha
Wt	Wild-type

11. Curriculum vitae

Persönliche Daten

Janos Michael Groh

geb. am 29.12.1981 in Schweinfurt

ledig

Berufliche Tätigkeiten

ab 7/2012	Wissenschaftlicher Mitarbeiter, Neurologische Klinik und Poliklinik, Experimentelle Entwicklungsneurobiologie, Prof. Dr. Rudolf Martini, Julius-Maximilians-Universität, Würzburg; IZKF
11/2010 - 6/2012	Wissenschaftlicher Mitarbeiter, Neurologische Klinik und Poliklinik, Experimentelle Entwicklungsneurobiologie, Prof. Dr. Rudolf Martini, Julius-Maximilians-Universität, Würzburg; finanziert durch einen Forschungszuschuss
10/2008 - 10/2010	Stipendiat der NCL Stiftung, Hamburg; Doktorarbeit, Neurologische Klinik und Poliklinik, Experimentelle Entwicklungsneurobiologie, Prof. Dr. Rudolf Martini, Julius-Maximilians-Universität, Würzburg; Titel: „Pathogenic impact of immune cells in mouse models of neuronal ceroid lipofuscinosis"
3/2008 - 9/2008	Wissenschaftlicher Mitarbeiter, Neurologische Klinik und Poliklinik, Experimentelle Entwicklungsneurobiologie, Prof. Dr. Rudolf Martini, Julius-Maximilians-Universität, Würzburg; SFB
5/2007 - 2/2008	Studentische Hilfskraft; Diplomarbeit, Neurologische Klinik und Poliklinik, Experimentelle Entwicklungsneurobiologie, Prof. Dr. Rudolf Martini, Julius-Maximilians-Universität, Würzburg; Titel: „Role of Cytokines in Connexin32-deficient myelin mutants"; SFB

Studium

10/2001 - 04/2007   Studium der Biologie (Diplom), Julius-Maximilians-Universität Würzburg; Schwerpunkte: Neurobiologie, Genetik und physiologische Chemie

Schulbildung

1992 - 2001   Allgemeine Hochschulreife, Franken-Landschulheim Schloss Gaibach

1988 -1992   Grundschule, Volksschule Volkach

12. Publications

Original articles in peer-reviewed international journals

Groh J, Kühl TG, Ip CW, Nelvagal HR, Sri S, Duckett S, Mirza M, Langmann T, Cooper JD, Martini R (2013) Immune cells perturb axons and impair neuronal survival in a mouse model of infantile neuronal ceroid lipofuscinosis. Brain 136:1083-1101.

Ip CW, Kroner A, **Groh J**, Huber M, Klein D, Spahn I, Diem R, Williams SK, Nave KA, Edgar JM, Martini R (2012) Neuroinflammation by cytotoxic T-lymphocytes impairs retrograde axonal transport in an oligodendrocyte mutant mouse. PLoS One 7:e42554.

Groh J, Weis J, Zieger H, Stanley ER, Heuer H, Martini R (2012) Colony-stimulating factor-1 mediates macrophage-related neural damage in a model for Charcot-Marie-Tooth disease type 1X. Brain 135:88-104.

van Alen T, Claus H, Zahedi RP, **Groh J**, Blazyca H, Lappann M, Sickmann A, Vogel U (2010) Comparative proteomic analysis of biofilm and planktonic cells of Neisseria meningitidis. Proteomics 10:4512-21.

Groh J, Heinl K, Kohl B, Wessig C, Greeske J, Fischer S, Martini R (2010) Attenuation of MCP-1/CCL2 expression ameliorates neuropathy in a mouse model for Charcot-Marie-Tooth 1X. Hum Mol Genet 19:3530-3543.

Kohl B, Fischer S, **Groh J**, Wessig C, Martini R (2010a) MCP-1/CCL2 modifies axon properties in a PMP22-overexpressing mouse model for Charcot-Marie-tooth 1A neuropathy. Am J Pathol 176:1390-1399.

Kohl B, **Groh J**, Wessig C, Wiendl H, Kroner A, Martini R (2010b) Lack of evidence for a pathogenic role of T-lymphocytes in an animal model for Charcot-Marie-Tooth disease 1A. Neurobiol Dis 38:78-84.

Book chapters

Martini R, **Groh J**, Bartsch U (2010) Comparative Biology of Schwann cells and oligodendrocytes. In: The Biology of Oligodendrocytes (P. J. Armati and E.K. Mathey, eds). Cambridge University Press ISBN: 9780521899659

Magazines

Janos Groh und Thomas Kühl

8. Nationaler NCL-Kongress

GenomXpress 3.09; Band 9, Ausgabe 3 - September 2009: 33-34.

Oral presentations

Groh J, Klein D, Patzko A, Martini R (2012) Die immunologische Komponente genetisch bedingter Myelinerkrankungen. Arbeitstagung der Bayerischen Neuromuskulären Zentren, Würzburg, Germany, September 15, 2012.

Groh J, Kühl TG, Ip CW, Kroner A, Crocker P, Cooper JD, Martini R (2011) Immune cells are pathogenic mediators in neuronal ceroid lipofuscinosis (NCL or Batten disease). 1st JNCL PhD Symposium, Hamburg, Germany, July 29-31, 2011.

Groh J and Martini R (2010) Endoneurial M-CSF is a crucial factor for macrophage-mediated neuropathy in a mouse model for Charcot-Marie-Tooth 1X. Experimentelle PNS-Forschung, Düsseldorf, Germany, December 4, 2010.

Groh J, T. Kühl TG, Kroner A, Crocker P, Cooper JD, Martini R (2010) Immune cells are pathogenic mediators in neuronal ceroid lipofuscinosis (NCL or Batten disease). 40th Meeting of the Society for Neuroscience, San Diego, USA, November 13-17, 2010.

Groh J, Fischer S, Martini R (2009) MCP-1 and M-CSF are pathogenetically relevant in a mouse model for CMT-1X. Meeting of the Peripheral Nerve Society, Würzburg, Germany, July 4-8, 2009.

Poster presentations

Groh J, Klein I, Wettmarshausen J, Hollmann C, Klein D, Martini R (2013) Schwann cell dedifferentiation and myelin damage in a mouse model of CMT1X is mediated by CSF-1-related activation of macrophages. Current Topics in Myelin Research, Kassel, Germany, February 28 - March 2, 2013.

Groh J, Weis J, Zieger H, Stanley ER, Heuer H, Martini R (2012) Colony-stimulating factor-1 mediates macrophage-related neural damage in a model for Charcot-Marie-Tooth disease type 1X. Myelin Gordon Research Conference, Lucca, Italy, April 29 - May 4, 2012.

Groh J, Spahn I, Friedman H, Peterson A, Martini R (2012) Generation of oligodendrocyte-mutant mice as models for secondary immune-mediated neural perturbation. International Symposium SFB 581, Würzburg, Germany, April 19-21, 2012.

Groh J, Kühl TG, Ip CW, Mirza M, Crocker P, Langmann T, Cooper JD, Martini R (2012) Immune cells are pathogenic mediators in the visual system of two mouse models of Neuronal Ceroid Lipofuscinosis. 13th International Conference on Neuronal Ceroid Lipofuscinoses (Batten Disease), London, UK, March 28-31, 2012.

Groh J, Zieger H, Heuer H, Martini R (2011) Endoneurial M-CSF is a crucial factor for macrophage-mediated neuropathy in a mouse model for CMT1X. Current Topics in Myelin Research, Kassel, Germany, March 10-12, 2011.

Groh J, Heinl K, Kohl B, Wessig C, Greeske J, Fischer S and Martini R (2010) Attenuation of MCP-1/CCL2 expression ameliorates axon damage in a mouse model for Charcot-Marie-Tooth 1X. Workshop "Molecular and Cellular Mechanisms of Axon Degeneration", Eibsee, Germany, October 3-6, 2010.

Groh J, Kühl TG, Ip CW, Kroner A, Crocker P, Cooper JD, Martini R (2010) Immune cells are pathogenic mediators in infantile neuronal ceroid lipofuscinosis (INCL). Workshop "Molecular and Cellular Mechanisms of Axon Degeneration", Eibsee, Germany, October 3-6, 2010.

Pontikis CC, **Groh J**, Kühl TG, Pressey SNR, Kroner A, Mitchison HM, Martini R, Pearce DA, Cooper JD (2009) Progressive neuronal loss and evidence for abnormal glial responses within the thalamocortical system of Cln3-/- mice. 12th International Congress on Neuronal Ceroid Lipofuscinoses (NCL), Hamburg, Germany, June 3-6, 2009.